https://doi.org/10.15388/vu.thesis.396
https://orcid.org/0000-0002-2957-3123

VILNIUS UNIVERSITY
CENTER FOR PHYSICAL SCIENCES AND TECHNOLOGY

Šarūnas Žukauskas

Glucose biosensors and glucose-powered biofuel cells

DOCTORAL DISSERTATION

Natural Sciences,
Chemistry (N 003)

VILNIUS 2022

The dissertation was prepared between 2017 and 2021 at the Faculty of Chemistry and Geosciences at Vilnius University

Academic supervisors:
prof. habil. dr. Arūnas Ramanavičius (Vilnius University, Natural Sciences, Chemistry – N 003). From 2020-12-18 until 2022-09-30;
prof. dr. Aušra Valiūnienė Vilnius University, Natural Sciences, Chemistry – N 003). From 2017-10-01 until 2020-12-17.

Academic consultant – Dr. Gintautas Bagdžiūnas (Vilnius University, Natural Sciences, Chemistry – N 003).

This doctoral dissertation will be defended in a public/closed meeting of the Dissertation Defense Panel:

Chairman – prof. dr. Rasa Pauliukaitė (Center for Physical and Chemical Sciences, Natural Sciences, Chemistry – N 003).
Members:
prof. dr. Artūras Katelnikovas (Vilnius University, Natural Sciences, Chemistry – N 003);
prof. habil. dr. Eugenijus Norkus (Center for Physical and Chemical Sciences, Natural Sciences, Chemistry – N 003
prof. dr. Vida Vičkačkaitė (Vilnius University, Natural Sciences, Chemistry – N 003);
dr. Roman Viter (University of Latvia, Natural Sciences, Physics – N 002).

The dissertation will be defended at a public meeting of the Defense Council on 18 November 2022 at 14:00. Inorganic Chemistry, Faculty of Chemistry and Geosciences. Address: Naugarduko g. 24, LT03225, Vilnius, Lithuania, tel. (8 5) 219 3108; e-mail: info@chgf.vu.lt
The dissertation can be viewed at the Vilnius University, the Centre for Physical Sciences and Technology libraries and on the VU website at:
www.vu.lt/lt/naujienos/ivykiu-kalendorius

https://doi.org/10.15388/vu.thesis.396
https://orcid.org/0000-0002-2957-3123

VILNIAUS UNIVERSITETAS
FIZINIŲ IR TECHNOLOGIJOS MOKSLŲ CENTRAS

Šarūnas Žukauskas

Gliukozės biojutikliai ir gliukozės biokuro elementai

DAKTARO DISERTACIJA

Gamtos mokslai,
Chemija (N 003)

VILNIUS 2022

Disertacija rengta 2017-2021 metais Vilniaus universiteto Chemijos ir Geomokslų fakultete.

Moksliniai vadovai:
prof. habil. dr. Arūnas Ramanavičius (Vilniaus universitetas, gamtos mokslai, chemija – N 003). Nuo 2020-12-18 iki 2022-09-30;
prof. dr. Aušra Valiūnienė (Vilniaus universitetas, gamtos mokslai, chemija – N 003). Nuo 2017-10-01 iki 2020-12-17.

Mokslinis konsultantas – dr. Gintautas Bagdžiūnas (Vilniaus universitetas, gamtos mokslai, chemija – N 003).

Gynimo taryba:
Pirmininkė – prof. dr. Rasa Pauliukaitė (VTMI Fizinių ir technologijos mokslų centras, gamtos mokslai, chemija – N 003).
Nariai:
prof. dr. Artūras Katelnikovas (Vilniaus universitetas, gamtos mokslai, chemija – N 003);
prof. habil. dr. Eugenijus Norkus (VMTI Fizinių ir technologijos mokslų centras, gamtos mokslai, chemija – N 003);
prof. dr. Vida Vičkačkaitė (Vilniaus universitetas, gamtos mokslai, chemija – N 003);
dr. Roman Viter (Latvijos universitetas, gamtos mokslai, fizika – N 002).

Disertacija ginama viešame gynimo tarybos posėdyje 2022 m. lapkričio mėn. 18 d. 14 val. Chemijos ir geomokslų fakulteto Neorganinės chemijos auditorijoje. Adresas: Naugarduko g. 24, LT03225, Vilnius, Lietuva, tel. (8 5) 219 3108; el. paštas: info@chgf.vu.lt
Disertaciją galima peržiūrėti Vilniaius universiteto, Fizinių ir technologijos mokslų centro bibliotekose ir VU interneto svetainėje adresu:
https://www.vu.lt/naujienos/ivykiu-kalendorius

ABSTRACT

We aim to introduce and describe several glucose biosensor and glucose-powered biofuel cell technologies. We describe a bio electrochemical application of electrochemically generated hole-transporting (p-type) polymeric semiconductors(HTPS), which are based on carbazole derivatives and triphelamine as direct charge transfer glucose sensors. Electrodes based on indium tin oxide and graphite were electrochemically modified with a layer of HTPS and a monolayer of covalently immobilized glucose oxidase (GOx). The HTPS/GOx-based electrodes were investigated for an evaluation of direct hole-transfer between the enzyme and electrode at a bio-electrochemically relevant potential. The broad linear relationship between the peak-current density and glucose concentration was observed.

The development of high-power biofuel cells has been limited in the past by slow or indirect charge transfer. Enzymatic biofuel cell (EBFC) systems were explored with different redox mediator materials used to evaluate their applicability. Redox mediators of different natures have been selected to provide a deeper understanding of the charge transfer system and their effects on the characteristics of biofuel cells. Cytochrome c, Chlorophyll a, and supernatant of ultrasonically disrupted algae Chlorella vulgaris cells were examined as potential redox mediators. The effect of heparin on the EBFC was also evaluated under the same analytical conditions. The measurements of open circuit potential (OCP) and the evaluation of the current response in two modes of measurements (i) during potential cycling in cyclic voltammetry measurements or (ii) at the constant potential value in chronoamperometry were applied for the evaluation of EBFCs.

Further microbial fuel cells (MFBC) are unique biocatalytic systems, which transform chemical energy accumulated in renewable organic fuels, such as glucose into electrical energy. However, not all microorganisms during metabolic/catalytic processes generate sufficient redox potential. In our research, we have assessed the applicability of the microorganism *Rhizobium anhuiense* as a catalyst suitable for the design of microbial fuel cells. The *Rhizobium anhuiense* bacteria were cultivated in a high glucose environment and to improve the charge transfer, several redox mediators were tested, namely menadione, riboflavin, and 9,10-phenanthrenequinone (PQ).

CONTENTS

LIST OF ORIGINAL PUBLICATIONS:

P1, Gintautas Bagdžiūnas, Šarūnas Žukauskas, Arūnas Ramanavičius "Insights into a hole transfer mechanism between glucose oxidase and a p-type organic semiconductor", Biosensors and Bioelectronics, Volume 102, 15 April 2018, Pages 449-455.
https://doi.org/10.1016/j.bios.2017.11.053

P2, Šarūnas Žukauskas, Gintautas Bagdžiūnas, Arūnas Ramanavičius "Organic Semiconductors with Carbazole and Triphenylamine Moieties for Glucose Oxidase-Based Biosensors", Journal of The Electrochemical Society, 166 B316 2019
https://doi.org/10.1149/2.0291906jes

P3, Urte Samukaitė-Bubnienė, Šarūnas Žukauskas, Vilma Ratautaitė, Monika Vilkienė, Ieva Mockevičienė, Viktorija Liustrovaitė, Maryia Drobysh, Aurimas Lisauskas, Simonas Ramanavičius, Arūnas Ramanavičius, "Assessment of natural redox mediators for enzymatic biofuel cells powered by glucose" Energies 2022, 15(18), 6838
https://doi.org/10.3390/en15186838

LIST OF CONFERENCES

C1, Šarūnas Žukauskas, Gintautas Bagdžiūnas, Arūnas Ramanavičius „Application Hole Transporting Organic Semiconductors for Biosensors“ 23rd Topical Meeting of the Internaitonal society of Electrochemistry 2018m., Vilnius, Lietuva

C2, Deimantas Palinauskas, Šarūnas Žukauskas, Gintautas Bagdžiūnas „Electropolymerization of indole derivatives and their electrochromic properties“ 62nd international conference for students of physics and natural sciences 2019m., Vilnius, Lietuva

C3, Arūnas Ramanavičius, Eivydas Andriukonis, Vilma Ratautaite, Ieva Balevičiūtė, Natalija German, Asta Kaušaitė-Minkštimienė, Šarūnas Žukauskas, Aura Kiseliūtė, Almira Ramanavičienė „Formation of Conducting Polymer based Structures Suitable for Sensor Design“, 2nd INTERNATIONAL CONGRESS on ANALYTICAL and BIOANALYTICAL CHEMISTRY, 2020m., Antalya, Turkija

C4, Šarūnas Žukauskas, Deimantė Stankūnaitė, Arūnas Ramanavičius „Application of biosensor systems in the production of enzymatic biofuel cells“, Advanced Materials and Technologies 2021. 2021m., Palanga, Lietuva

ACKNOWLEDGEMENTS

I would like to express my deepest appreciation to professors Arūnas Ramanavičius, Aušta Valiūnienė and to dr. Gintautas Bagdžiūnas. I would also like to extend my gratitude to colleagues from the department of physical chemistry in Vilnius University, NanoTechnas research laboratory in the institute of chemistry, and department of Nanotechnology in the center for physical science and technology.

With special mentions to Alma, Almira, Anton, Aura, Benas, Eivydas, Inga, Lina, Povilas, Raimonda, Simonas, Urte, Viktorija, Vilma and Vincentas.

I have learned an immense amount from each and every one of them.

LIST OF ABBREVIATIONS

GOx - glucose oxidase
EBFC - enzymatic biofuel cell
MBFC - microbial biofuel cell
HTPS - hole transporting (p-type) polymeric semiconductor
FAD - flavin adenine dinucleotide
CT - charge-transfer
DT - direct charge transfer
ITO - indium tin oxide
DCM - Dichloromethane
$TBAPH_6$ - Tetrabutylammonium hexafluorophosphate
PBS - phosphate-buffered saline solution
CzO - 9-(oxiran-2-ylmethyl)-9H-carbazole
CzS - 9-(thiiran-2-ylmethyl)-9H-carbazole
CzEt - 9-ethyl-9*H*-carbazole
CzPh - 9-phenyl-9*H*-carbazole
TPA - *N*,*N*,*N*-triphenylamine
OCP - open circuit potential
CV - cyclic voltammetry
SEM - scanning electron microscopy
$EBFC_{CC}$ - cytochrome c mediated biofuel cell
$EBFC_{CA}$ - chlorophyll a mediated biofuel cell
$EBFC_{ChV}$ - *chlolera vulgaris* supernatant mediated biofuel cell
$EBFC_{Hep}$ - heparin mediated biofuel cell

1. INTRODUCTION

Glucose is a carbohydrate, a simple sugar, that is abundant throughout nature. Produced through the process of photosynthesis by algae and plants, it is widely utilized as a means of energy storage, as a natural building block, and for aerobic and anaerobic cellular respiration. As a molecule it is ever present in our lives in agriculture, natural and industrial products, within our own bodies. As such it is vital to study it, to expand our understanding of how it can be further utilized. In this study we focus on electrochemical technologies for detecting and measuring glucose, as well as technologies that allow the conversion of glucose to electrical energy.

The ability to detect and measure glucose is of vital importance to the medical and food industry. Our bodies function by maintaining a narrow concentration range of glucose in our bloodstream, roughly 5±2 mM, and in cases where it cannot do so due to illness (such as diabetes) or otherwise, it must be regulated through external methods. As such technologies to accurately track glucose concentrations in real time or near real time conditions were developed. These technologies are also widely used in the food industry, the amount of glucose present in foodstuff changes overtime and by tracking these changes we can quantitively analyze the ripeness of fruits, track fermentation or even assess unwanted microbial growth.

Glucose, being the most common carbohydrate in nature, is also very appealing for its potential use as a bio-friendly form of electrochemical energy storage. As the body utilizes glucose for cellular respiration so can we also utilize it to power industrial or agricultural applications. Energy is ever in demand and by making use of glucose as a fuel source, we could obtain alternative ways of utilizing excess waste plant matter, spoiled food... etc. It could also potentially function as an energy source for electromechanical devices within living bodies such as pacemakers or sensors.

1.1. Glucose sensor technologies

In this work we focus on second and third generation glucose sensors. Second generation sensors require a mediator to facilitate charge transfer, third generation sensor attempt to bypass a mediator and to utilize direct charge transfer to the electrode. However, the actual probability of "direct CT" depends significantly on the distance between a redox-active center and the electrode as well as the nature and/or modification of the electrode surface[1]. One of many of such enzymes is glucose oxidase (GOx) [2], which is the most

frequently applied in the design of amperometric biosensors as a biological recognition part [3] and has a great potential in development of enzymatic biofuel cells [4]. On the other hand, direct CT is the main advantage of the third-generation biosensors, which leads to a high selectivity and lower operational potential of the enzymatic electrode. While designing direct CT based electrodes, a high rate of charge transfer between the active site of enzyme and electrode surface is the crucial and most challenging factor. Wittekindt et al. deduced that the aromatic amino acids, such as tyrosine (Tyr) and tryptophan (Trip) are involved in CT of various biological systems [5]. Ayranci et al., have reported that polymers based on thiophene and (1*H*-pyrrol-1-yl)aniline as monomers can be used as the matrices for the immobilization of GOx and applied for glucose determination [6]. Later, Winkler and Gray proposed that hole-hopping should protect enzymes from oxidative damage. This CT mechanism prevents the formation of harmful molecular oxidants [7,8]. Eventually, this hole-transfer mechanism can be applied to establish CT between enzymes and electrodes, which are used in the design of biosensors and biofuel cells. However, according to the best of our knowledge, the hole-transport mechanism has not been realized and proved in above mentioned enzymatic devices so far. On the other hand, hole (p-type) transporting organic semiconductors (for example that are based on carbazole derivatives and polymers) have been employed in the organic electronics, such as organic light emitting diodes (OLED) [9–11]. In our research, an investigation of charge (hole) transfer between the enzyme and electrode was performed on electrodes based on indium tin oxide (ITO) and graphite electrochemically modified with a hole-transporting (p-type) polymer-semiconductor (HTPS) based on carbazole derivatives, TPA and covalently immobilized GOx monolayer. Charge transfer rate constants between HTPS and GOx as well as sensitivity to glucose were determined.

1.2. Biofuel cell technologies

Biofuel cells are primarily separated into two types – microorganisms-based biofuel cells [12] and enzyme-based biofuel cells [13]. Enzymatic biofuel cells are attractive because of the type of catalysts they use. An excellent feature of enzymes, as catalysts, is that they are highly selective, because– they catalyze only specific reactions, therefore, most of them are harmless, active at room and/or human body temperature, and at near to neutral pH values, hence they can be compatible with living organisms. One of the advantages is that biofuel cells can produce more energy than conventional

batteries because the fuel in the system can be constantly renewed almost without any limitations, which makes such systems very attractive. However, relatively low power output is still being exhibited. To overcome this problem, redox mediators are introduced into the system.

1.3. Redox mediated systems

High fuel cell standards require that a biofuel cell must be simple, efficient, long-lasting, stable, easily compatible, and most importantly, commercially viable. By changing the types of electrodes [14], their modification methods [15], the composition of the buffer solutions [16,17], enzymes themselves [18], and mediators used [19], different efficiencies can be obtained, and thus the characteristics of the biofuel cell can be improved. A considerable amount of research to make this fuel-producing equipment economically viable is spent and systems are being improved in various ways. The enzymatic fuel cell can be mediated and unmediated. Most enzyme-based cells are electrochemically active, although charge transfer from an enzyme to the electrode can be facilitated more effectively *via* the mediators.

A very important characteristic of enzymatic biofuel cells is the efficiency of electron transfer between the reactive site of the enzyme and the electrode surface. The key to achieving efficient enzymatic biofuel cells is related to the speed of this process, and the best performance will depend on the electrochemical reaction rate. Depending on how the electric connection between a particular electrode/enzyme pair is realized, enzymatic biofuel cells can be divided into two main groups, which are based on: (i) direct electron transfer, where the enzyme is able to communicate directly with the electrode, (ii) mediated electron transfer, in which redox species either in solution or as immobilized redox polymers are used to channel the electrons to (and from) the electrode surface [20]. But the major problem encountered in enzymatic fuel cell studies is a rather slow charge transfer between the enzyme and the electrode. To mediate the charge transfer between the enzyme and the surface of electrode, low molecular weight redox compounds, such as cytochromes, are used as redox mediators. Higher power generation and minimal interference effects at a lower cell potential are achieved by using a mediator in fuel cell systems. A mediator should possess the following characteristics: fast electrochemical kinetics and oxidation states that do not interfere with the enzyme and chemical stability. Also, choosing a mediator that has a redox potential close to that of the fuel increases the power density [19].

In previous studies, some mediators were described [13]: phenanthrenequinone [21] ubiquinone/ubiquinol [22] ferrocene methanol, methylene blue or 2,2'-azinobis(3-ethylbenzothiazoline-6-sulfonic acid) [23], 9,10-phenanthroline-5,6-dione [13], or methyl-1,4-naphthoquinone [24] were used as anodic redox mediators. There are several aspects that should be carefully considered while selecting appropriate redox mediators for the microbial biofuel cells. One of them is the solubility of a mediator in the media. Mediators are categorized according to their solubility in water-based media or organic solvent-based media. The most often used example of the hydrophilic mediator is potassium ferricyanide/ferrocyanide. In the case of microbial biofuel cells, the examples of a lipophilic redox mediator are 1,10-phenanthroline-5,6-dione or 9,10-phenanthrenequinone.

In this research we have evaluated the applicability of several potential redox mediators, namely cytochromes, chlorophylls, and the supernatant of ultrasonically disrupted algae *Chlorella vulgaris* cells. The applicability of these materials as redox mediators was evaluated by means of power density, cyclic voltammetry, and chronoamperometry. During the evaluation of the cyclic voltammetry results, the focus was on the value of the potential at which oxidation is observed. Meanwhile, during the evaluation of chronoamperometry results, the focus was on the changes of current in respect of glucose concentration in the solution. In addition, the effect of heparin on the EBFC characteristics also was evaluated.

Cytochromes are heme-based proteins, designed for charge transfer. The transfer of electrons is facilitated by an oscillation of the heme iron between the ferrous and the ferric forms [25]. They are a very large class of metalloproteins. The heme group confers functionality, which can include oxygen-carrying, oxygen reduction, electron transfer, and other processes [25,26]. The heme consists of iron cation bound at the center of the conjugate base of the porphyrin, as well as other ligands attached to the "axial sites" of the iron. The iron is typically Fe^{2+} or Fe^{3+}. Hemeproteins have diverse biological functions including oxygen transport, which is completed via hemeproteins including hemoglobin, myoglobin, neuroglobin, cytoglobin, and leghemoglobin. Some hemeproteins – cytochrome P450s, cytochrome c oxidase, ligninases, catalase, and peroxidases – are enzymes. They often activate O_2 for oxidation or hydroxylation. Hemeproteins also enable electron transfer as they form part of the electron transfer chain. Cytochrome a, cytochrome b, and cytochrome c possess electron transfer functions [27], which can be well exploited in biofuel cells [26]. Due to their oxidative reducing properties, heme proteins are good electron carriers and can therefore be mutual intermediaries between the electrode and the enzyme. Also, heme iron-

containing proteins are less sensitive to halides (e.g., chloride and fluoride) compared to some enzymes such as laccase, and chloride ions are known to be found in numerous biofuel cell systems [26].

Heparin is a highly sulfated glycosaminoglycan that has been used as a clinical anticoagulant for more than 90 years [28]. Heparin is a carbohydrate that is part of the glycosaminoglycan family of molecules, which includes a variety of closely related members such as heparin sulfate. Heparin is usually processed from porcine or bovine intestine tissues in the pharmaceutic industry and has various molecular lengths ranging from 2000 up to 40,000 Dalton [29]. Heparin has been found to play a role in a wide variety of cellular functions, and the importance and diversity of their possible uses have only recently begun to be fully recognized. Heparin acts by binding to the lysyl residues on antithrombin and accelerating the rate of the complex formation [30].

Chlorophylls are natural green pigments ubiquitously present in the plant kingdom, which play an important role in the photosynthetic process. Chlorophylls are found in diverse plants, algae, and cyanobacteria [31]. Chlorophyll is formed up of carbon and nitrogen atoms along with a magnesium ion in a central position. Chlorophyll is found in almost every green part of plants, i.e., leaves and stems, within the chloroplast. Chloroplast can be referred to as the "food factory" of the plant cell because it produces energy and glucose for the whole plant in association with CO_2, water, and sunlight. Initially, chlorophyll was classified into four classes – Chlorophyll a, Chlorophyll b, Chlorophyll c, and chlorophyll d [32] Chlorophylls play a pivotal role in photosynthesis. They have a unique capacity to trap light energy and utilize it in the photolysis of water molecules to replenish the reducing power of the cells, this energy is needed in carbon assimilation in subsequent steps of photosynthesis. This property of the pigment is unique and can be exploited in various anthropogenic applications. Chlorophyll could be used as a redox mediator. Apart from this, Chlorophyll has also been observed to possess other important activities that add to the suitability of the molecule for different applications. The fluorescence activity of chlorophyll allows it to be used extensively to develop optical biosensors.

Chlorella vulgaris microalgae store valuable amounts of lipids, especially the appropriate fatty acid profile, which can be used to produce biofuels. One of the most desirable particulars is its high growth rate. The *Chlorella* sp. has been widely studied from the bioenergy perspective. Also, it is known to fare well in algae-based biofuel cells studies [33–35]. There are many studies, where the supernatant of ultrasonically disrupted *Chlorella vulgaris* cells is used in biofuel cell cathodes, where bacteria could oxidize organic matter and produce

e^-, H^+, and CO_2. The supernatant of ultrasonically disrupted *Chlorella vulgaris* cells in the cathodic area could use CO_2, as well as nitrogen and phosphorus released by the sediment during photosynthesis under the light, and produce O_2, which serves as the electron acceptor for the generation of electricity. Photosynthesizing algae in the cathode will not only solve the problem of cathode electron acceptor restriction, but also absorb CO_2, nitrogen, and phosphorus without requiring an additional energy source [36]. Algae-based systems work well in biomass generation as algae grow faster, have low land requirements, and have better photosynthetic efficiency. However, algae systems are sensitive to contaminations, and sudden changes in cultivation conditions and require careful monitoring and regular harvesting of algae biomass. On the other hand, plant systems require a higher start-up time because plants grow slowly and have lower efficiencies but require less careful maintenance [37].

1.4. Microbial biofuel cells

Microbial biofuel cells (MBFC) are bio-electrochemical devices that are driven by the metabolic activities of microorganisms [38], which can produce electricity through the oxidation of reducing organic substrates during metabolic processes occurring in the microorganisms and charge transfer to electrodes [39]. The selection of the most suitable microorganisms is an important issue during the development of MBFCs. Both aerobic and anaerobic microorganisms have been utilized in the MBFCs design and are serving as biocatalysts in anode compartment. Several research reported great applicability of redox-active microbes in MBFCs design [39,40]. These 'electroactive' microbes can perform extracellular electron transfer *via* several different pathways, e.g.: *c*-type cytochromes (cyt *c*) [41], type IV pili/nanowire [42], chemically incorporated conducting polymers [43,44], and redox mediators [45,46]. Depending on the nature and redox state of the applied redox mediator and their contribution to redox processes, two main types of MBFCs are reported: MBFCs based on mediated and on direct electron transfer [47]. *Shewanella putrefaciens* [48], *Geobacter sulfurreducens*, *Geobacter metallicreducens* [49], *Aeromonas hydrophila* [50], and *Rhodoferax ferrireducens* [51] are most commonly used in direct electron transfer-based MBFCs; While various endogenous and exogenous mediators (e.g.: methylene blue [52], menadione [53], riboflavin[54], and some other redox materials) can be applied in mediated electron transfer based MBFCs. However, to estimate the fuel cell efficiency, it is not sufficient just to know the charge transfer principle and the

rate of fuel conversion into reaction products [38,55], because some other characteristics are also critically important during the assessment of MBFCs performance. The most important characteristics include: (i) metabolic capacities of the chosen microorganisms; (ii) charge transfer rate from the microorganism towards electrode; (iii) the efficiency of semi-permeable membrane; (iv) electrical resistance of applied solutions, electrodes, and some other parts of the bio-electrochemical system; (v) diffusion rates of used organic fuel molecules and during metabolic processes generated products [56]. Depending on the operational parameters of the MBFC, different metabolic pathways of applied bacteria can be exploited for the oxidation of various organic fuels. These parameters are determined by the selection and performance of specific microorganisms. The efficiency of MBFCs can be significantly advanced by the application of 3D electrodes. The immobilization of microorganisms is an important issue during the development of MBFCs, various strategies can be applied to solve this problem, e.g.: electrostatic forces can be exploited to mediate the interaction/attachment of bacteria to electrodes. In cell wall of gram-negative bacteria the negatively charged phosphate and carboxyl groups are outweighing the positively charged amino groups, therefore, these conditions determines rather low surface zeta potential of mentioned microbes[57].

Ecosystems that can utilize large colonies of microorganisms living in the natural environment such as water and soil are the most promising for the design of MBFCs. Some soil bacteria are an auspicious for the design of MBFCs because they can be easily electrostatically attracted/fixed on the electrode surface. *Rhizobia* are among the best-studied soil microbes associated with plants. This group of bacteria can proliferate free in the soil, or establish symbiosis with some legumes, mostly with peas [58]. *Rhizobia* bacteria exhibit an oligotrophic lifestyle, belonging to either α-proteobacteria or β-proteobacteria. The interaction is reciprocal where plants selectively enrich beneficial bacteria attaching to their roots, and the *Rhizobia* bacteria infect and colonize plant epidermis, form bacteroids, and then start to fix atmospheric nitrogen, this process is essential for the development of plants. In most agroecosystems, *Rhizobia* are one of the common soil bacteria, especially if legumes are incorporated into the rotation [58]. The *Rhizobia* related are gram-negative nitrogen-fixing bacteria and are commonly found across the whole of Eurasia in an endosymbiotic relationship with the nodule of legume plants. *Rhizobia*-related species could serve as good candidates for MBFCs design because they are a non-pathogenic, facultative anaerobe group of microbes. Moreover, *Rhizobium* species have wide capacities decompose

organic substrates, roots exudates including C4 dicarboxylates (malate, fumarate, and succinate) and some other short chain fatty acids. In the native habitat, most of the extracted electrons are usually channeled to nitrogenase to fix atmospheric nitrogen to ammonia. It is used by legume hosts, and a small amount is released into the soil. Dicarboxylate decomposition and nitrogen fixation processes are tightly regulated by metabolic processes performed within the hosing plant. According to scientific research it is well known that *Rhizobia* species are well equipped with highly efficient metabolic systems capable to extract electrons from organic compounds [59]. It should be noted that in laboratory conditions in the absence of a specific host and conditions in the surrounding environment, these regulatory signals, which are inducing nitrogen fixation, will be absent and all captured electrons will increase the reduction potential of the *Rhizobia* bacteria-based system. All the traits indicate that microbes, which interact with plant roots in the rhizosphere, can be used to develop a new design of microbial fuel cells and *Rhizobium bacteria* are among the most attractive candidates for this purpose. However, despite numerous attempts, MBFCs are still nascent yet promising technology that could provide solutions to our global energy and environmental problems. MBFCs are still the only technology, generating electricity from organic waste and reducing the concentration of hazardous materials. Nevertheless, more research is needed to tackle some bottlenecks including the complete utilization of substrate to enable the generation of sufficient voltage and power. The assessment of microorganisms with strong electron scavenging capacity can provide solutions for the development of MBFCs.

1.5. The aim of this study:

To develop and design functioning glucose biosensors and glucose-powered biofuel cells utilizing direct and indirect charge transfer technologies and microorganisms.

1.6. The objectives of this study:

To design, create and evaluate a GOx-based bioelectrochemical systems utilizing direct electron transfer technology.

To design, create and evaluate a GOx-based bioelectrochemical systems utilizing mediated charge transfer technology.

To design, create and evaluate a microorganism-based bioelectrochemical systems powered by glucose.

1.7. Academic novelty

P-type polymer semiconductors have been shown to be able to participate in direct electron transfer with proteins.

One of the first times that cytochrome-mediated bioelectrochemical systems of glucose have been investigated.

One of the first papers describing the use of nitrogen-fixing bacteria to generate electricity.

2. MATERIALS AND INSTRUMENTS

2.1. Reagents

All materials used were of reagent grade unless specifically stated.

D–(+)–glucose, Glutaraldehyde (50% V) Carl Roth (Karlsruhe, Germany)

The solution of 0.5 M glucose was prepared in distilled water at least 24 h before use to allow for the mutarotation of D-(+)-glucose; to reach equilibrium between the α- and β-forms.

Glucose oxidase (GOx) from *Aspergillus niger* with catalytic activity of 208 U/mg Fluka (Buchs, Switzerland)

2-methyl-1,4-naphthoquinone, riboflavin. Alfa Aesar (Haverhill, MA, USA).

Sodium molybdate and 9,10-phenanthrenequinone were purchased from Merck (Darmstadt, Germany).

Tetrabutylammonium hexafluorophosphate ($TBAPH_6$). Sigma-Aldritch (Berlin, Germany). Was used as an ion carrier in organic solvents

125 μg/mL heparin medicinal product. Rotexmedica (Trittau, Germany)

Ethanol. Riedel-de Haën (Seelze, Germany)

Dichloromethane (DCM) was distilled over CaH_2 and under Ar atmosphere and stored over 3 Å microsieves.

Sodium acetate – acetic acid buffer, pH 4.0, and phosphate-buffered saline solution, pH 7.2, pH 7.4 (PBS)

Precursors of organic polymers as semiconductors (OS) were prepared according to the following literature the 9-(oxiran-2-ylmethyl)-9H-carbazole (CzO) [60], and 9-(thiiran-2-ylmethyl)-9H-carbazole (CzS) [61], further organic polymers as semiconductors used were 9-ethyl-9*H*-carbazole (CzEt), 9-phenyl-9*H*-carbazole (CzPh), *N*,*N*,*N*-triphenylamine (TPA)

Cytochrome c electrophoresed from lysed spirulina cells. Norsk institut for vannforskning, (Oslo, Norway).

Chlorella vulgaris preparation was obtained according to protocol: firstly, Chlorella vulgaris algal cells were broken down ultrasonically. The ultrasonicated cells were centrifuged; the remaining supernatant after centrifugation was used in the experiments

Chlorophyll a was extracted manually. 7.2 grams of fresh spinach were broken down mechanically using a porcelain mortar and pestle while adding 20 mL of toluene and methanol solution (molar ratio 8:2). The solution was then filtered through a Buchner funnel. For Chlorophyll, an extraction

silica gel and toluene were used to load the column up to 15 cm and then the filtrate was added. The column was washed with toluene until the yellow fraction containing carotenes was collected. The green fraction containing Chlorophyll a was collected within 50 mL of a toluene-methanol solution mixed at a molar ratio of 8:2. The toluene and methanol solutions were separated from each other using a separator funnel and then the toluene solution (containing dissolved Chlorophyll a) was evaporated. After the extraction, the Chlorophyll a was dissolved in methanol.

Yeast cell extract and glucose used for MBFC were of microbiological grade.

2.2. Instrumentation

Graphite rods, Sigma-Aldrich (Berlin, Germany) (99.99%, 3 mm in diameter with an active surface area of 0.071 cm^2) and ITO coated glass (working area 0.65cm^2) Sigma-Aldrich (Berlin, Germany) were used as working electrodes

The voltages were reported with reference to the Ag/AgCl in 3 M KCl solution electrode in aqueous solutions and against a silver wire electrode coated with AgCl in non-aqueous-media solutions

Titan plate electrode (partially coated with platinum) with the electrochemically active-area of 1.0 cm^2, platinum wire (working area 0.24 cm^2) were used as counter electrodes in aqueous media and graphite rods, Sigma-Aldrich (Berlin, Germany) (99.99%, 3 mm in diameter with an active surface area of 2.5 cm^2) and platinum wire (working area 0.24 cm^2) were used as counter electrodes in non-aqueous media, with a ferocene/ferocenium couple employed as the external reference.

The electrochemical experiments were performed by using an Autolab PGSTAT 30 Potentiostat/Galvanostat from Autolab (Utrecht, The Netherlands) with the Nova v. 1.10 and 2.10 software packages

Attenuated total reflection infrared (ATR IR) spectra were recorded using a Bruker VERTEX 70 spectrometer. The static contact angle was measured using a Theta Lite optical tensiometer and contact angle meter from Biolin Scientific. The atomic force microscopy (AFM) was carried out using a WITec Alpha300R microscope. Zeta potential was assessed using Zetasizer Nano series Nano-ZS, Malvern Industries (United Kingdom). Electrodes were imaged using E-SEM SU-70 scanning electron microscope Hitachi (Japan). Biofuel cell power measurements were obtained using the benchtop multimeter UT8802E UNI T from TEM Electronic components (Łódź, Poland) and Autolab PGSTAT 30 Potentiostat/Galvanostat from Autolab (Utrecht, The Netherlands)

3. METHODOLOGY

3.1.Electrode cleaning and preparation

Before further modification of ITO-modified glass electrodes were cut to size 75 mm by 26 mm, the electrodes were washed with distilled water and acetone; afterwards they were electrochemically cleaned by 10 potential cycles in the range from -1000 to +1000 mV vs Ag/AgCl, at 200 mV/s scan rate in PBS buffer solution.

Graphite rod electrodes were cut to the required size and polished by hand with abrasives using the Figure 9 method, until an even reflective surface was obtained.

The counter electrode was treated with fire and cleaned with acetone and DI water to burn off any accumulation of organic residue in the process of experimentation.

The surface area of the electrodes was limited and maintained constant during electrochemical tests using silicone tubing and Teflon tape.

3.2. Modification of electrodes with organic polymers as semiconductors

The p-type semiconducting polymer was deposited on graphite and ITO electrodes under potentiodynamic conditions by using the cyclic voltammetry method. The parameters for the deposition were chosen experimentally.

CzO, CzS organic polymer precursors were deposited on cleaned ITO electrodes electrochemically using 10 potential cycles in a solution of 0.5 mg/ml of the organic precursor with 0.1 M $TBAPH_6$ dissolved in dry DCM at the scan rate of 50 mV/s. During this modification (the potential was swept from -200 mV to +1500 mV vs Ag/AgCl for polymerization of CzO and CzS) cyclic voltammograms were registered. To clean the newly formed ITO/poly-CzO and ITO/poly-CzS electrodes they were washed with distilled water before and after each treatment step. An electrochemical characterization was performed with the same electrochemical devices and software which were used for the modification of ITO electrodes.

TPA, CzEt and CzPh organic polymer precursors were deposited on cleaned graphite electrodes electrochemically using 20 potential cycles in a solution of 0.5 mg/ml of the organic precursor with 0.1 M $TBAPH_6$ dissolved in dry DCM at the scan rate of 50 mV/s. During this modification (the

potential was swept from -200 mV to +1500 mV vs Ag wire coated with AgCl for polymerization of TPA, CzEt and CzPh) cyclic voltammograms were registered. To clean the newly formed graphite/poly-TPA, graphite/poly-CzEt, graphite/poly-CzPh electrodes were washed with distilled water before and after each treatment step. An electrochemical characterization was performed with the same electrochemical devices and software which were used for the modification of graphite electrodes.

3.3. Crosslinking organic semiconducting polymer modified electrodes with GOx enzymes

The polymer-modified electrodes were crosslinked with GOx enzyme by utilizing a two-step process. The electrodes were being incubated for 1 hour at room temperature in a solution 2.5% of glutaraldehyde in water. The electrodes were washed with distilled water before and after each treatment step. Finally, the following electrodes were immersed to a GOx (5 mg/mL) solution in PBS buffer (pH 7.2) and stored overnight at +4°C temperature. Prior to the electrochemical measurements, the electrodes were thoroughly washed with distilled water to remove: the non-immobilized enzyme; the dissociated GOx cofactor – FAD; and other un/non-immobilized materials, which were present in the enzyme samples used for electrode modification. Moreover, an immobilization of the pure FAD cofactor on the ITO/poly-CzS -electrode was not observed using the UV-vis spectroscopy due to a low nucleophilicity of the amino group of the FAD cofactor adenine. The prepared electrodes had been kept in a closed vessel over PBS, at +4°C until they were used in the experiments.

3.4. Mediated EBFC electrode preparation

3 µL of assessed material solution and 5 µL of glucose oxidase. were physically deposited on the polished graphite electrode surface. The deposited solution is left to partially evaporate to reduce in volume. We waited until a drying outer edge could begin to be observed on the electrode's outer circumference, but the central section was still wet. Once enough liquid had evaporated, the system was transferred into a chamber saturated with glutaraldehyde vapor to chemically bond the structure with the electrode. Such systems were indicated based on the assessed material: $EBFC_{CC}$ – the system with Cytochrome c, $EBFC_{CA}$ – the system with Chlorophyll a, $EBFC_{ChV}$ – the

system with the supernatant of ultrasonically disrupted Chlorella vulgaris cells, and $EBFC_{Hep}$ – the system with heparin.

3.5. MBFC electrode preparation

Gram-negative *Rhizobium anhuiense* bacteria obtained from Lithuanian Research Center for Agriculture and Forestry (Vėžaičiai, Lithuania) microbial strain collection. Bacteria were cultivated in Norris medium [62], in a high glucose environment, pH 7.0, composed of nitrogen-fixing bacteria strains. Prior to the use in experiments, the *Rhizobium ahnuiense* bacteria were reinoculated on an inclined Norris medium supplemented with agar and left to grow for 48 hours at 28°C. Afterward, 5 µL of an autoclaved Norris medium solution was used to fill the test tube with inoculums and carefully suspended. The mixture was vortexed for several minutes to ensure that the majority of the bacteria gets lifted from solid media. Then, the bacterial suspension was transferred and diluted in a fresh autoclaved Norris medium to obtain a density of colony-forming units (CFU) equal to 1 × 107 CFU mL^{-1} [63]. A single chamber MBFC cell was assembled, where a two-electrode electrochemical system was utilized, a graphite electrode was used as the working electrode and a large-area platinum wire served as a counter electrode. Bacterial samples were immobilized on a graphite electrode by letting it lightly dry for two minutes. A polycarbonate membrane with 1 µm holes was used to separate the specimen from the surrounding environment to ensure attachment to the anode.

3.6. Assessment of Zeta potential

The prepared samples were diluted 10-fold in a medium with appropriate ionic strength (0.01 mM, 0.05 mM, 0.1 mM, 0.3 mM, 10 mM, 50 mM, 100 mM, 300 mM) and pH of 5.0, 6.0, 7.0 or 8.0 were adjusted immediately prior to zeta potential measurement. The resulting suspension was used to fill clear disposable 'zeta cells' (ATA scientific, Australia) immediately prior to zeta potential measurements. The ionic strength was measured at pH 7.0, while pH investigations were conducted in 0.1 mM PBS solution. The electrophoretic mobility of bacterial cells was measured with a zeta potential analyzer at 80 V (Zetasizer Nano series Nano-ZS; Malvern Industries Ltd, Malvern, United Kingdom) and converted to zeta potentials [64]. Measurements were performed at 25°C in standard a Norris medium, pH 7.0.

The sample was measured five times on two separate days to determine the reproducibility of the results. Between each measurement, electrodes were rinsed with copious amounts of Milli-Q^{TM} water, followed by the test bacterial suspension.

3.7. Electrochemical assessment of modified electrode sensitivity to glucose

A three-electrode system was used to assess the modified electrodes, with the modified electrode serving as the working electrode (working area 0.071 cm^2) and a platinum wire (working area 0.24 cm^2) as the counter electrode. The voltages were measured against a commercial Ag/AgCl electrode. The functionality and viability of the created GOx-modified organic semiconductor-based electrodes were assessed using the CV method. Throughout this experiment, glucose solution was continuously added to the PBS buffer solution; after each addition, the resulting solution was run through two cyclic voltammetry cycles from -0.2 V to 0.4 V vs Ag/AgCl at a potential sweep rate of 30 mVs^{-1}. In all the cyclic voltammetry-based assessments, the data of the second potential cycle was evaluated. For further electrochemical analysis, the modified electrodes were investigated by CV in the absence of glucose at potential sweep rates from 5 to 100 mVs^{-1}.

Mediated EBFC modified electrodes were assessed using a wider potential range -1.5V to 1.5V at 50 mVs^{-1} due to the higher oxidation potential observed during the experiments. These systems were also assessed using chronoamperometry at the respective oxidation potential measured in each system.

3.8. Biofuel cell design

A single chamber cell design using a two-electrode system was used to assess the modified electrodes for their applicability in biofuel cells. The modified working electrodes were tested versus a commercial Ag/AgCl electrode while testing EBFC modified electrodes, and vs a platinum wire electrode (working area 0.24cm^2) in MBFC systems. The chamber was filled with PBS, pH 7.0, and the systems' open current potential (OCP) was measured. Afterward, various external resistors (10 MΩ, 1 MΩ, 390 kΩ, 220 kΩ, 180 kΩ, 130 kΩ, 100 kΩ, 68 kΩ, 56 kΩ, 33 kΩ, 10 kΩ, 1 kΩ) were connected in parallel to the electrical circuit to imitate external loads and to

assess the power density of the bacterial samples. The potential changes were recorded.

4. RESULTS AND DISCUSSION

4.1. Formation of poly-CzO/GOx, poly-CzS/GOx modified electrodes

It is universally accepted that during electrochemical oxidation carbazole derivatives mostly couple to each other via 3- and 6-position because these molecules have the highest electron densities at these positions [65]. The electrochemical deposition of polymers poly-CzO and poly-CzS on ITO surface was performed under potentiodynamic conditions (Figure 1a and b). The onset ionization potentials (IP) of monomer and polymer were measured during the 1st and 10th potential cycles of electrochemical polymerization, respectively. The ionization potentials were calculated to be 1.15/1.12 V vs Ag/AgCl (5.61/5.58 eV vs vacuum) and 0.882/0.773 V (5.34/5.24 eV) for CzO/CzS monomers and poly-CzO/poly-CzS polymers, respectively. Furthermore, poly-CzS is obtained at a lower ionization potential than poly-CzO due to the longer polymer chains and their higher conjugations.

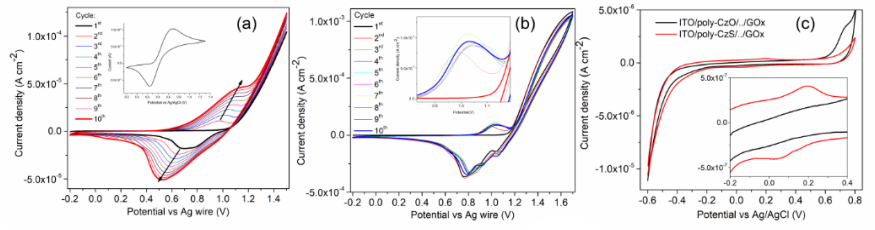

Figure 1. Electrode modification and evaluation. Cyclic voltammogram (CV) profiles of ITO-electrode during potential cycling based electrochemical polymerization of (a) CzS and (b) CzO in DCM 0.1 M of $TBAPF_6$ at scan rate of 50 mV s^{-1},1st to 10th cycle (Inset: CV of ferrocene as external standard), (c) CVs of ITO/poly-CzO and poly-CzS/amine/aldehyde/GOx in buffer, pH 4.0, (Inset: increased spectral range from -0.2 to 0.4 V)

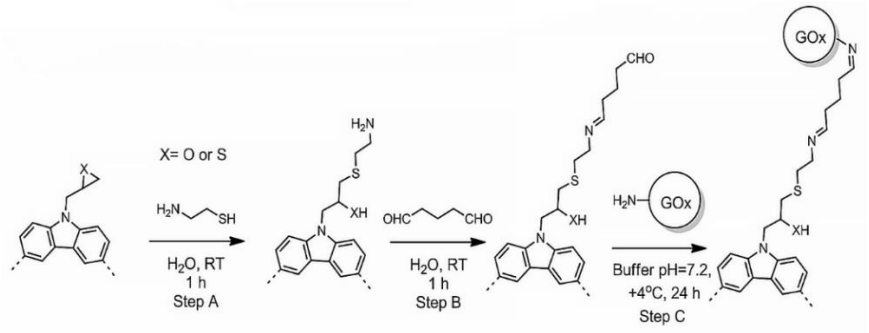

Figure 2. Schematic representation of step-by-step self-assembly-based immobilization of GOx on ITO/poly-CzO and ITO/poly-CzS electrodes.

During the verification of the polymer's chemical structure, both monomer and polymer films on ITO were analyzed using attenuated total reflection infrared (ATR IR) spectroscopy. The bending vibrations situated at 747 cm^{-1} and 749 cm^{-1} for CzO and CzS, respectively, corresponded to the vibration of carbazyl core. Moreover, the formation of polymeric carbazyl in electrochemical deposition film was approved by IR spectra in accordance with the appearance of new peaks at 826 cm^{-1} and 832 cm^{-1}, which indicated the formation of trisubstituted carbazole moieties [66]. Furthermore, the stability of oxirane and thiirane groups during electrochemical deposition was evaluated by IR. In the spectrum of CzO, medium intensive C-O bond vibration signals of oxirane group were observed at 861 cm^{-1} and 908 cm^{-1}, which correspond to scissoring and symmetric stretching of the oxirane cycle (Figure 3). After electrochemical polymerization, the peak in poly-CzO spectra shifted to the 883 cm^{-1} [67]. For CzS, a band at about 598 cm^{-1} could be attributed to C-S bond vibrations in thiirane group [68]. The corresponding band in the spectrum of poly-CzS film at 560 cm^{-1} was indicated (Figure 4). The results indicate that the successful generation of the polycarbazole films has been achieved by the polymerization of the CzO and CzS precursors. A step-by-step covalent-binding-based assembly was applied for the immobilization of GOx [69]. First, the electrodes with polycarbazole films were incubated in the aqueous cysteamine solution. At this stage, monolayer containing the amine groups was formed (Figure 2, Step A).

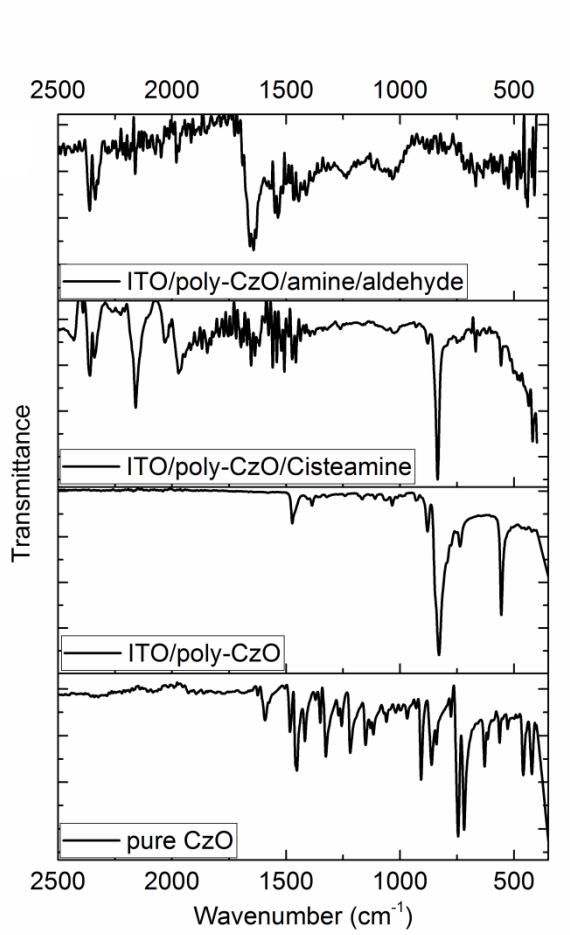

Figure 3. ATR-IR spectra of pure CzO, both deposited on ITO/poly-CzO, ITO/poly-CzO/amine, ITO/poly-CzO/amine/aldehyde.

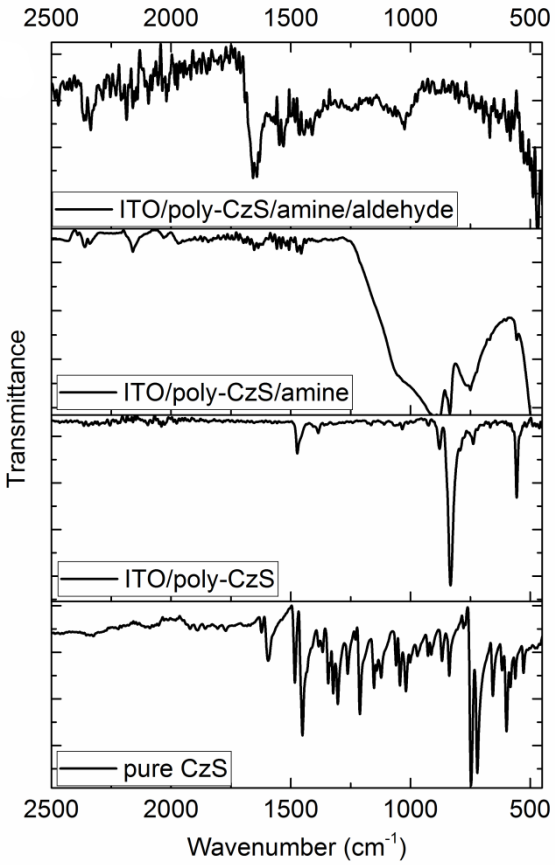

Figure 4. ATR-IR spectra of pure CzS, both deposited on ITO/poly-CzS, ITO/poly-CzS/amine, ITO/poly-CzO/amine/aldehyde.

Secondly, the free terminal amine groups were functionalized with glutaraldehyde in water (step B) via the aldehyde and amine condensation reaction to imine at a room temperature. From IR spectra of both ITO/CzS(O)/amine/aldehyde surfaces, the signal of aldehyde C=O group vibration at 1730 cm^{-1} was observed (Figure 3 and Figure 4). Finally, ITO/CzS(O)/amine/aldehyde electrodes were incubated in GOx (5 mg mL^{-1}) solution in buffer, pH 7.2, and stored for 24 hours at +4 °C temperature. It should be noted that the immobilization of GOx directly on the poly-CzO and poly-CzS surfaces does not occur because these surfaces are hydrophobic (evaluated below) and the oxiran(or thiiran)-2-ylmethyl tags are too short (only 4 Å) for imine formation reaction. Moreover, water solvation shell, which is formed around the hydrophobic side chains on the enzyme surface

that is in the range of ~10 Å, prevents the reaction with too short tags [70]. ITO/poly-CzS surface is more hydrophilic in comparison to that of ITO/poly-CzO as can be seen in Figure 5.

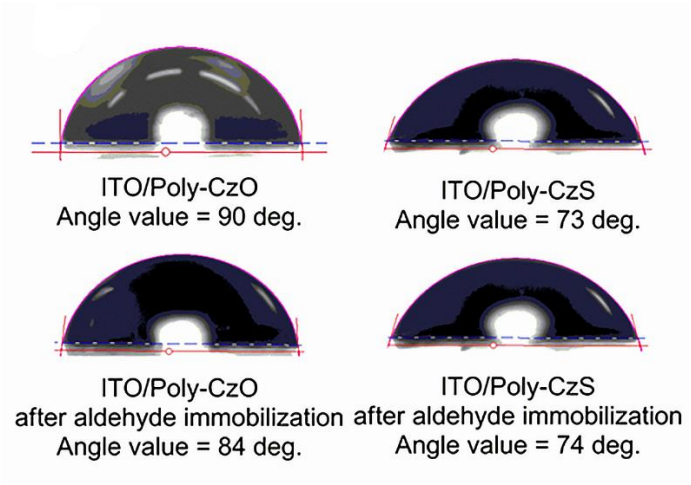

Figure 5. Water contact angle measurements of ITO/poly-CzO(S) electrode before and after the treatment with glutaraldehyde. Measurements were repeated three times, the mean values are displayed.

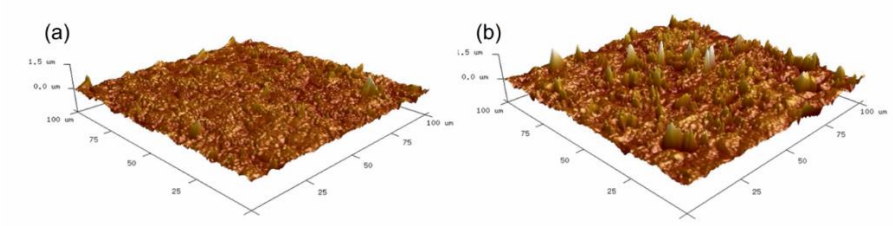

Figure 6. AFM images of (a) ITO/poly-CzS and (b) the same surface after GOx immobilization.

However, small differences of surface roughness between the immobilized and pure polymer surfaces were observed by AFM imaging (Figure 6). It should be noted that the surface wettability is significantly influenced by surface roughness [71].

4.2. Formation of poly-TPA/GOx, poly-CzEt/GOx, poly-CzPh/GOx modified electrodes

N,N,N-triphenylamine (TPA), 9-ethyl-9H-carbazole (CzEt) and 9-phenyl-9H-carbazole (CzPh) were used as starting compounds for the modification of electrodes by p-type organic semiconductor layers. The electropolymerization of CzEt and CzPh starts at around 1.1 V vs Ag/AgCl and some indications of electrochemical formation of polymer film are observed even in the first cycle of CV. This potential is sufficient for the oxidation of carbazole moiety into the corresponding radical cation [72]. After the 10th CV cycle, the onsets of anodic process of CV for these samples stabilize at 0.75 V vs Ag/AgCl. Carbazole based monomers easily oxidize, and if a substitution is present by the nitrogen atom (in our case, the phenyl and ethyl groups, respectively), it forms a bicarbazole alongside the 3,6-positions, which can oxidize further producing oligomers [73]. The oxidation of the TPA monomer was observed at a slightly lower potential of 0.9 V vs Ag/AgCl, and it functioned in accordance with other research [74,75]. In all the deposition cases, when using the three tested monomers, a saturation of current is reached before the 10th CV cycle, after which a yellow-green residue for the carbazole-based monomers and a blue-green residue for TPA could be observed in the solution around the electrodes. Considering the residue, we can assume that there is a low and finite limit to the amount of material that can be deposited on the working electrode while utilizing this system. Moreover, we can still see a clear difference in the SEM pictures of the electrochemically modified electrodes if compared to the control surface in Figure 7. All the three tested monomers produce a limited coverage of the surfaces. The surface of the electrode with deposited CzPh appears to be patchy with no visible crystallizations, and a gradient in the deposition of the material can be seen towards the edge, which implies that the oligomers are much more likely to deposit on rougher surfaces with sharp features. The surface of the CzEt modified electrode appears to have developed as a coarse film that is densely covered by small sub 100 nm crystalline particles and the overall coverage is uniform. The TPA modified electrode displays an amorphous and continuous surface coverage. This macrostructure appears as

a “hyphae-like” fractal structure, which has been observed over the electrode surface. However, all these above-mentioned surface features cannot be observed on the control electrode, where only the underlying graphite platelets can be clearly seen.

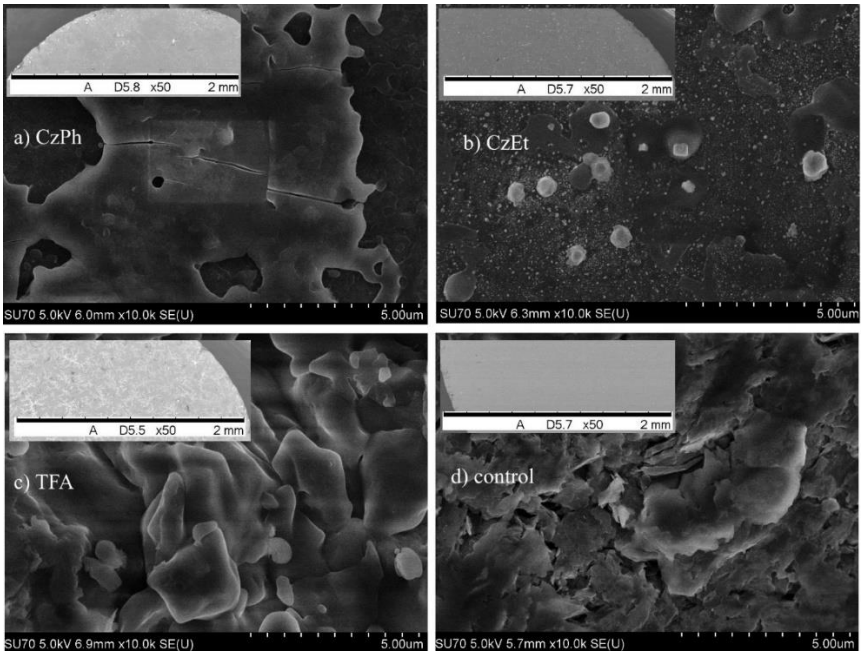

Figure 7. Scanning electron microscopy surface images of a) covered with polymer based on CzPh as a monomer; b) CzEt; c) TPA and d) graphite as control electrodes.

4.3.Electrochemical evaluation of poly-CzO/GOx, poly-CzS/GOx modified electrodes

The electrochemical experiments were carried out to verify the mechanism and efficiency of charge transfer (CT) between the GOx-cofactor and semiconducting poly-CzS or poly-CzO layers, surface-activity, and the diffusion rate coefficient. However, the CT from GOx only in ITO/poly-CzS/GOx-based electrode was observed (Figure 1c) due to a higher conductivity and lower ionization potential (5.58 eV vs. 5.24 eV) of poly-CzS. CVs illustrated that CT in ITO/poly-CzS/GOx-based electrode is quasi-reversible and surface-controlled. Moreover, any new signals in the CVs and FT-IR spectra were observed in the bare ITO electrode after the immobilization. Efficiency of charge (either electrons or holes) transfer was

estimated from the peak shape of CV. It is diagnostic of the homogeneity of the monolayer and can be evaluated by the full width at half of the peak full width at half maximum (FWHM) as described by equation 1:

$$n = \frac{3.53\ RT}{FWHM \times F} = \frac{90.6\ mV}{FWHM} \qquad (1)$$

where n is the number of charge carriers (electrons or holes), R is an ideal gas constant, T is an absolute temperature and F is a Faraday constant.

The values of FWHM can be larger or smaller than theoretical FWHM have been attributed to electrostatic effects incurred by the neighboring charged species. According to the electrochemical measurements, a quasi-reversible surface-controlled electrochemical process was observed and the full width at half of the peaks maximum heights (FWHM) were calculated to be 115 and 120 mV for the positive and negative signals of the ITO/poly-CzS/GOx system, respectively, which satisfies the one electron (or one hole) based charge transfer process. Moreover, the oxidation peaks at pH 4.0 and 7.2 registered at scan rate of 10 mV s^{-1} was observed at 181 mV and 76 mV vs Ag/AgCl (4.82 eV and 4.71 eV), what corresponds to the reversible/monoelectronic oxidation of $FADH_2$ to $FADH_2^+$. To evaluate the reversible charge transfer phenomenon in more detail, CVs at different scan rates at pH 4.0 and 7.2 were recorded (Figure 8).

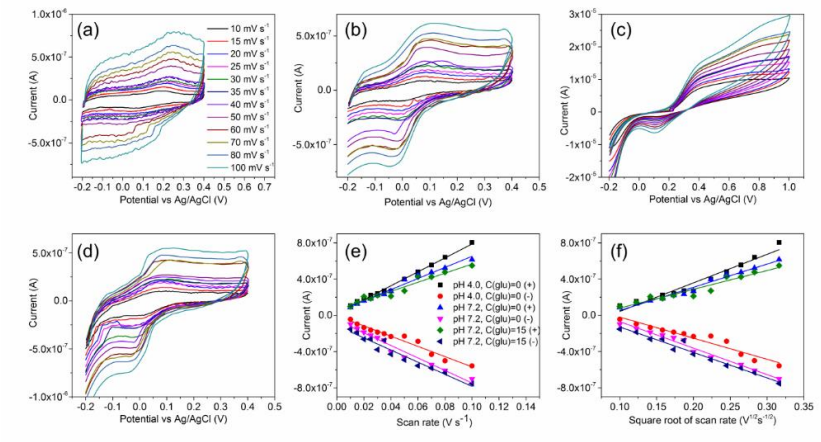

Figure 8. (a) CVs at different scan rates when pH 4.0 and C(glu)=0, (b) pH 7.2 and c(glu)=0, (c), pH 4.0 and c(glu)=15 mM, (d) pH 7.2 and C(glu)=15 mM, (d) current vs scan rate and (f) current vs square root of scan rate and the corresponding fitting lines. Scan rates in the range from 10 to 100 mV s^{-1} were used for all CV experiments.

The surface activity Γ (coverage), which in this system is the activity of the GOx immobilized on the electrode-surface, and it was determined from the slope of the line of I vs ν, using equation 2:

$$\Gamma = \frac{4IRT}{n^2F^2A}\nu \qquad (2)$$

where I is peak current, ν is potential sweep rate, A is area of the electrode. Activity of ITO/poly-CzS/GOx-surface at pH 4.0 and 7.2 without glucose were calculated from the slope of the linear oxidation current dependence vs sweep rate to be about 3×10^{-12} mol cm^{-2}. For the calculation of theoretical surface-coverage, a diameter of GOx monomer of 65 Å and a filling ratio of 0.8 were proposed. Then the theoretical surface-concentration of the GOx molecules on the surface of electrode (coverage of electrode by GOx) was calculated to be 4×10-12 mol cm-2. This value is in-line with experimental Γ value. Very similar activity of ITO/poly-CzS/GOx-electrode was observed after one month storage at +4 °C in the buffer solution. Therefore, we think that the hole-hopping-based charge-transfer from GOx to organic semiconductor protected the enzyme from oxidative damage.

In order to determine the effective diffusion-coefficient, the Randles-Sevcik equation 3 was applied:

$$I = 0.4463\, n\, A\, F\, C\sqrt{\frac{nF\nu D_{eff}}{RT}} \qquad (3)$$

where C is a concentration of enzyme on the surface. Then, Deff was estimated from the slope of linear dependency of I vs √ν in the range of scan rates of 10-100 mV s-1. The enzyme concentration within the monolayer was estimated by considering the surface-coverage and thickness (h) of enzyme (GOx) as $C = \Gamma \times h^{-1}$. This thickness consists of tag length of 15 Å and diameter of enzyme monomer of 65 Å estimated from single crystal X-ray analysis of GOx (*Aspergillus niger*) [76]. Rate constants from the diffusion coefficients data were calculated employing the equation 4. The summary of diffusion coefficients and rate constants is presented in Table 1.

$$D_{CT} = \frac{1}{6} h_{CT}^2 k_{CT} \qquad (4)$$

Table 1. Surface activity, diffusion coefficients and rate constants of ITO/CzS/GOx structure at different pHs and glucose concentrations.[a,b]

#	pH	C (gluc)/ mM	$\vec{\Gamma}$ ×10^{-12} / mol cm^{-2}	$\overleftarrow{\Gamma}$ ×10^{-12}/ mol cm^{-2}	$\vec{D}$ ×10^{-12}/ cm^2 s^{-1}	$\overleftarrow{D}$ ×10^{-12}/ cm^2 s^{-1}	$\vec{k}_{CT}$ / s^{-1}	$\overleftarrow{k}_{CT}$ / s^{-1}
1	4.0	0	3.0±0.2	2.8±0.3	1.4±0.2	3.1±0.2	70±10	150±20
2	4.0	15	77±6	25±3	25±3[b]	8.4±0.6[b]	-	-
3	7.2	0	2.5±0.3	2.8±0.2	2.7±0.3	3.5±0.3	130±20	160±20
4	7.2	15	2.1±0.2	2.8±0.2	2.7±0.4	3.2±0.3	130±20	150±20

[a] Indexes '→' and '←'indicate the anodic (oxidation) and cathodic (reduction) processes, respectively;

[b] Diffusion coefficients were calculated using Randles-Sevcik equation and C(glu)= 15 mM.

The monoelectronic oxidation and reduction CT rate-constants were calculated to be 70±10 s^{-1} and 150±20 s^{-1} at pH 4.0 and 130±20 s^{-1} and 160±20 s^{-1} at pH 7.2, respectively. For comparison, in the previous reports, the CT rates of a FAD redox system (i.e., the reduction potentials are about -0.3 V vs Ag/AgCl) were measured for electron transfer: the rate constants of 0.1 s^{-1} on a bare silver electrode [77], 0.03 s^{-1} on a short self-assembled monolayer on gold surface [78], 1.6 s^{-1} on a boron-doped carbon nanotubes modified electrode [79] and 350 s^{-1} on aminophenol nitriloacetic acid modified glassy carbon electrode [80] have been determined. Moreover, Willner et al. [81] have reported a method used to assemble a GOx monolayer on the Au electrode via reconstitution of the apo-protein with the pyrroloquinoline quinine/FAD monolayer, which yields a functionalized electrode for electrooxidation of glucose at an unprecedentedly high rate constant of about 600 s^{-1}.

The pH influence on the rate-constants of ITO/poly-CzS/GOx structure at pH 4.0 and 7.2 was investigated and compared. First, the surface-activities for oxidation and reduction at pH 7.2 and 4.0 are very similar, i.e., about 3×10^{-12} mol cm^{-2}. Secondly, considering the influence of glucose on the charge transfer, ITO/poly-CzS/GOx-electrode at pH 4.0 and 7.2 was investigated employing a relatively high glucose concentration of 15 mM. The oxidation and reduction rate constants at pH 7.2 were estimated as being

statistically of the same value with that one registered in a similar system without glucose (Table 1, entry 3 and 4) because this is a charge (hole) transfer process from the HTPS to the cofactor. However, for a system with glucose at pH 4.0, a new irreversible peak at about 800 mV was observed (Figure 9c). The first signal at about 180 mV (onset) exhibits oxidation of the cofactor to the radical cation via holes from the organic semiconductor. The second signal at about 800 mV can be assigned to the oxidation of the FAD-glucose complex to gluconic acid and FAD (see below). According to [82], the second order rate constant of glucose oxidation in the presence of GOx is about 3×10^4 $M^{-1}s^{-1}$. Therefore, the pseudo-first order rate constant at 15 mM of glucose of this process was calculated to be 450 s^{-1}. The lower k_{CT} of reduction process at pH 4.0 than oxidation of glucose suggests that glucose can moderate the CT kinetics in the enzyme. Recently, Bartlett and Al-Lolage [83] have analyzed the scientific papers, which reported electrochemical biosensors based on glucose oxidase (GOx), that were purified by different suppliers from different GOx-producing microorganisms. They have predicted that the redox peaks in cyclic voltammograms, which are usually attributed to charge transfer of GOx sometimes arise from free FAD, and possibly from catalase and/or other impurities, which are present in the as supplied commercial enzyme that are also adsorbed at the electrode's surface. It was reported, that in the case of immobilized catalase, a more negative obvious catalytic reduction peak is observed [84] when compared to that observed in our recent research. Free FAD has been washed out by a tough washing procedure of GOx-modified electrodes. Moreover, the possibility that some free FAD cofactor is released from the slowly dissociating GOx and can be oxidized/reduced on the electrode's surface cannot be excluded, because the cofactor – FAD – binds with apo-GOx non-covalently, therefore this binding is relatively weak and holo-GOx tends to dissociate slowly into apo-GOx and FAD.

Volt-amperometric behaviour of ITO/poly-CzS/GOx-electrode was investigated by cyclic voltammetry in potential range from -200 mV until +1000 mV in the presence of different glucose concentrations (1-15 mM) in buffer, pH 4.0, and containing dissolved oxygen (Figure 9a). After addition of glucose, the difference of current for the oxidation (at 800 mV) peaks was calculated. A broad linear relationship of the peak-current density and glucose concentration from 2 to 15 mM was observed (Figure 9a, inset); with correlation coefficient of 0.982 for the oxidation currents. Moreover, from the slope of linear fitting, the sensitivity to glucose is estimated to be 0.64±0.03 $\mu A\ mM^{-1}\ cm^{-2}$. According to [85], the second-order rate constant for oxidation of $FADH_2$ in GOx by oxygen at low pH was estimated to be $1.6 \times 106\ M^{-1}\ s^{-1}$. Therefore, the pseudo-first order oxidation rate constant at ~0.2 mM of O2

dissolved in water was calculated to be ~300 s-1. This rate constant is a little higher but of the same order of magnitude as that for $FADH_2$ oxidation by CzS. In this case, the sensitivity of ITO/poly-CzS/GOx-electrode is average because oxygen competes with CzS in the oxidation of $FADH_2$.

Based on the obtained results, the mechanism of glucose oxidation via holes and without involvement of dissolved oxygen was proposed (Figure 9b). First of all, holes from the electrode in reversible way oxidize the $FADH_2$ cofactor into radical cation – $FADH_2^+$.

Therefore, the oxidation and reduction peaks are observed in the CV at around +400 mV and +100 mV, respectively (Figure 8a). A second step is a nucleophilic addition of glucose to this radical cation ($FADH_2^+$) and the formation of transition state (TS). Recently, similar TS of the FAD-glucose complex has been successfully identified using a mass spectrometry [86]. Finally, the formed TS is oxidized by second hole from the electrode to form initial $FADH_2$ and gluconic acid.

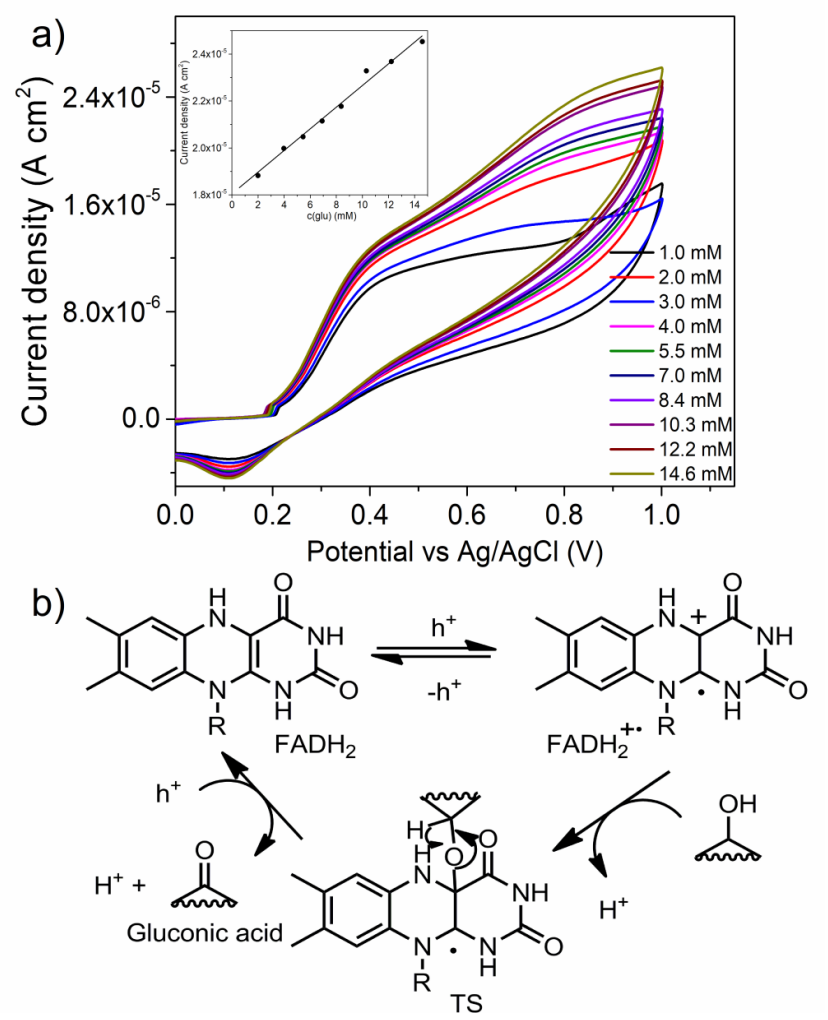

Figure 9. (a) Dependence of electrode current on glucose concentration. CVs of ITO/poly-CzS/GOx electrode in the absence of glucose at a scan rate of 50 mV s^{-1} (Inset: current vs glucose concentration dependence at +800 mV). (b) Proposed mechanism of glucose oxidation via holes.

4.4. Electrochemical evaluation of poly-TPA/GOx, poly-CzEt/GOx, poly-CzPh/GOx modified electrodes

The resulting electrodes were modified with a thin layer of immobilized GOx by cross-linking with glutaraldehyde, and they were tested for the response towards glucose; the measurement results are presented in Figure 10. By adding glucose to the PBS solution, we can observe a

continuously increasing overall current response in all the tested electrodes. Starting with the glucose concentration of 0.50 mM and higher for the CzPh-based polymer (poly-CzPh) modified electrode, 1.0 mM and higher for the CzEt-based polymer (poly-CzEt) modified electrode, a continuously increasing and defined oxidation peak-based sensor response has been observed in the voltammograms at a potential of around 0.15 V vs Ag/AgCl. The response saturates at higher concentrations of glucose. A peak response could also be seen while using the polymerized TPA (poly-TPA) modified electrode, however, the characteristics of the electrode were different. The oxidation peak observed in CVs was significantly more diffused and less defined, therefore, the overall signal-to-noise ratio was lower and proportional potential drift vs the concentration of glucose was observed. Unfortunately, chronoamperometry method did not provide substantial information during the attempts to evaluate the variation of current density vs glucose concentration because too high of a noise level of the current was observed.

The obtained measurement data at the peak position of 0.15 V vs Ag/AgCl was used to produce the data presented in Figure 11. Responses of both the poly-CzPh/GOx and poly-CzEt/GOx electrodes appear to be saturated at around 5 mM concentration of glucose. While the current density of the poly-TPA/GOx electrode was continuously increasing alongside with the increasing glucose concentration, we could not obtain enough data points for a calibration curve. Unexpectedly, a characteristic peak of the poly-TPA/GOx electrode displayed a significant potential drift while reacting to glucose concentrations. By increasing the glucose concentration from 0.5 to 14 mM, we measured a 15 mV difference in the observed potential of the CV oxidation peak. However, the peak's position could not be identified accurately at lower concentrations than 0.5 mM for all the electrodes. As it can be seen in Figure 10, the current response to different concentrations of glucose for the poly-CzEt/GOx, poly-CzPh/GOx and poly-TPA/GOx electrodes appear to be parallel, thus, the largest measurable difference in this area would always be at the observable peak. Moreover, the preliminary tests on possible interfering species, such as ascorbic acid, uric acid, lactose, sucrose, and hydrogen peroxide, indicate that the combined choice of GOx as a specific catalyst as well as a low working potential of 0.15 V did not display any signal towards the presence of these interfering materials.

The limits of detection (LOD) were determined from the low concentration linearity range of the calibration curves according to Equation (5):

$$LOD = \frac{3.0\,\sigma}{slope} \qquad (5)$$

where σ is the standard deviation of the response. The average sensitivities were estimated as the slope of the current density vs glucose contraction which was determined from calibration curves. Values of LOD of 240 and 230 μM by taking signal to noise ratio of 3.0 and the average sensitivities of 3.3 and 3.7 μA cm^{-2} mM^{-1} of the biosensors based on poly-CzEt and poly-CzPh active layers were calculated, respectively.

By taking the difference in current density at the observed peak voltage and the base current density (J0 is current density at 0 mM glucose), we have determined the electrode's sensitivity to glucose. The resulting calibration curve follows the dependency of Michaelis-Menten kinetics. The Michaelis constants (KM) values have been calculated by employing the Lineweaver-Burk approach (Equation 6) [87,88]:

$$\frac{1}{J} = \frac{1}{J_{max}} + \frac{K_M}{J_{max}C} \qquad (6)$$

where J_{max} is the maximal current density and C is the concentration of glucose. Figure 11b shows a linear dependence for all the substrate concentration points of all the electrodes. Moreover, the Michaelis constants have been estimated to be 1.1, 2.0 and 1.4 mM for poly-CzPh/GOx, poly-CzEt/GOx poly-CzEt and poly-TPA/GOx electrodes, respectively. These constants are one level of magnitude higher than Michaelis constant of native GOx, which is around 0.3 mM with respect to dissolved oxygen[89] and it indicates that the maximum rate in our case has been achieved at a higher substrate concentration.

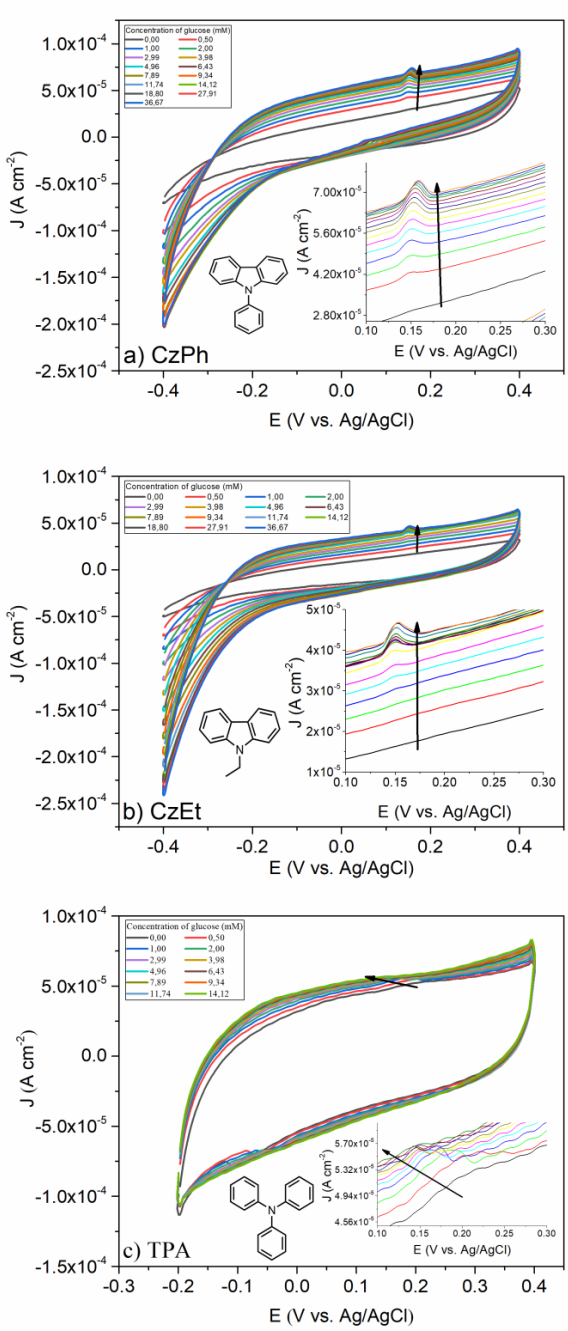

Figure 10. Cyclic voltammograms of a) poly-CzPh, b) poly-CzEt, c) poly-TPA covered electrodes modified with cross-linked GOx at different concentrations of glucose in a PBS solution, 7.2 pH at scan rate of 30 mV s^{-1}

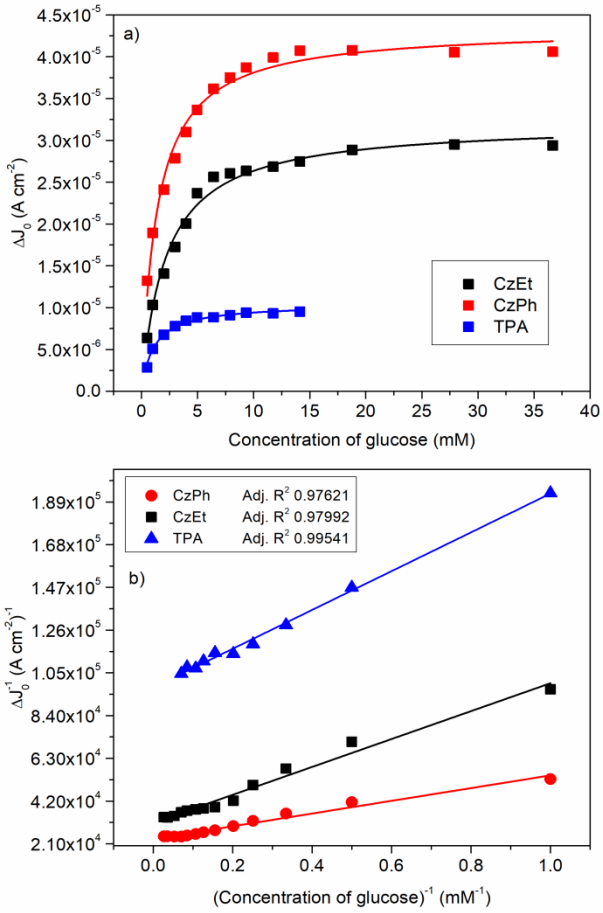

Figure 11. The dependence of the poly-CzPh/GOx, poly-CzEt/GOx and poly-TPA/GOx electrodes of current density on the concentration of glucose in solution at 7.2 pH: a) calibration curve, b) regression analysis.

To study the activity of GOx on the electrode surfaces, the activity Γ (coverage) has been determined from the slope of the line of I vs ν, by using Equation 3:[75]

$$I = \frac{n^2 F^2 A \Gamma}{4RT} \nu \qquad (7)$$

where n represents the number of charges involved in the reaction, A (cm^2) is the electrode area, F is the Faraday constant, Γ (mol cm^{-2}) is the surface density/activity of reactant species, ν (V s^{-1}) is the potential sweep rate, R is the ideal gas constant, and T is the absolute temperature. To calculate a

charge number, the peak shape of CV has been evaluated. It represents the homogeneity of the layers which can be evaluated by the full width at half of the peak's full height (FWHM) as described in equation 1[90]

In this case, n is estimated to be around 1 for all the electroactive materials. We can calculate the surface density of the reactant species by using the current measurement value in the expected peak position at 0.15 V vs Ag/AgCl. As compared to the result obtained in our previous work, the obtained surface density is in the order of 10^{-9}-10^{-10} mol cm^{-2}, which is significantly larger (by three orders of magnitude) if compared with that calculated for the monolayer of GOx (i.e., around 10^{-12} mol cm^{-2}). Such a large increase can be justified by the fact that when utilizing a different immobilization method, i.e. by crosslinking the adsorbed GOx molecules on the surface, we no longer produce a structured surface monolayer of GOx, and dense unordered agglomerates of GOx on the electrodes' surface are produced instead.

Table 2. Comparison of the three produced amperometric glucose biosensors with data available in literature.

Active layer	Linear range, mM	Average sensitivity, μA cm^{-2} mM^{-1}	LOD, μM	Γ $\times 10^{-10}$, mol cm^{-2}	K_M, mM	Ref.
Poly-CzEt/GOx	1-5	3.3	240	3.5	2.0	This work
Poly-CzPh/GOx	2-5	3.7	230	3.7	1.1	This work
Poly-TPA/GOx	-	-	-	19	1.4	This work
PEDOT-NFs/GOx	0-5	6.4	260	-	-	[8]
PEDOT/GOx	0-10	9.24	100	-	11.6	[12]
Poly-2,2'-BT/GOx	0.09-5.2	-	30	-	-	[9]
Poly-4,4'-bBT/GOx	0.15-5.2	-	50	-	-	[9]

SBEDOT/GOx	1-20	12.6	-	-	-	[11]
Poly-SNS-NH_2/GOx	1-10	2.7	903	-	-	[13]
PPX-GOx	3-8	-	-		66	[14]
Poly-CzS/GOx	2-15	0.46	240	0.03	-	[20]

Abbreviations: NFs: nanofibers; 2,2'-BT: 2,2′-bithiophene; 4,4′-bBT: 4,4′-bis(2-methyl-3-butyn-2-ol)-2,2′-bithiophene; SBEDO: sulfobetaine-3,4-ethylenedioxythiophene; SNS-NH_2: 4-(2,5-di(thiophen-2-yl)-1*H*-pyrrol-1-yl)aniline; PPX: β-(10-phenoxazinyl)propionic acid; CzS: 9-(thiiran-2-ylmethyl)-9H-carbazole.

The obtained analytical parameters of the designed biosensor based on the carbazole derivatives bio composite have been compared with some other GOx-based glucose biosensors reported previously, where a linear range of current – concentration was determined at a positive potential vs Ag/AgCl, and the data are presented in table 2. The determined linear range, sensitivity, and detection limit values for the poly-CzEt/GOx and poly-CzPh/GOx-based biosensor remained at a similar level to the other electrochemical approaches described in the literature (see Table 2). By comparing our prepared biosensors, it has been found out that the carbazole-based electrodes have a higher sensitivity than the triphenylamine-based electrode because these electropolymers have a more conjugated aromatic system and, as a result, charge carrier mobilities in these electropolymers are higher than in poly-TPA. Moreover, the limit of detection (LOD) shows the minimum amount of analyte that can be detected by biosensors. These values of LOD are equal to the concentration of oxygen in air-saturated aqueous solution of around 200 μM. Therefore, oxygen molecules compete in the oxidation of reduced cofactor ($FADH_2$) by the charge carrier (hole) from the electrode in/to GOx. Although these third-generation biosensors, based on the hole injecting/transporting materials, have excellent stability, they have a low sensitivity and a medium linear range because charge tunneling toward the electrode is a limiting step of overall process in these biosensors.[91]

4.5. Assessment of Cytochrome c and Chlorophyll a as natural redox mediators for EBFCs powered by glucose

4.5.1. Determination of power density

The stability of current, the maximum value of the power output, and a large electromotive force are three key features of the biofuel cell [92]. In this study, firstly an attempt was made to determine a system that generates sufficient power for the biofuel cell. Hence the power and surface power density of the biofuel cell were calculated using Ohm's law and power calculation formula based on the surface area of the graphite electrode. The whole-cell OCP was calculated via the following equation 9:

$$OCP = (E_k\text{-}E_{ref})\text{-}(E_a\text{-}E_{ref}) \qquad OCP = \frac{(E_k - E_{ref})}{(E_a - E_{ref})} \qquad (9)$$

where E_k is a potential value of the cathode, and E_a is a potential value of the anode.

The power density of EFC was calculated according to equation $P = U^2/R$ and dividing it by the geometric surface area.

The results of the power density calculations are presented in Figure 12. The highest power density was generated by the system $EBFC_{CA}$. The surface power density of this system is about 2500 – 4000 nW/cm^2 (Figure 12). While the power density values generated by the other systems $EBFC_{CC}$, $EBFC_{ChV}$, and $EBFC_{Hep}$ were about 10 times lower. As expected, the power density generated by the system without any redox mediator was the lowest. Some differences were observed between the values of the carbon composite resistor load used to obtain the maximum power density. The maximum power density generated by the system with redox-mediated by Chlorophyll a was registered at a biofuel cell potential of 125 mV. The power density has succeeded the comparably high value in the system employing heparin, with a potential of 35 mV. The potentials generated by other biofuel cells $EBFC_{CC}$ and $EBFC_{ChV}$, based on cytochromes and the supernatant of ultrasonically disrupted *Chlorella vulgaris* cells, were rather similar, but the potential of $EBFC_{CC}$ was 80 mV and of $EBFC_{ChV}$ was 143 mV.

In a similar system with a substrate of redox-mediated Chlorophyll a, a power density of 2397 nW/cm^2 was reached using a mix of water treatment sludge and fruit juice effluent 3:1 [93]. In another study, the peak power densities were compared in different seasons of the year and the power density value of

5700 nW/cm^2 was achieved in spring and only 110 nW/cm^2 MBFCs in summer using biomass with the Chlorophyll a in the microbial fuel cell [94]. The biofuel cell system generated a power density of 1510 nW/cm^2 at a glucose concentration of 20 g/l in the synthetic wastewater [95]. Biofuel cell technology is used for wastewater bio-depuration using *Chlorella vulgaris* and bio-electrogenic activity has increased from 2317 nW/cm^2 to 32767 nW/cm^2 [96].

In conclusion of power density evaluation, it can be noted that Chlorophyll a substrate in $EBFC_{CA}$ is the best choice of the assessed redox mediators used to construct the EBFC.

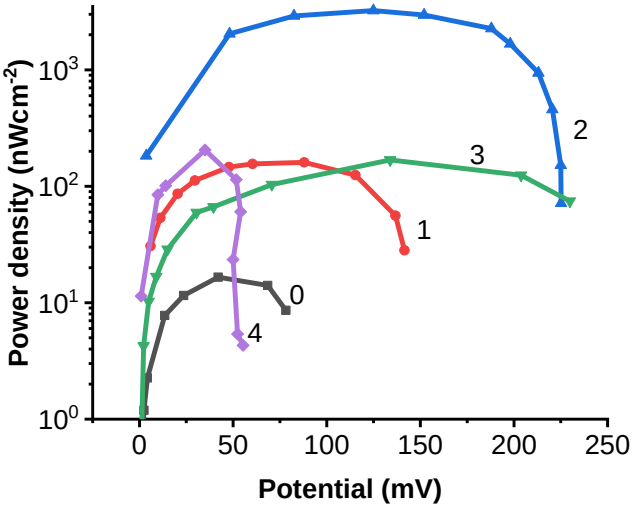

Figure 12. The dependencies of the maximum power density on the potential when the system is: 0 – control of the study, 1 – $EBFC_{CC}$; 2 – $EBFC_{CA}$; 3 – $EBFC_{ChV}$; and 4 – $EBFC_{Hep}$.

Glucose is considered an ideal ecological fuel for direct-type biofuel cells. An advantage of glucose is that it can be produced in abundance from both natural plants and industrial processes. The effect of glucose concentration on the system power density and the electromotive force was measured by adding a certain amount of glucose to here evaluated five systems. Increasing glucose concentration from 0,10 and 100 mM (Figure 13), has decreased biofuel cell potential, and in the case of a biofuel cell based on chlorophyll, by increasing the glucose concentration to 100 mM, the system hardly generates power – the surface power density is very close to 0 nW/cm^2. When cytochrome c was used as the redox mediator in the $EBFC_{CC}$ system (Figure 13), the power generated increased with increasing glucose concentration. Although the maximum power density is lower than in $EBFC_{CA}$ or $EBFC_{Ch}$ systems and reaches about 160 nW/cm^2, the signal of this system increases when the amount of glucose in the electrolyte solution has increased, and such a system was much more stable.

Control of the study was performed only with a polished graphite electrode – the maximum surface power density was 24.71 nW/cm^2 in the absence of glucose in the system. Increasing glucose concentration reduces the power density of a biofuel cell. It can be argued that these redox mediators increase the efficiency of biofuel cells because they generate much higher maximum surface power.

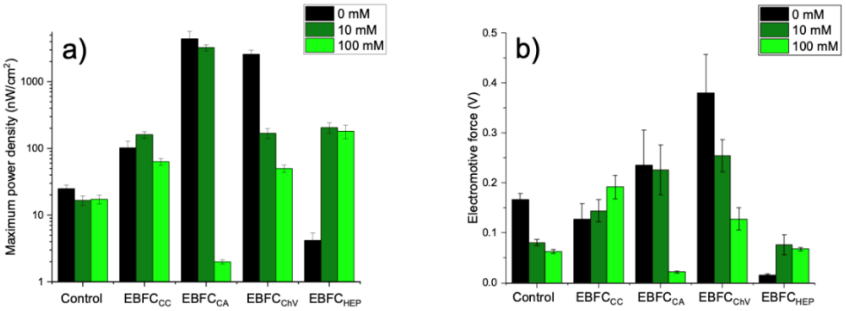

Figure 13. Dependences at different glucose concentrations of a) the electric power; b) the electromotive force. 0 – control of the study; 1 – $EBFC_{CC}$; 2 – $EBFC_{CA}$; 3 – $EBFC_{ChV}$; 4 – $EBFC_{Hep}$.

Figure 13 compares the power density (Figure 13A) and electromotive force (Figure 13B) of all biofuel cells at a glucose concentration of 10 mM in the solution. The voltage decrease usually is registered when the load of the external circuit increases [97]. Although the power density of such biofuel cells is usually reported in terms of the active surface area of the electrode, rather than volume, as it is often the case for many other energy sources because more advanced calculations are not possible due to problems related to active surface calculation in the entire volume of the electrode.

4.5.2. Cyclic voltammetry-based evaluation of mediated EBFCs

During the evaluation of the cyclic voltammetry results, the focus was on the value of the potential at which oxidation peak is observed in the cyclic voltammogram (CV). During this experiment the potential was changed in a rather broad range of the potential values, i.e., the potential was changed from -1.5 V to +1.5 V at the scan rate of 50 mV/s (Figure 14). The potential cycling in such a broad range of electrode potentials required very careful removal of dissolved oxygen by degassing the electrochemical system with a nitrogen stream. It was observed that in the system without any redox mediator (Figure 14A) no clearly distinguished oxidation peak was observed. However, in this system, it was followed by a slightly expressed current density increase at the potential value of 1.1 V. The current density changes correspond to the linear correlation with R^2=0.95 and y=0.11x + 1.85. The current density was rather different in the evaluated EBFC systems. In the $EBFC_{CC}$ (Figure 14B), it was observed a shift in the oxidation peak potential value. The observed potential value was shifted to higher potential values with increased glucose concentration. The potential values were shifted from 0.63 V to 0.77 V.

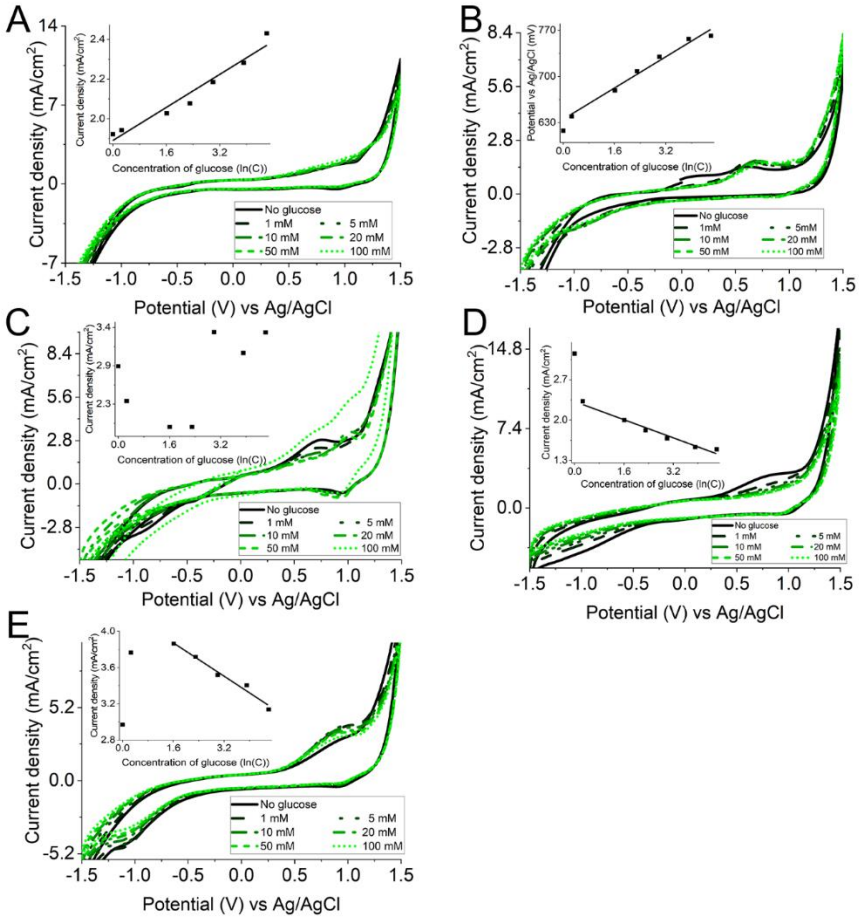

Figure 14. Cyclic voltammograms when the working electrode is A. control of the study; B. $EBFC_{CC}$; C. $EBFC_{CA}$; D. $EBFC_{ChV}$; and E. $EBFC_{Hep}$.

Meanwhile no current density dependence on glucose concentration was observed in this system. Such a shift of the potential value was not observed in any other evaluated system. During potential cycling at the increased glucose concentrations, the drop in current density was observed in the $EBFC_{CA}$ (Figure 14C) and $EBFC_{Hep}$ (Figure 14E). No current or potential dependencies were observed in $EBFC_{ChV}$.

Some researchers [92] revealed the occurrence of ineligible reactions – parasitic O_2 reactions. The scientific group described that depending on the experimental conditions, parasitic reactions may appear when using redox mediators of extremely negative or positive redox potentials. O_2 reduction at redox polymers, which is observed at low potential bioanodes, or the oxidation

of some other electroactive species, which are observed at high potentials applied at biocathodes, are objectionable effects.

Table 3. The summary of values of the potential at which occurs oxidation on $EBFC_{CC}$, $EBFC_{CA}$, $EBFC_{ChV}$, and $EBFC_{Hep}$ electrodes.

Name of the system	The value of the potential at which occurs oxidation, V
The control of the system	1.1 V
$EBFC_{CC}$	0.6 V
$EBFC_{CA}$	0.8 V
$EBFC_{ChV}$	0.9 V
$EBFC_{Hep}$	0.9 V

The values of the potential at which occurs oxidation in all evaluated systems $EBFC_{CC}$, $EBFC_{CA}$, $EBFC_{ChV}$, and $EBFC_{Hep}$ are summarized in table 3. According to the data displayed in table 3, the value of the potential at which occurs oxidation was decreased in all systems.

4.5.3. Chronoamperometry-based evaluation of mediated EBFCs

The characteristics of the electrochemical system as a second-generation biosensor were investigated by chronoamperometry. $EBFC_{CC}$, $EBFC_{CA}$, $EBFC_{ChV}$, and $EBFC_{Hep}$ responded to changes in glucose at a steady state. This effect is well seen from the graphs (Figure 15) that when using an $EBFC_{ChV}$, a constant drop in current is observed, and the equilibrium of the system is difficult to stabilize. Using an $EBFC_{Hep}$, a constant increase in current is observed. Such systems are not considered stable enough to develop a biosensor.

The electrodes $EBFC_{CA}$ and $EBFC_{CC}$ were suitable for the development of EBFC. It was determined that by increasing the glucose content in the system, the current density increases, and the equilibrium is reached quickly. Due to the highly variable base levels, it is difficult to assess and compare the systems directly from the data of the chronoamperometry. Measurement results, which are presented in Figure 16, are based on the data presented in Figure 15 because by measuring the change in current density we can more easily compare the efficiency of the tested systems. All the tested systems react to the addition of glucose, gradually increased glucose concentration increases the observed change in current density by nearly an order of magnitude, with the highest overall increase observed in the $EBFC_{CC}$, when saturated with

glucose it displayed a 15× times increase in change of current density compared to the control system. The $EBFC_{ChV}$ also displays a large relative change of current, over an order of magnitude, but appears to saturate quickly, offering a decreased response range saturating at 20 mM/L of glucose, whereas all the other tested systems displayed a change in current density throughout the tested 0 – 100 mM/L glucose range.

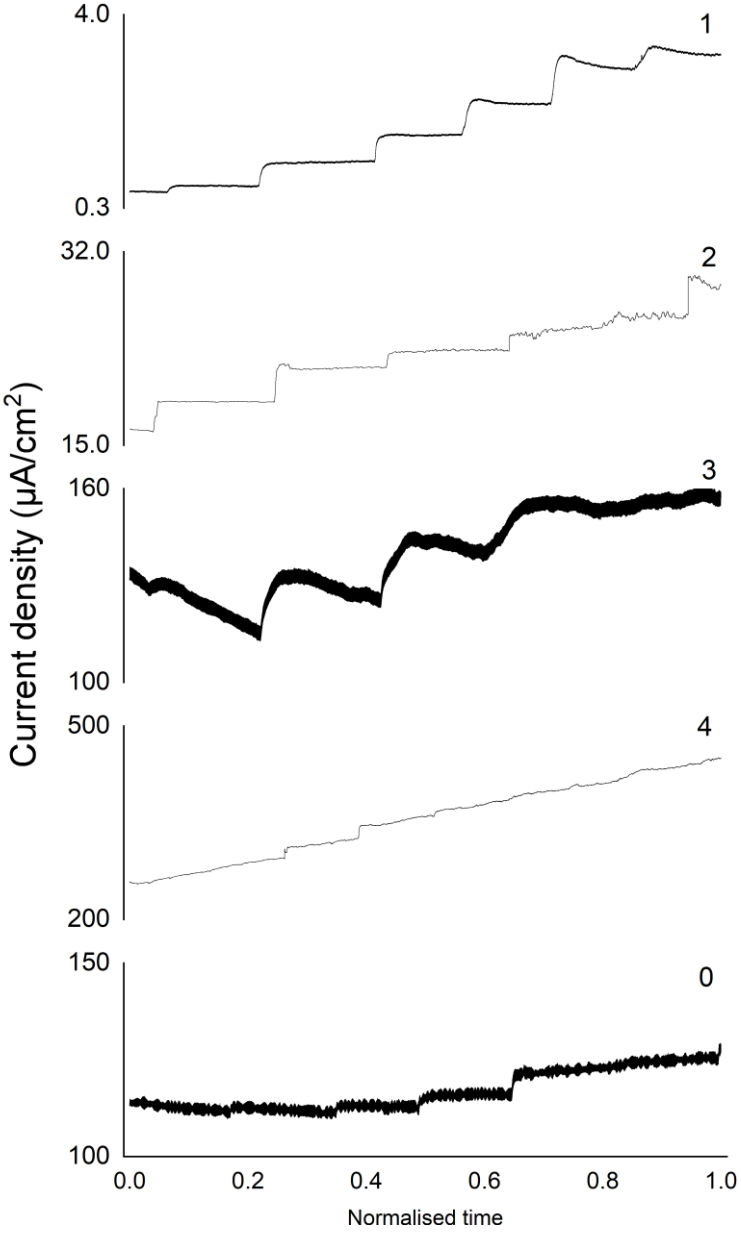

Figure 15. Chronoamperometry data on: 0 – control of the study; 1 – $EBFC_{CC}$; 2 – $EBFC_{CA}$; 3 – $EBFC_{ChV}$; and 4 – $EBFC_{Hep}$ electrodes.

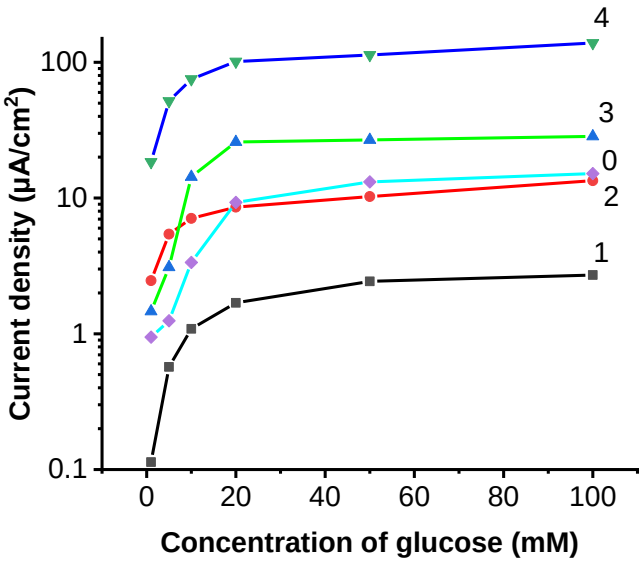

Figure 16. Current density dependency on glucose concentration. ΔJ, log10($J_i - J_0$) from the concentration of glucose, where J_i – current density is measured after the addition of glucose, and J_0 – current density is measured at the start of the experiment. 0 – control of the study; 1 – $EBFC_{CC}$; 2 – $EBFC_{CA}$; 3 – $EBFC_{ChV}$; and 4 – $EBFC_{Hep}$.

All samples follow expected Michael-Menten kinetics curves. Displayed as such, $EBFC_{Hep}$ and 'Control' samples represent an inaccurate view due to the nature of their response as seen in the chronoamperometry data. Both $EBFC_{Hep}$ and 'Control' samples do not reach equilibrium and continuously increase.

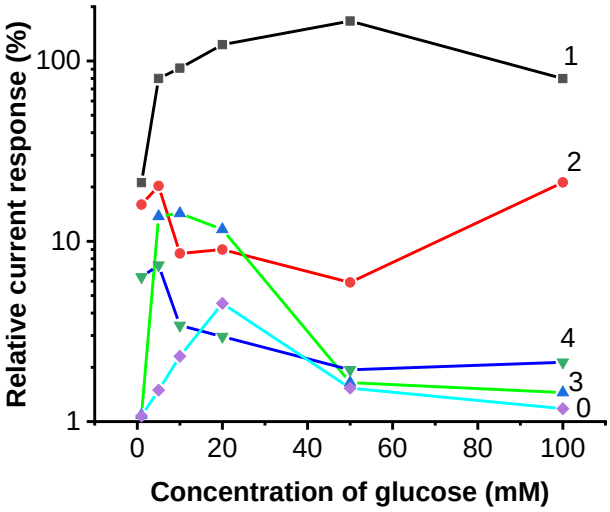

Figure 17. The dependence of relative change in current density from glucose concentration. 0 – control; 1 – $EBFC_{CC}$ – the system with Cytochrome c substrate; 2 – $EBFC_{CA}$ – the system with Chlorophyll a substrate; 3 – $EBFC_{ChV}$ – the system with the supernatant of ultrasonically disrupted *Chlorella vulgaris* cells substrate; 4 – $EBFC_{Hep}$ – the system with heparin.

The relative change in current density was calculated according to equation 10:

$$log10\,\frac{J_i - J_{i-1}}{J_0 * 100\%} \qquad (10)$$

where J_i – current density after the addition of glucose, J_{i-1} – current density before the addition of glucose, and J_0 – current density measured at the start of the experiment.

The application of cytochromes in the $EBFC_{CC}$ produced the greatest relative current response to the further increase of glucose concentration. Also, it was observed from the Figure 17 that the system retains a high amount of sensitivity throughout the assessed concentration range, displaying the increase of registered current up to 50 mM of glucose, with further increases gradually lowering the current response rate. Increasing glucose concentration from 20 mM to 50 mM we observed a 167% increase in registered current, by further increasing the concentration by 50 mM we observed an increase of 80%, and the response rate follows a bell-shaped curve over the entire tested

concentration range. The high relative sensitivity suggests a possibility for further iterative improvement, as the system is currently held back only due to small absolute signal current values.

$EBFC_{CA}$ also produced a relatively linear current response to the increase of glucose throughout the range.

$EBFC_{ChV}$ displayed a strong response in the lower boundaries of the concentration range and plateaus at concentrations above 20 mM. $EBFC_{Hep}$ and control samples had a relatively low response to noise ratio and both samples reacted strongly in a very limited concentration range in the lower boundaries of the tested range.

4.6. Assessment of *Rhizobium anhuiense* bacteria as a potential biocatalyst for microbial biofuel cell design

Zeta potential measurements were performed to evaluate the electrical potential of the cell surface, which depends on environmental conditions [98]. The surface of the majority of gram-negative bacteria at neutral pH is mostly negatively charged. This effect is predetermined by negatively charged phosphate and carboxylate groups containing lipopolysaccharides [39] and balanced by oppositely charged counter ions present in the surrounding media, leading to the formation of the electrical double layer.

Menadione (MQ) is a redox cycling compound, with the empiric $C_6H_4(CO)_2C_2H(CH_3)$ formula, it is also known as a vitamin K_3, and it's an analog of 1,4-naphthoquinone having additional methyl group. Menadione is a prooxidant generating superoxide anion radicals. *Rhizobia* exposed to menadione responds by inactivation of free anion radicals generated by this exposure [62]. The optical density growth curve (Figure 18) was used to assess the doubling period and to check whether bacteria remained metabolically active.

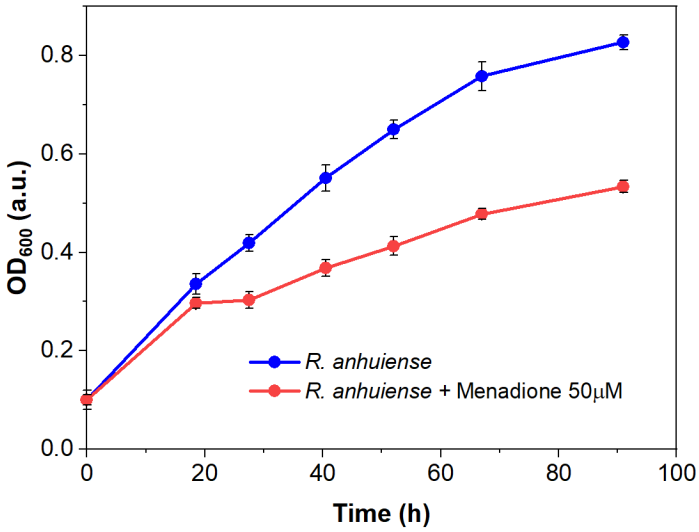

Figure 18. Growth curve optical density (OD) values of *Rhizobium anhuiense* bacteria in Norris medium with or without Menadione.

In this research at low concentration menadione acts as a stressor, therefore, it did not kills the bacteria but strengthens their resistance and increases their charge-transfer efficiency after the adaptation period. At ion

concentration below 1 mM, the zeta potential was independent of ionic strength (Figure 19A), and the bacteria displayed minor variation of zeta potential in the presence of menadione, and this effect was not dependent on the duration of incubation. When ion concentration exceeded 1 mM, then the zeta potential of all samples increased together with increasing ionic strength. No meaningful difference in zeta potential was observed between the presence or absence of various mediators and the duration of incubation. The influence of pH on the zeta potential of *Rhizobium anhuiense* was assessed. Considering that a natural living environment of the bacteria is ~pH 7.0, and due to metabolic processes and secretion of various metabolites the pH is often changed to the acidic side, further investigations in pH range between 5.0 and 8.0 were performed. The research revealed that these pH alterations have not significantly influenced the zeta potential of the bacteria. Zeta potential remained negative over a wide pH range (Figure 19B). This reveals that the variation of pH does not influence electrostatic interactions between the bacteria and anode. The influence of the cultivation medium on the zeta potential of bacteria was also evaluated (Figure 19C). A Norris medium, pH 7.0, 25g/L glucose, also positively influenced zeta potential. The average zeta potential of bacteria increased to –25 mV compared to an average zeta potential of bacteria, which is –60 mV in PBS-based solutions with low ionic strength. This phenomenon is observed most likely due to the presence of different dissolved ions in PBS and Norris medium.

Bacterial cells with inherent negative charges are more favorable to adhere and subsequently immobilize to the positively charged electrode due to the electrostatic attraction. In this research, we observed a highly negative zeta potential in solutions with low ionic strength. Observation suggests that *Rhizobium anhuiense* possesses the inherent ability to adhere strongly to the surface of the anode.

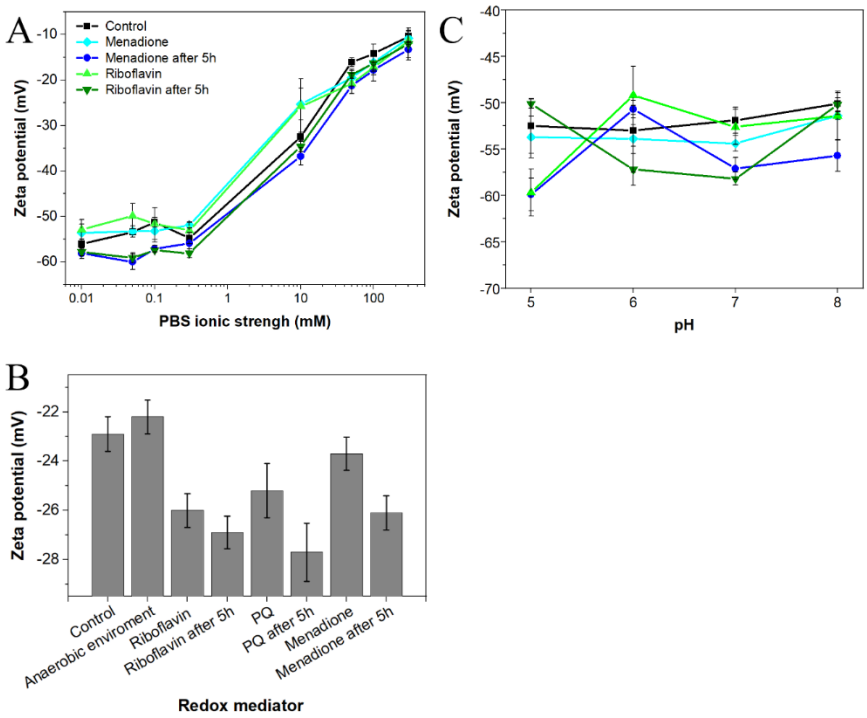

Figure 19. Zeta potential (mean ± SD) of *Rhizobium anhuiense* at mid-logarithmic phase: A) Zeta potential as a function of ionic strength; B) Zeta potential measured in 0.1 mM PBS as a function of pH; C) Zeta potential in growing Norris medium, pH 7.0. Measurements were performed in PBS, pH 7.0, the presence of several redox mediators (5 mM of menadione, 0.2 µM of riboflavin, and 4 mM of 9,10-phenanthrenequinone) and at anaerobic conditions.

Open circuit potential (OCP) was determined at loads of external circuits and power density was calculated using these measurement results.

Power density curves and polarization were gathered for BFC based on a *Rhizobium anhuiense* bacteria, which were treated with several redox mediators in different environments, (Figure 20 and Figure 21).

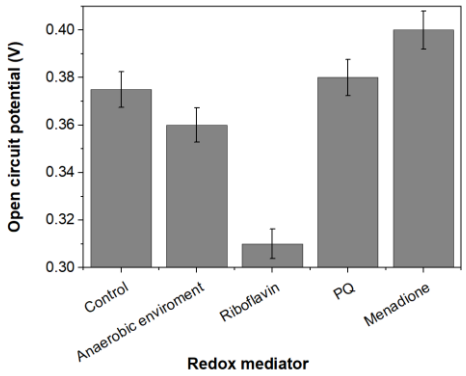

Figure 20. The dependence of capabilities to generate an electrochemical potential of *Rhizobium anhuiense* in 0.1 mM PBS, pH 7.0, the presence of several redox mediators (5 mM of menadione, 0.2 µM of riboflavin, and 4 mM of 9,10-phenanthrenequinone) and at anaerobic conditions.

Menadione is serving as an organic hydrophobic redox mediator enhancing charge transfer [53,54]. The efficiency of redox mediators at large extent depends on the oxidation and reduction potentials of the applied redox mediator. Redox mediators with a higher redox potential will more efficiently capture electrons from electron donors, however, electron transfer from redox mediators, which are characterized by a very high redox potential, to the charge transfer chain is not very efficient [99]. Electrical potential and power density of here designed MBFC is displayed in Figure 21.

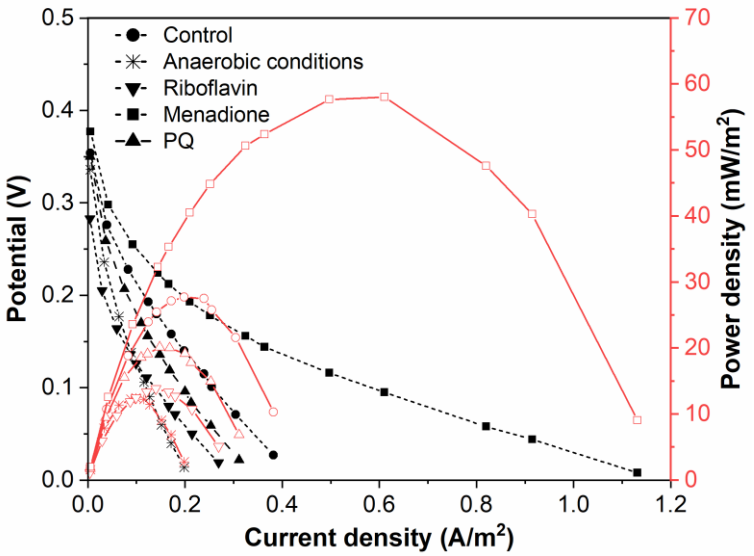

Figure 21. Polarization and power density curves of *Rhizobium anhuiense-based* BFC in 0.1 mM PBS, pH 7.0, the presence of several redox mediators (5 mM of menadione, 0.2 µM of riboflavin, and 4 mM of 9,10-phenanthrenequinone) and at anaerobic conditions.

Riboflavin is known as an endogenous redox mediator facilitating electron transfer rate promoted less of the generated power. Functional devices that have their energy supplied by fuel cells need to operate in conditions up to or equal to the power density maximum to function at high efficiency. Electrons transferred during this process are directly associated with the chemical reactions catalyzed by enzymes involved in the metabolic processes of microorganisms. Bacteria-based fuel cells are characterized by nonlinear power density. This nonlinearity can be used for efficient energy saving while adapted to activate performance to a certain set of characteristics. A larger overall power density at higher potential is a goal during the development of such systems because at the maximum value of power density it enables the generation of the greatest amount of electric current.

Application of natural redox mediator – menadione – in MBFC design enables to increase of both the voltage and power of the designed MBFC and this well increases their applicability. In contrast, no positive effect was observed when riboflavin was applied instead of menadione. This effect can be related to different solubility of both these natural redox mediators, because menadione is soluble in a hydrophobic environment and enters the phospholipid membrane, whereas riboflavin is water-soluble and can be dissolved within the cell, as within the extracellular environment. However,

riboflavin is not well suitable to shoot electrons through the cell membrane. Therefore, we can propose that a menadione can more efficiently shuttle charge through phospholipid membrane towards the electrodes in comparison to charge transfer ability of riboflavin (Figure 20).

It is known that *Rhizobium anhuiense* can function in both anaerobic and aerobic conditions. Therefore, the ability of power generation of *Rhizobium anhuiense* was additionally tested in anaerobic conditions by the protrusion and saturation of the system with nitrogen gas. However, under anaerobic conditions, a significant decrease in all power generation-related characteristics was determined (Figure 18 and Figure 21).

It should be noted that the current density generated by here reported MBFC, like in most of MBFCs, is not very high, therefore, to increase the density of current 3D electrode materials [100] and/or conducting polymer-based structures [101] can be applied, which will enable to increase the magnitude of current by several orders [64].

5. CONCLUSIONS

1. We have found that hole-transporting (p-type) organic/polymer semiconductors can be used in the construction of biosensor electrodes. Electrochemical experiments have shown that, at relatively low ionisation potentials, a direct transfer of holes from the electrode to the enzyme occurs. A broad linear dependence between current density and glucose concentration from 2 to 15 mM and a high stability of the ITO/poly-CzO/GOx-electrode were observed, while the highest sensitivity was found for the graphite/poly-CzPh/GOx-electrode at 3,7 $\mu A\ cm^{-2}\ mM^{-1}$.

2. We have constructed and tested redox mediator-based bioelectrochemical systems utilizing different redox mediators. Chlorophyll A and cytochrome-mediated systems showed the highest sensitivity to variable glucose concentrations, with a measured power density of 2.5-4 $\mu W/cm^2$. However, these systems were inhibited with further increases in glucose concentrations. For the chlorophyll-a mediated system, the power density dropped to < 10 nW/cm^2 when the glucose concentration was increased to 100 mM.

3. Using *Rhizobium anhuiense* bacteria, we further developed fuel cells based on electrocatalytic processes. In order to improve charge transfer, we tested several redox mediators: menadione, riboflavin and 9,10-phenanthrquinone. The best results were found in a Rhizobium anhuiense-based bioanode cultured in a high glucose environment, mediated by menadione, with an open circuit potential of 0.385 mV, and a maximum power density of 5.5 $\mu W/cm^2$, which generated an anodic current of 50 $\mu A/cm^2$.

6. REFERENCES

1. Wang, J. Electrochemical Glucose Biosensors. *Chem Rev* **108**, 814–825 (2008).
2. Wilson, R. & Turner, A. P. F. Glucose oxidase: an ideal enzyme. *Biosens Bioelectron* **7**, 165–185 (1992).
3. Chen, C. *et al.* Recent advances in electrochemical glucose biosensors: a review. *RSC Adv.* **3**, 4473–4491 (2013).
4. Ramanavicius, A., Kausaite, A. & Ramanaviciene, A. Enzymatic biofuel cell based on anode and cathode powered by ethanol. *Biosens Bioelectron* **24**, 761–766 (2008).
5. Wittekindt, C., Schwarz, M., Friedrich, T. & Koslowski, T. Aromatic Amino Acids as Stepping Stones in Charge Transfer in Respiratory Complex I: An Unusual Mechanism Deduced from Atomistic Theory and Bioinformatics. *J Am Chem Soc* **131**, 8134–8140 (2009).
6. Ayranci, R. *et al.* Comparative investigation of spectroelectrochemical and biosensor application of two isomeric thienylpyrrole derivatives. *RSC Adv.* **5**, 52543–52549 (2015).
7. Winkler, J. R. & Gray, H. B. Electron flow through biological molecules: does hole hopping protect proteins from oxidative damage? *Q Rev Biophys* **48**, 411–420 (2015).
8. Gray, H. B. & Winkler, J. R. Hole hopping through tyrosine/tryptophan chains protects proteins from oxidative damage. *Proceedings of the National Academy of Sciences* **112**, 10920–10925 (2015).
9. Bagdžiūnas, G. *et al.* Green and red phosphorescent organic light-emitting diodes with ambipolar hosts based on phenothiazine and carbazole moieties: photoelectrical properties, morphology and efficiency. *RSC Adv.* **6**, 61544–61554 (2016).
10. Reig, M. *et al.* Easy accessible blue luminescent carbazole-based materials for organic light-emitting diodes. *Dyes and Pigments* **137**, 24–35 (2017).
11. Bezuglyi, M., Ivaniuk, K., Volyniuk, D., Gražulevičius, J. v & Bagdžiūnas, G. An approach to discovering novel exciplex supramolecular complex based on carbazole-containing 1,8-naphthalimide. *Dyes and Pigments* **149**, 298–305 (2018).
12. Kisieliute, A. *et al.* Towards microbial biofuel cells: Improvement of charge transfer by self-modification of microoganisms with conducting polymer – Polypyrrole. *Chemical Engineering Journal* **356**, 1014–1021 (2019).

13. Ramanavicius, A. *et al.* Biofuel cell based on glucose oxidase from Penicillium funiculosum 46.1 and horseradish peroxidase. *Chemical Engineering Journal* **264**, 165–173 (2015).
14. A. Karim, N. & Yang, H. Mini-Review: Recent Technologies of Electrode and System in the Enzymatic Biofuel Cell (EBFC). *Applied Sciences* vol. 11 Preprint at https://doi.org/10.3390/app11115197 (2021).
15. Rewatkar, P., Kothuru, A. & Goel, S. PDMS-Based Microfluidic Glucose Biofuel Cell Integrated With Optimized Laser-Induced Flexible Graphene Bioelectrodes. *IEEE Trans Electron Devices* **67**, 1832–1838 (2020).
16. Qiang, L., Yuan, L. & Ding, Q. [Influence of buffer solutions on the performance of microbial fuel cell electricity generation]. *Huan Jing Ke Xue* **32**, 1524–1528 (2011).
17. Mukherjee, S., Ganguly, A. & Ghosh, A. A comparative study on the energy generation through wastewater purification in microbial fuel cell. *Mater Today Proc* (2022) doi:https://doi.org/10.1016/j.matpr.2021.12.326.
18. Kwon, C. H. *et al.* High-power hybrid biofuel cells using layer-by-layer assembled glucose oxidase-coated metallic cotton fibers. *Nat Commun* **9**, (2018).
19. Anson, C. W. & Stahl, S. S. Mediated Fuel Cells: Soluble Redox Mediators and Their Applications to Electrochemical Reduction of O(2) and Oxidation of H(2), Alcohols, Biomass, and Complex Fuels. *Chem Rev* **120**, 3749–3786 (2020).
20. Haque, S. U., Duteanu, N., Ciocan, S., Nasar, A. & Inamuddin. A review: Evolution of enzymatic biofuel cells. *J Environ Manage* **298**, 113483 (2021).
21. Giroud, F., Gondran, C., Gorgy, K., Vivier, V. & Cosnier, S. An enzymatic biofuel cell based on electrically wired polyphenol oxidase and glucose oxidase operating under physiological conditions. *Electrochim Acta* **85**, 278–282 (2012).
22. Cinquin, P. *et al.* A glucose biofuel cell implanted in rats. *PLoS One* **5**, e10476–e10476 (2010).
23. Trifonov, A. *et al.* Enzyme-Capped Relay-Functionalized Mesoporous Carbon Nanoparticles: Effective Bioelectrocatalytic Matrices for Sensing and Biofuel Cell Applications. *ACS Nano* **7**, 11358–11368 (2013).
24. Rozene, J., Morkvenaite-Vilkonciene, I., Bruzaite, I., Zinovicius, A. & Ramanavicius, A. Baker's Yeast-Based Microbial Fuel Cell Mediated

by 2-Methyl-1,4-Naphthoquinone. *Membranes* vol. 11 Preprint at https://doi.org/10.3390/membranes11030182 (2021).
25. Everse, J. Heme Proteins. in (eds. Lennarz, W. J. & Lane, M. D. B. T.-E. of B. C. (Second E.) 532–538 (Academic Press, 2013). doi:https://doi.org/10.1016/B978-0-12-378630-2.00015-3.
26. Ramanavicius, A. & Ramanaviciene, A. Hemoproteins in Design of Biofuel Cells. *Fuel Cells* **9**, 25–36 (2009).
27. Kumari, A. Chapter 3 - Electron Transport Chain. in (ed. Kumari, A. B. T.-S. B.) 13–16 (Academic Press, 2018). doi:https://doi.org/10.1016/B978-0-12-814453-4.00003-0.
28. Hemker, H. C. A century of heparin: past, present and future. *J Thromb Haemost* **14**, 2329–2338 (2016).
29. Lima, M., Rudd, T. & Yates, E. New Applications of Heparin and Other Glycosaminoglycans. *Molecules* **22**, (2017).
30. Atallah, J., Khachfe, H. H., Berro, J. & Assi, H. I. The use of heparin and heparin-like molecules in cancer treatment: a review. *Cancer Treat Res Commun* **24**, 100192 (2020).
31. Singh, A. K., Rana, H. K. & Pandey, A. K. Chapter 19 - Analysis of chlorophylls. in (eds. Sanches Silva, A., Nabavi, S. F., Saeedi, M. & Nabavi, S. M. B. T.-R. A. in N. P. A.) 635–650 (Elsevier, 2020). doi:https://doi.org/10.1016/B978-0-12-816455-6.00019-6.
32. Ropp, R. C. Chapter 1 - The Alkaline Earths as Metals. in (ed. Ropp, R. C. B. T.-E. of the A. E. C.) 1–23 (Elsevier, 2013). doi:https://doi.org/10.1016/B978-0-444-59550-8.00001-6.
33. Jadhav, D. A., Carmona-Martínez, A. A., Chendake, A. D., Pandit, S. & Pant, D. Modeling and optimization strategies towards performance enhancement of microbial fuel cells. *Bioresour Technol* **320**, 124256 (2021).
34. Khandelwal, A., Vijay, A., Dixit, A. & Chhabra, M. Microbial fuel cell powered by lipid extracted algae: A promising system for algal lipids and power generation. *Bioresour Technol* **247**, 520–527 (2018).
35. Yadav, G. *et al.* Mechanism and challenges behind algae as a wastewater treatment choice for bioenergy production and beyond. *Fuel* **285**, 119093 (2021).
36. Song, X. *et al.* Chlorella vulgaris on the cathode promoted the performance of sediment microbial fuel cells for electrogenesis and pollutant removal. *Science of The Total Environment* **728**, 138011 (2020).

37. Kumar, P. K. *et al.* Biomass production from microalgae Chlorella grown in sewage, kitchen wastewater using industrial CO2 emissions: Comparative study. *Carbon Resources Conversion* **2**, 126–133 (2019).
38. Logan, B. E., Rossi, R., Ragab, A. & Saikaly, P. E. Electroactive microorganisms in bioelectrochemical systems. *Nat Rev Microbiol* **17**, 307–319 (2019).
39. Ramanavicius, S. & Ramanavicius, A. Charge Transfer and Biocompatibility Aspects in Conducting Polymer-Based Enzymatic Biosensors and Biofuel Cells. *Nanomaterials* **11**, (2021).
40. Rozene, J., Morkvenaite-Vilkonciene, I., Bruzaite, I., Dzedzickis, A. & Ramanavicius, A. Yeast-based microbial biofuel cell mediated by 9,10-phenantrenequinone. *Electrochim Acta* **373**, 137918 (2021).
41. El-Naggar, M. Y. *et al.* Electrical transport along bacterial nanowires from Shewanella oneidensis MR-1. *Proceedings of the National Academy of Sciences* **107**, 18127–18131 (2010).
42. Reguera, G. Harnessing the power of microbial nanowires. *Microb Biotechnol* **11**, 979–994 (2018).
43. Kisieliute, A. *et al.* Towards microbial biofuel cells: Improvement of charge transfer by self-modification of microoganisms with conducting polymer – Polypyrrole. *Chemical Engineering Journal* **356**, 1014–1021 (2019).
44. Apetrei, R.-M. *et al.* Cell-assisted synthesis of conducting polymer – polypyrrole – for the improvement of electric charge transfer through fungal cell wall. *Colloids Surf B Biointerfaces* **175**, 671–679 (2019).
45. Anson, C. W. & Stahl, S. S. Mediated Fuel Cells: Soluble Redox Mediators and Their Applications to Electrochemical Reduction of O2 and Oxidation of H2, Alcohols, Biomass, and Complex Fuels. *Chem Rev* **120**, 3749–3786 (2020).
46. Ramanavicius, S. & Ramanavicius, A. Progress and Insights in the Application of MXenes as New 2D Nano-Materials Suitable for Biosensors and Biofuel Cell Design. *Int J Mol Sci* **21**, (2020).
47. Aiyer, K. S. How does electron transfer occur in microbial fuel cells? *World J Microbiol Biotechnol* **36**, 19 (2020).
48. Gorby, Y. A. *et al.* Electrically conductive bacterial nanowires produced by Shewanella oneidensis strain MR-1 and other microorganisms. *Proceedings of the National Academy of Sciences* **103**, 11358–11363 (2006).
49. R, B. D. & R, L. D. Electricity Production by Geobacter sulfurreducens Attached to Electrodes. *Appl Environ Microbiol* **69**, 1548–1555 (2003).

50. Park, H. S. *et al.* A Novel Electrochemically Active and Fe(III)-reducing Bacterium Phylogenetically Related to Clostridium butyricum Isolated from a Microbial Fuel Cell. *Anaerobe* **7**, 297–306 (2001).
51. Chaudhuri, S. K. & Lovley, D. R. Electricity generation by direct oxidation of glucose in mediatorless microbial fuel cells. *Nat Biotechnol* **21**, 1229–1232 (2003).
52. Rahimnejad, M., Najafpour, G. D., Ghoreyshi, A. A., Shakeri, M. & Zare, H. Methylene blue as electron promoters in microbial fuel cell. *Int J Hydrogen Energy* **36**, 13335–13341 (2011).
53. Petroniene, J. *et al.* Evaluation of Redox Activity of Human Myocardium-derived Mesenchymal Stem Cells by Scanning Electrochemical Microscopy. *Electroanalysis* **32**, 1337–1345 (2020).
54. Wu, S. *et al.* Riboflavin-mediated extracellular electron transfer process involving Pachysolen tannophilus. *Electrochim Acta* **210**, 117–121 (2016).
55. Jong, B. C. *et al.* Enrichment, Performance, and Microbial Diversity of a Thermophilic Mediatorless Microbial Fuel Cell. *Environ Sci Technol* **40**, 6449–6454 (2006).
56. Oliveira, V. B., Simões, M., Melo, L. F. & Pinto, A. M. F. R. Overview on the developments of microbial fuel cells. *Biochem Eng J* **73**, 53–64 (2013).
57. Juang, D. F., Yang, P. C., Lee, C. H., Hsueh, S. C. & Kuo, T. H. Electrogenic capabilities of gram negative and gram positive bacteria in microbial fuel cell combined with biological wastewater treatment. *International Journal of Environmental Science & Technology* **8**, 781–792 (2011).
58. Yang, J. *et al.* Mechanisms underlying legume–rhizobium symbioses. *J Integr Plant Biol* **64**, 244–267 (2022).
59. Zhang, Y. J. *et al.* Rhizobium anhuiense sp. nov., isolated from effective nodules of Vicia faba and Pisum sativum. *Int J Syst Evol Microbiol* **65**, 2960–2967 (2015).
60. Humphries, P. S. *et al.* Carbazole-containing sulfonamides and sulfamides: Discovery of cryptochrome modulators as antidiabetic agents. *Bioorg Med Chem Lett* **26**, 757–760 (2016).
61. Swinarew, A. *et al.* Star-shaped poly(2-(9-carbazolyl)methylthiirane): Synthesis, analysis and photoluminescencent properties. *J Mol Struct* **1005**, 129–133 (2011).
62. Ranganayaki, S. & Mohan, C. Effect of sodium molybdate on microbial fixation of nitrogen. *Z Allg Mikrobiol* **21**, 607–610 (1981).

63. Sijilmassi, B. *et al.* Assessment of Genetic Diversity and Symbiotic Efficiency of Selected Rhizobia Strains Nodulating Lentil (Lens culinaris Medik.). *Plants* **10**, (2021).
64. Wilson, W. W., Wade, M., Holman, S. & Champlin, F. Status of Methods for Assessing Bacterial Cell Surface Charge Properties Based on Zeta Potential Measurements. *J Microbiol Methods* **43**, 153–164 (2001).
65. Karon, K. & Lapkowski, M. Carbazole electrochemistry: a short review. *Journal of Solid State Electrochemistry* **19**, 2601–2610 (2015).
66. Liu, C. *et al.* Luminescent network film deposited electrochemically from a carbazole functionalized AIE molecule and its application for OLEDs. *J. Mater. Chem. C* **3**, 3752–3759 (2015).
67. Nikolic, G. *et al.* Fast Fourier Transform IR Characterization of Epoxy GY Systems Crosslinked with Aliphatic and Cycloaliphatic EH Polyamine Adducts. *Sensors* **10**, 684–696 (2010).
68. Allen, W. D. *et al.* The experimental vibrational spectra, vibrational assignment, and normal coordinate analysis of thiirane-h4 and -d4 and cis- and trans-1,2-dideuteriothiirane: Ab initio theoretical IR spectra of thiirane, thiirene, and isotopically substituted derivatives. *J Chem Phys* **84**, 4211–4227 (1986).
69. Samanta, D. & Sarkar, A. Immobilization of bio-macromolecules on self-assembled monolayers: methods and sensor applications. *Chem. Soc. Rev.* **40**, 2567–2592 (2011).
70. Fogarty, A. C. & Laage, D. Water Dynamics in Protein Hydration Shells: The Molecular Origins of the Dynamical Perturbation. *J Phys Chem B* **118**, 7715–7729 (2014).
71. Marmur, A. Soft contact: measurement and interpretation of contact angles. *Soft Matter* **2**, 12–17 (2006).
72. Karon, K. & Lapkowski, M. Carbazole electrochemistry: a short review. *Journal of Solid State Electrochemistry* **19**, 2601–2610 (2015).
73. Li, M. C3−C3′ and C6−C6′ Oxidative Couplings of Carbazoles. *Chemistry – A European Journal* **25**, 1142–1151 (2019).
74. Bagdziunas, G., Surka, M. & Ivaniuk, K. High triplet energy exciton blocking materials based on triphenylamine core for organic light-emitting diodes. *Org Electron* **41**, 122–129 (2017).
75. Córdoba-Torres, P., Mesquita, T. J. & Nogueira, R. P. Relationship between the Origin of Constant-Phase Element Behavior in Electrochemical Impedance Spectroscopy and Electrode Surface Structure. *The Journal of Physical Chemistry C* **119**, 4136–4147 (2015).

76. Wohlfahrt, G. *et al.* 1.8 and 1.9Å resolution structures of the Penicillium amagasakiense and Aspergillus niger glucose oxidases as a basis for modelling substrate complexes. *Acta Crystallographica Section D* **55**, 969–977 (1999).
77. Wen, Z., Ye, B. & Zhou, X. Direct electron transfer reaction of glucose oxidase at bare silver electrodes and its application in analysis. *Electroanalysis* **9**, 641–644 (1997).
78. Liu, J., Agarwal, M. & Varahramyan, K. Glucose sensor based on organic thin film transistor using glucose oxidase and conducting polymer. *Sens Actuators B Chem* **135**, 195–199 (2008).
79. Deng, C. *et al.* Direct electrochemistry of glucose oxidase and biosensing for glucose based on boron-doped carbon nanotubes modified electrode. *Biosens Bioelectron* **23**, 1272–1277 (2008).
80. Demin, S. & Hall, E. A. H. Breaking the barrier to fast electron transfer. *Bioelectrochemistry* **76**, 19–27 (2009).
81. Willner, I. *et al.* Electrical Wiring of Glucose Oxidase by Reconstitution of FAD-Modified Monolayers Assembled onto Au-Electrodes. *J Am Chem Soc* **118**, 10321–10322 (1996).
82. Tao, Z., Raffel, R. A., Souid, A.-K. & Goodisman, J. Kinetic Studies on Enzyme-Catalyzed Reactions: Oxidation of Glucose, Decomposition of Hydrogen Peroxide and Their Combination. *Biophys J* **96**, 2977–2988 (2009).
83. Bartlett, P. N. & Al-Lolage, F. A. There is no evidence to support literature claims of direct electron transfer (DET) for native glucose oxidase (GOx) at carbon nanotubes or graphene. *Journal of Electroanalytical Chemistry* **819**, 26–37 (2018).
84. Salimi, A., Noorbakhsh, A. & Ghadermarz, M. Direct electrochemistry and electrocatalytic activity of catalase incorporated onto multiwall carbon nanotubes-modified glassy carbon electrode. *Anal Biochem* **344**, 16–24 (2005).
85. Su, Q. & Klinman, J. P. Nature of Oxygen Activation in Glucose Oxidase from Aspergillus niger: The Importance of Electrostatic Stabilization in Superoxide Formation. *Biochemistry* **38**, 8572–8581 (1999).
86. Wang, Y., Sun, M., Qiao, J., Ouyang, J. & Na, N. FAD roles in glucose catalytic oxidation studied by multiphase flow of extractive electrospray ionization (MF-EESI) mass spectrometry. *Chem. Sci.* **9**, 594–599 (2018).
87. Inzelt, G. & Láng, G. Model dependence and reliability of the electrochemical quantities derived from the measured impedance

spectra of polymer modified electrodes. *Journal of Electroanalytical Chemistry* **378**, 39–49 (1994).

88. Day, N. U., Walter, M. G. & Wamser, C. C. Preparations and Electrochemical Characterizations of Conductive Porphyrin Polymers. *The Journal of Physical Chemistry C* **119**, 17378–17388 (2015).
89. Rubinson, J. F. & Kayinamura, Y. P. Charge transport in conducting polymers: insights from impedance spectroscopy. *Chem. Soc. Rev.* **38**, 3339–3347 (2009).
90. Reig, M., Bagdziunas, G., Ramanavicius, A., Puigdollers, J. & Velasco, D. Interface engineering and solid-state organization for triindole-based p-type organic thin-film transistors. *Phys. Chem. Chem. Phys.* **20**, 17889–17898 (2018).
91. Bagdžiūnas, G. & Ramanavičius, A. Towards direct enzyme wiring: a theoretical investigation of charge carrier transfer mechanisms between glucose oxidase and organic semiconductors. *Physical Chemistry Chemical Physics* **21**, 2968–2976 (2019).
92. Conzuelo, F., Marković, N., Ruff, A. & Schuhmann, W. The Open Circuit Voltage in Biofuel Cells: Nernstian Shift in Pseudocapacitive Electrodes. *Angewandte Chemie International Edition* **57**, 13681–13685 (2018).
93. Gonzalez del Campo, A. *et al.* Study of a photosynthetic MFC for energy recovery from synthetic industrial fruit juice wastewater. *Int J Hydrogen Energy* **39**, 21828–21836 (2014).
94. Venkata Mohan, S., Srikanth, S., Chiranjeevi, P., Arora, S. & Chandra, R. Algal biocathode for in situ terminal electron acceptor (TEA) production: Synergetic association of bacteria-microalgae metabolism for the functioning of biofuel cell. *Bioresour Technol* **166**, 566–574 (2014).
95. Yakar, A., Türe, C., Türker, O. C., Vymazal, J. & Saz, Ç. Impacts of various filtration media on wastewater treatment and bioelectric production in up-flow constructed wetland combined with microbial fuel cell (UCW-MFC). *Ecol Eng* **117**, 120–132 (2018).
96. Huarachi-Olivera, R. *et al.* Bioelectrogenesis with microbial fuel cells (MFCs) using the microalga Chlorella vulgaris and bacterial communities. *Electronic Journal of Biotechnology* **31**, 34–43 (2018).
97. Malekmohammadi, S. & Ahmad Mirbagheri, S. A review of the operating parameters on the microbial fuel cell for wastewater treatment and electricity generation. *Water Science and Technology* **84**, 1309–1323 (2021).

98. Jaszek, M., Janczarek, M., Kuczyński, K., Piersiak, T. & Grzywnowicz, K. The response of the Rhizobium leguminosarum bv. trifolii wild-type and exopolysaccharide-deficient mutants to oxidative stress. *Plant Soil* **376**, 75–94 (2014).
99. Fang, D. *et al.* Redox Mediator-Based Microbial Biosensors for Acute Water Toxicity Assessment: A Critical Review. *ChemElectroChem* **7**, 2513–2526 (2020).
100. Yang, Y. *et al.* Boosting Power Density of Microbial Fuel Cells with 3D Nitrogen-Doped Graphene Aerogel Electrode. *Advanced Science* **3**, 1600097 (2016).
101. Ramanavicius, S. & Ramanavicius, A. Conducting Polymers in the Design of Biosensors and Biofuel Cells. *Polymers (Basel)* **13**, (2021).

6. SANTRAUKA

Šiame darbe siekiame pristatyti ir aprašyti keletą gliukozės biojutiklių ir gliukozę vartojančių biokuro elementų technologijų. Aprašome elektrocheminiu būdu sukurtų skylėmis pernešančių (p tipo) polimerinių puslaidininkių (HTPS), kurių pagrindą sudaro karbazolo dariniai ar triphelaminas, kaip tiesioginio krūvio pernešimo gliukozės jutiklių biocheminį taikymą. Indžio alavo oksido ir grafito pagrindu pagaminti elektrodai buvo elektrochemiškai modifikuoti HTPS sluoksniu ir kovalentiškai imobilizuotas gliukozės oksidazės (GOx) monosluoksniu. HTPS ir GOx pagrindu pagaminti elektrodai buvo tiriami siekiant įvertinti tiesioginį skylių perdavimą tarp fermento ir elektrodo esant bioelektrochemiškai tinkamam potencialui. Pastebėta plati tiesinė priklausomybė tarp smailės srovės tankio ir gliukozės koncentracijos.

Naujų didelės galios biokuro elementų kūrimą praeityje ribojo lėtas arba netiesioginis krūvio pernešimas. Siekiant įvertinti jų pritaikomumą, buvo ištirtos fermentinių biokuro elementų (EBFC) sistemos su skirtingomis redokso mediatorių medžiagomis. Skirtingos prigimties redokso mediatoriai buvo parinkti siekiant geriau suprasti krūvio perdavimo sistemą ir jų poveikį biokuro elementų savybėms. Citochromas c, chlorofilas a ir ultragarsu suardytų dumblių *Chlorella vulgaris* ląstelių supernatantas buvo tiriami kaip potencialūs redokso mediatoriai. Tomis pačiomis analitinėmis sąlygomis buvo įvertintas ir heparino poveikis EBFC. EBFC vertinti buvo taikomi atvirosios grandinės potencialo (OCP) matavimai ir srovės atsako įvertinimas dviem matavimo režimais: i) ciklinės voltamperometrijos matavimų metu, kai potencialas ciklišKai keičiasi, arba ii) esant pastoviai potencialo vertei, kai taikoma chronoamperometrija.

Mikrobiniai kuro elementai (MFBC) - tai unikalios biokatalizės sistemos, kurios cheminę energiją, sukauptą atsinaujinančiuose organiniuose degaluose, pavyzdžiui, gliukozėje, paverčia elektros energija. Tačiau ne visi mikroorganizmai medžiagų apykaitos ir (arba) katalizės procesų metu sukuria pakankamą redokso potencialą. Savo tyrime įvertinome mikroorganizmo *Rhizobium anhuiense,* kaip katalizatoriaus, tinkamo mikrobiniams kuro elementams kurti, pritaikomumą. *Rhizobium anhuiense* bakterijos buvo kultivuojamos didelio gliukozės kiekio aplinkoje, o krūvio perdavimui pagerinti buvo išbandyti keli redokso mediatoriai: menadionas, riboflavinas ir 9,10-fenantrenchinonas (PQ).

6.1. Įvadas

Gliukozė - tai angliavandenis, paprastasis cukrus, kurio gausu visoje gamtoje. Gliukozė gaminama dumblių ir augalų fotosintezės proceso metu ir plačiai naudojama kaip energijos kaupimo priemonė, natūrali statybinė medžiaga ir aerobiniam bei anaerobiniam ląstelių kvėpavimui. Kaip molekulė jis nuolat aptinkamas mūsų gyvenime žemės ūkyje, gamtiniuose ir pramoniniuose produktuose, mūsų pačių kūnuose. Todėl labai svarbu ją tyrinėti, kad geriau suprastume, kaip ją galima toliau panaudoti. Šiame tyrime daugiausia dėmesio skiriame elektrocheminėms gliukozės aptikimo ir matavimo technologijoms, taip pat technologijoms, leidžiančioms gliukozę paversti elektros energija.

Gebėjimas nustatyti ir išmatuoti gliukozę yra labai svarbus medicinos ir maisto pramonei. Mūsų organizmas funkcionuoja palaikydamas siaurą gliukozės koncentracijos diapazoną kraujyje, maždaug 5±2 mM, o tais atvejais, kai dėl ligos (pvz., diabeto) ar kitų priežasčių to padaryti negali, gliukozės koncentraciją reikia reguliuoti išoriniais metodais. Todėl buvo sukurtos technologijos, leidžiančios tiksliai sekti gliukozės koncentraciją realiuoju arba beveik realiuoju laiku. Šios technologijos taip pat plačiai naudojamos maisto pramonėje - gliukozės kiekis maisto produktuose kinta visą laiką, o sekdami šiuos pokyčius galime kiekybiškai analizuoti vaisių sunokimą, stebėti fermentaciją ar net įvertinti nepageidaujamą mikrobų augimą.

Gliukozė, kuri yra labiausiai paplitęs gamtoje angliavandenis, taip pat yra labai patraukli, nes ją galima naudoti kaip biologiškai draugišką elektrocheminės energijos kaupimo formą. Kaip organizmas naudoja gliukozę ląstelių kvėpavimui, taip ir mes galime ją panaudoti pramonėje ar žemės ūkyje. Energijos nuolat reikia, o panaudodami gliukozę kaip kuro šaltinį, galėtume gauti alternatyvius būdus, kaip panaudoti perteklines augalines atliekas, sugedusį maistą ir t. t. Gliukozė taip pat galėtų būti energijos šaltinis gyvų kūnų elektromechaniniams prietaisams, pavyzdžiui, širdies stimuliatoriams ar jutikliams.

6.1.1. Šio tyrimo tikslas:

Sukurti ir suprojektuoti veikiančius gliukozės biojutiklius ir gliukoze varomus biokuro elementus, naudojant tiesioginio ir netiesioginio krūvio perdavimo technologijas ir mikroorganizmus.

6.1.2. Šio tyrimo tikslai:

1. Suprojektuoti, sukurti ir įvertinti GOx pagrindu veikiančias bioelektrochemines sistemas, naudojančias tiesioginę elektronų perdavimo technologiją.
2. Suprojektuoti, sukurti ir įvertinti GOx pagrindu veikiančias bioelektrochemines sistemas, naudojančias tarpininkaujamą krūvio perdavimo technologiją.
3. Suprojektuoti, sukurti ir įvertinti mikroorganizmų pagrindu veikiančias bioelektrochemines sistemas, maitinamas gliukoze.

6.1.3. Mokslinis naujumas

Įrodyta, kad P-tipo polimeriniai puslaidininkiai gali dalyvauti tiesioginės elektronų pernašos sistemoje su baltymais.

Vienas iš pirmųjų kartų, kai buvo ištirtos cytochromomis medijuojamos gliukozės bioelektrocheminės sistemos.

Vienas pirmųjų darbų aprašančių azotą fiksuojančių bakterijų panaudojimą elektros energijos generavimui.

6.2. Metodika

6.2.1. Elektrodų valymas ir paruošimas

Prieš tolimesnę modifikaciją ITO modifikuoto stiklo elektrodai buvo supjaustyti iki 75 mm x 26 mm dydžio, elektrodai buvo nuplauti distiliuotu vandeniu ir acetonu; po to jie buvo elektrochemiškai valyti 10 potencialo ciklų nuo -1000 iki +1000 mV prieš Ag/AgCl, esant 200 mV/s skenavimo greičiui PBS buferiniame tirpale.

Grafitiniai strypiniai elektrodai buvo supjaustyti iki reikiamo dydžio ir poliruojami rankiniu būdu naudojant abrazyvus pagal 9 pav. metodą, kol buvo gautas tolygus atspindintis paviršius.

Priešpriešinis elektrodas buvo apdorotas ugnimi ir nuvalytas acetonu bei DI vandeniu, kad eksperimento metu būtų sudegintos organinės liekanos.

Atliekant elektrocheminius bandymus elektrodų paviršiaus plotas buvo ribojamas ir palaikomas pastovus naudojant silikoninius vamzdelius ir teflono juostą.

6.2.2. Elektrodų modifikavimas organiniais polimerais kaip puslaidininkiais

P tipo puslaidininkinis polimeras buvo nusodintas ant grafito ir ITO elektrodų potenciodinaminėmis sąlygomis, taikant ciklinės voltamperometrijos metodą. Nusodinimo parametrai buvo parinkti eksperimentiškai.

CzO, CzS organinių polimerų pirmtakai buvo nusodinti ant išvalytų ITO elektrodų elektrocheminiu būdu, naudojant 10 potencialo ciklų 0,5 mg/ml organinio pirmtako tirpale su 0,1 M $TBAPH_6$, ištirpintame sausame DCM, esant 50 mV/s skenavimo greičiui. Šios modifikacijos metu (potencialas buvo keičiamas nuo -200 mV iki +1500 mV prieš Ag/AgCl, kad būtų galima polimerizuoti CzO ir CzS) buvo registruojamos ciklinės voltamperogramos. Siekiant išvalyti naujai suformuotus ITO/poli-CzO ir ITO/poli-CzS elektrodus, prieš kiekvieną apdorojimo etapą ir po jo jie buvo plaunami distiliuotu vandeniu. Elektrocheminis charakterizavimas atliktas naudojant tuos pačius elektrocheminius prietaisus ir programinę įrangą, kurie buvo naudojami ITO elektrodams modifikuoti.

TPA, CzEt ir CzPh organinių polimerų pirmtakai buvo nusodinti ant išvalytų grafito elektrodų elektrocheminiu būdu, naudojant 20 potencialo ciklų 0,5 mg/ml organinio pirmtako tirpale su 0,1 M $TBAPH_6$, ištirpintame sausame DCM, skenuojant 50 mV/s greičiu. Šios modifikacijos metu (potencialas buvo keičiamas nuo -200 mV iki +1500 mV prieš Ag vielą, padengtą AgCl, skirtą TPA, CzEt ir CzPh polimerizacijai) buvo registruojamos ciklinės voltamperogramos. Siekiant išvalyti naujai suformuotus grafito/poli-TPA, grafito/poli-CzEt, grafito/poli-CzPh elektrodus, prieš kiekvieną apdorojimo etapą ir po jo jie buvo plaunami distiliuotu vandeniu. Elektrocheminis charakterizavimas atliktas naudojant tuos pačius elektrocheminius prietaisus ir programinę įrangą, kurie buvo naudojami modifikuojant grafito elektrodus.

6.2.3. Organinių puslaidininkinių polimerų, modifikuotų GOx fermentais, kovalentinė imobilizacija

Polimerais modifikuoti elektrodai buvo susieti GOx fermentu naudojant dviejų etapų procesą. Elektrodai 1 valandą kambario temperatūroje buvo inkubuojami 2,5 % glutaraldehido tirpale vandenyje. Prieš kiekvieną apdorojimo etapą ir po jo elektrodai buvo plaunami distiliuotu vandeniu.

Galiausiai šie elektrodai buvo panardinti į GOx (5 mg/ml) tirpalą PBS buferiniame tirpale (pH 7,2) ir laikomi per naktį +4 °C temperatūroje. Prieš atliekant elektrocheminius matavimus, elektrodai buvo kruopščiai nuplauti distiliuotu vandeniu, kad būtų pašalinti: neimobilizuotas fermentas; disocijuotas GOx kofaktorius - FAD; ir kitos neimobilizuotos medžiagos, kurių buvo fermentų mėginiuose, naudotuose elektrodams modifikuoti. Be to, gryno FAD kofaktoriaus imobilizacija ant ITO/poli-CzS elektrodo nebuvo pastebėta naudojant UV-vis spektroskopiją dėl mažo FAD kofaktoriaus adenino aminogrupės nukleofiliškumo. Paruošti elektrodai buvo laikomi uždarame inde su PBS, +4 °C temperatūroje, kol buvo naudojami eksperimentams.

6.2.4. EBFC elektrodų ruošimas

Ant poliruoto grafito elektrodo paviršiaus buvo fiziškai nusodinta 3 µL vertinamos medžiagos tirpalo ir 5 µL gliukozės oksidazės. Nusodintas tirpalas paliktas iš dalies išgaruoti, kad sumažėtų jo tūris. Laukėme, kol ant elektrodo išorinio perimetro pradės matytis džiūstantis išorinis kraštas, tačiau centrinė dalis vis dar buvo drėgna. Kai išgaravo pakankamai skysčio, sistema buvo perkelta į kamerą, prisotintą glutaraldehido garų, kad chemiškai sujungtų struktūrą su elektrodu. Tokios sistemos buvo nurodytos pagal įvertintą medžiagą: $EBFC_{CC}$ - sistema su citochromu c, $EBFC_{CA}$ - sistema su chlorofilu a, $EBFC_{ChV}$ - sistema su ultragarsu suardytų *Chlorella vulgaris* ląstelių supernatantu ir $EBFC_{Hep}$ - sistema su heparinu.

6.2.5. MBFC elektrodų paruošimas

Gramneigiamos *Rhizobium anhuiense* bakterijos, gautos iš Lietuvos agrarinių ir miškų mokslų centro (Vėžaičiai, Lietuva) mikrobų padermių kolekcijos. Bakterijos buvo auginamos Norriso terpėje [62], didelio gliukozės kiekio aplinkoje, pH 7,0, sudarytoje iš azotą fiksuojančių bakterijų padermių. Prieš naudojant eksperimentams, *Rhizobium ahnuiense* bakterijos buvo perskiepytos į pasvirusią Norris terpę, papildytą agaru, ir paliktos augti 48 val. 28 °C temperatūroje. Po to 5 µl autoklavuoto Norriso terpės tirpalo buvo užpildytas mėgintuvėlis su inokuliu ir atsargiai suspenduotas. Mišinys keletą minučių buvo sukamas sūkuriniu judesiu, kad didžioji dalis bakterijų pakiltų iš kietosios terpės. Tada bakterijų suspensija buvo perkelta ir praskiesta šviežia autoklavine Norris terpe, kad kolonijas sudarančių vienetų (KVV)

tankis būtų lygus 1 × 107 KVV mL [163]. Buvo surinkta vienos kameros MBFC celė, kurioje buvo panaudota dviejų elektrodų elektrocheminė sistema, grafito elektrodas buvo naudojamas kaip darbinis elektrodas, o didelio ploto platinos viela - kaip priešinis elektrodas. Bakterijų mėginiai buvo imobilizuoti ant grafito elektrodo, leidžiant jam lengvai išdžiūti dvi minutes. Bandiniui atskirti nuo jį supančios aplinkos buvo naudojama polikarbonato membrana su 1 µm skylutėmis, kad būtų užtikrintas prisitvirtinimas prie anodo.

6.2.6. Zeta potencialo įvertinimas

Paruošti mėginiai buvo 10 kartų praskiesti -terpėje su atitinkama jonine jėga (0,01 mM, 0,05 mM, 0,1 mM, 0,3 mM, 10 mM, 50 mM, 100 mM, 300 mM), o prieš pat zeta potencialo matavimą buvo sureguliuotas pH 5,0, 6,0, 7,0 arba 8,0. Gauta suspensija užpildytos skaidrios vienkartinės "zeta kameros" (ATA scientific, Australija) prieš pat zeta potencialo matavimus. Joninė jėga buvo matuojama esant pH 7,0, o pH tyrimai atlikti 0,1 mM PBS tirpale. Bakterijų ląstelių elektroforetinis judrumas buvo matuojamas 80 V įtampos zeta potencialo analizatoriumi (Zetasizer Nano series NanoZS-; Malvern Industries Ltd, Malvern, Jungtinė Karalystė) ir perskaičiuojamas į zeta potencialus [64]. Matavimai buvo atliekami 25 °C temperatūroje standartinėje Norriso terpėje, pH 7,0. Siekiant nustatyti rezultatų atkuriamumą, mėginys buvo matuojamas penkis kartus dvi skirtingas dienas. Tarp kiekvieno matavimo elektrodai buvo skalaujami dideliu kiekiu MilliQ™ vandens, po to - tiriamoji bakterijų suspensija.

6.2.7. Modifikuoto elektrodo jautrumo gliukozei elektrocheminis įvertinimas

Modifikuotiems elektrodams įvertinti buvo naudojama trijų elektrodų sistema, kurioje modifikuotas elektrodas buvo darbinis elektrodas (darbinis plotas 0,071 cm^2), o platinos viela (darbinis plotas 0,24 cm^2) - priešinis elektrodas. Įtampos buvo matuojamos lyginant su komerciniu Ag/AgCl elektrodu. Sukurtų GOx modifikuotų organinių puslaidininkių pagrindu sukurtų elektrodų funkcionalumas ir gyvybingumas buvo įvertintas CV metodu. Viso eksperimento metu į PBS buferinį tirpalą nuolat buvo pilamas gliukozės tirpalas; po kiekvieno papildymo gautas tirpalas buvo paleidžiamas per du ciklinės voltamperometrijos ciklus nuo -0,2 V iki 0,4 V prieš Ag/AgCl, kai potencialo svyravimo greitis buvo 30 mVs^{-1} . Atliekant visus ciklinės

Atlikus cikline voltamperometriją, buvo vertinami antrojo potencialo ciklo duomenys. Tolesnei elektrocheminei analizei modifikuoti elektrodai buvo tiriami CV metodu sistemoje be gliukozės, kai potencialo kitimo greitis buvo nuo 5 iki 100 mVs^{-1} .

EBFC modifikuoti elektrodai buvo vertinami naudojant platesnį potencialų diapazoną -1,5V-1,5V esant 50 mVs^{-1} dėl eksperimentų metu pastebėto didesnio oksidacijos potencialo. Šios sistemos taip pat įvertintos naudojant chronoamperometriją, esant atitinkamam kiekvienoje sistemoje išmatuotam oksidacijos potencialui.

6.2.8. Biodegalų elementų projektavimas

Siekiant įvertinti modifikuotų elektrodų pritaikomumą biokuro elementuose, buvo naudojamas vienos kameros elementas su dviejų elektrodų sistema. Atliekant EBFC modifikuotų elektrodų bandymus, modifikuoti darbiniai elektrodai buvo išbandyti lyginant su komerciniu Ag/AgCl elektrodu, o MBFC sistemose - su platinos vieliniu elektrodu (darbinis plotas 0,24 cm^2). Kamera buvo pripildyta PBS, pH 7,0, ir išmatuotas sistemų atviros srovės potencialas (OCP). Vėliau prie elektrinės grandinės lygiagrečiai buvo prijungti įvairūs išoriniai rezistoriai (10 MΩ, 1 MΩ, 390 kΩ, 220 kΩ, 180 kΩ, 130 kΩ, 100 kΩ, 68 kΩ, 56 kΩ, 33 kΩ, 10 kΩ, 1 kΩ), siekiant imituoti išorines apkrovas ir įvertinti bakterijų mėginių galios tankį. Buvo registruojami potencialo pokyčiai.

6.3. Rezultatai ir aptarimas

6.3.1. Poli-CzO/GOx, poli-CzS/GOx modifikuotų elektrodų formavimas

Elektrocheminės oksidacijos metu karbazolo dariniai dažniausiai jungiasi tarpusavyje per 3 ir 6 pozicijas, nes šiose padėtyse šių molekulių elektronų tankis yra didžiausias [65]. Elektrocheminis polimerų poli-CzO ir poli-CzS nusodinimas ant ITO paviršiaus buvo atliktas potenciodinaminėmis sąlygomis (1a ir b pav.). Monomero ir polimero jonizacijos pradžios potencialai (IP) buvo išmatuoti atitinkamai 1-ojo ir 10-ojo elektrocheminės polimerizacijos potencialo ciklų metu. Apskaičiuota, kad CzO/CzS monomerų ir poli-CzO/poli-CzS polimerų jonizacijos potencialai atitinkamai yra 1,15/1,12 V prieš Ag/AgCl (5,61/5,58 eV prieš vakuumą) ir 0,882/0,773 V (5,34/5,24 eV).

Be to, poli-CzS gaunamas esant mažesniam jonizacijos potencialui nei poli-CzO dėl ilgesnių polimerų grandinių ir didesnio jų konjugavimo.

Tikrinant polimero cheminę struktūrą, tiek monomero, tiek polimero plėvelės ant ITO buvo analizuojamos naudojant susilpnintą visiškojo atspindžio infraraudonąją (ATR IR) spektroskopiją. Lenkiamieji virpesiai, esantys ties 747 cm^{-1} ir 749 cm^{-1} atitinkamai CzO ir CzS, atitiko karbazilo branduolio virpesius. Be to, polimerinio karbazilo susidarymą elektrocheminio nusodinimo plėvelėje patvirtino IR spektrai pagal naujų smailių atsiradimą ties 826 cm^{-1} ir 832 cm^{-1} , o tai rodo, kad susidarė tripakeistos karbazolo dalys [66]. Be to, oksirano ir tiirano grupių stabilumas elektrocheminio nusodinimo metu buvo įvertintas IR metodu. CzO spektre pastebėti vidutinio intensyvumo oksirano grupės C-O ryšio virpesių signalai ties 861 cm^{-1} ir 908 cm^{-1} , kurie atitinka oksirano ciklo žirklinį ir simetrinį tempimą (3 pav.). Po elektrocheminės polimerizacijos poli-CzO spektrų smailė pasislinko į 883 cm^{-1} [67]. CzS atveju juosta ties maždaug 598 cm^{-1} gali būti priskirta tiirano grupės C-S ryšio virpesiams [68]. Poli-CzS plėvelės spektre buvo nurodyta atitinkama juosta ties 560 cm^{-1} (4 pav.). Gauti rezultatai rodo, kad polikarbazolo plėveles pavyko sukurti polimerizuojant CzO ir CzS pirmtakus. GOx imobilizacijai buvo pritaikytas laipsniškas kovalentiniu jungimu pagrįstas surinkimas [69]. Pirmiausia elektrodai su polikarbazolo plėvelėmis buvo inkubuojami cisteamino vandeniniame tirpale. Šiame etape susidarė monosluoksnis, kuriame yra amino grupių (2 pav., A etapas).

Antra, laisvosios terminalinės amino grupės buvo funkcionalizuotos glutaraldehidu vandenyje (B etapas) per aldehido ir amino kondensacijos reakciją iki imino kambario temperatūroje. Iš abiejų ITO/CzS(O)/amino/aldehido paviršių IR spektrų matyti aldehido C=O grupės virpesių signalas ties 1730 cm^{-1} (3 ir 4 pav.). Galiausiai ITO/CzS(O)/amino/aldehido elektrodai buvo inkubuoti GOx (5 mg ml^{-1}) tirpale buferiniame tirpale, pH 7,2, ir 24 valandas laikomi +4 °C temperatūroje. Reikėtų pažymėti, kad GOx imobilizacija tiesiogiai ant poli-CzO ir poli-CzS paviršių nevyksta, nes šie paviršiai yra hidrofobiški (įvertinta toliau), o oksiran(arba tiiran)-2-ilmetilo žymės yra per trumpos (tik 4 Å) imino susidarymo reakcijai. Be to, vandens solvatacijos apvalkalas, kuris susidaro aplink hidrofobines šonines grandines fermentų paviršiuje, siekiantis ~10 Å, neleidžia vykti reakcijai su per trumpomis žymėmis [70]. ITO/polis-CzS paviršius yra hidrofiliškesnis, palyginti su ITO/polis-CzO paviršiumi, kaip matyti 5 pav.

Tačiau atliekant AFM vaizdavimą pastebėti nedideli paviršiaus šiurkštumo skirtumai tarp imobilizuoto ir gryno polimero paviršių (6 pav.). Reikėtų

pažymėti, kad paviršiaus drėkinamumui didelę įtaką daro paviršiaus šiurkštumas [71].Poli-TPA/GOx, poli-CzEt/GOx, poli-CzPh/GOx modifikuotų elektrodų formavimas

N,N,N-trifenilaminas (TPA), 9-etil-9H-karbazolas (CzEt) ir 9-fenil-9H-karbazolas (CzPh) buvo naudojami kaip pradiniai junginiai modifikuojant elektrodus p tipo organinių puslaidininkių sluoksniais. CzEt ir CzPh elektropolimerizacija prasideda esant maždaug 1,1 V įtampai prieš Ag/AgCl, o tam tikri polimero plėvelės elektrocheminio susidarymo požymiai pastebimi jau pirmajame CV cikle. Šio potencialo pakanka karbazolo daliai oksiduotis į atitinkamą radikalo katijoną [72]. Po dešimtojo CV ciklo šių bandinių anodinio proceso pradžios CV stabilizuojasi ties 0,75 V prieš Ag/AgCl. Karbazolo pagrindo monomerai lengvai oksiduojasi, o jei prie azoto atomo yra pakaitalas (mūsų atveju atitinkamai fenilo ir etilo grupės), šalia 3,6 padėčių susidaro bikarbazolas, kuris gali oksiduotis toliau, susidarant oligomerams [73]. TPA monomero oksidacija buvo stebima esant šiek tiek mažesniam 0,9 V potencialui prieš Ag/AgCl ir veikė pagal kitus tyrimus [74,75]. Visais nusodinimo atvejais, kai naudojami trys tirti monomerai, srovės prisotinimas pasiekiamas iki 10-ojo CV ciklo, po kurio tirpale aplink elektrodus buvo galima pastebėti geltonai žalią karbazolo pagrindu pagamintų monomerų liekaną ir mėlynai žalią TPA liekaną. Atsižvelgiant į liekanas, galima daryti prielaidą, kad medžiagos, kurią galima nusodinti ant darbinio elektrodo naudojant šią sistemą, kiekis yra nedidelis ir ribotas. Be to, vis tiek matome aiškų skirtumą elektrochemiškai modifikuotų elektrodų SEM nuotraukose, jei palyginsime jas su kontroliniu paviršiumi, pavaizduotu 7 paveiksle. Visi trys tirti monomerai sukuria ribotą paviršių padengimą. Elektrodo su nusodintu CzPh paviršius atrodo netolygus, be matomų kristalizacijų, o medžiagos nusėdimo gradientas matomas link krašto, o tai reiškia, kad oligomerai daug dažniau nusėda ant šiurkštesnių paviršių su aštriais bruožais. Atrodo, kad CzEt modifikuoto elektrodo paviršius susidarė kaip šiurkšti plėvelė, kurią tankiai dengia mažos, mažesnės nei 100 nm kristalinės dalelės, o bendras padengimas yra tolygus. TPA modifikuotas elektrodas pasižymi amorfiniu ir vientisu paviršiaus padengimu. Ši makrostruktūra atrodo kaip fraktalinė struktūra, panaši į "hifą", kuri buvo pastebėta elektrodo paviršiuje. Tačiau visų šių minėtų paviršiaus savybių negalima pastebėti ant kontrolinio elektrodo, kur aiškiai matyti tik po juo esančios grafito plokštelės.

6.3.2. Poli-CzO/GOx, poli-CzS/GOx modifikuotų elektrodų elektrocheminis įvertinimas

Elektrocheminiai eksperimentai buvo atliekami siekiant patikrinti krūvio perdavimo tarp GOx-kofaktoriaus ir puslaidininkinių poli-CzS arba poli-CzO sluoksnių mechanizmą ir efektyvumą, paviršiaus aktyvumą ir difuzijos greičio koeficientą. Tačiau dėl didesnio laidumo ir mažesnio poli-CzS jonizacijos potencialo (5,58 eV, palyginti su 5,24 eV) buvo stebimas tik ITO/polis-CzS/GOx elektrodo CT iš GOx (1c pav.). CV parodė, kad ITO/poly-CzS/GOx pagrindu sukurto elektrodo KT yra kvaziteisminė ir kontroliuojama paviršiaus. Be to, po imobilizacijos nepridengtame ITO elektrode nepastebėta jokių naujų signalų CVs ir FT-IR spektruose. Pagal CV smailės formą buvo įvertintas krūvio (elektronų arba skylių) perdavimo efektyvumas. Jis yra monosluoksnio homogeniškumo diagnostinis rodiklis ir gali būti įvertintas pagal smailės pilnąjį plotį ties puse maksimumo (FWHM), kaip aprašyta 1 lygtyje:

$$n = \frac{3.53\ RT}{FWHM \times F} = \frac{90.6\ mV}{FWHM} \qquad (1)$$

kur n - krūvio nešėjų (elektronų arba skylučių) skaičius, R - idealiųjų dujų konstanta, T - absoliutinė temperatūra, o F - Faradėjaus konstanta.

FWHM reikšmės gali būti didesnės arba mažesnės už teorines FWHM reikšmes, nes tai susiję su gretimų įkrautų rūšių elektrostatiniais efektais. Remiantis elektrocheminiais matavimais, buvo stebimas kvazigrįžtamasis paviršiaus valdomas elektrocheminis procesas, o apskaičiuotas pilnas plotis ties puse maksimalaus smailės aukščio (FWHM) yra 115 ir 120 mV atitinkamai ITO/poli-CzS/GOx sistemos teigiamiems ir neigiamiems signalams, o tai atitinka vienu elektronu (arba viena skyle) pagrįstą krūvio pernašos procesą. Be to, oksidacijos smailės, užregistruotos esant pH 4,0 ir 7,2, kai nuskaitymo greitis 10 mV s^{-1} , buvo pastebėtos 181 mV ir 76 mV prieš Ag/AgCl (4,82 eV ir 4,71 eV), o tai atitinka grįžtamąją (monoelektroninę) $FADH_2$ oksidaciją į $FADH_2^+$. Siekiant išsamiau įvertinti grįžtamojo krūvio pernašos reiškinį, buvo užfiksuoti CV, esant skirtingiems skenavimo greičiams, esant pH 4,0 ir 7,2 (8 pav.).

Paviršiaus aktyvumas Γ (aprėptis), kuris šioje sistemoje yra ant elektrodo paviršiaus imobilizuoto GOx aktyvumas, buvo nustatytas pagal I ir ν tiesės nuolydį, naudojant 2 lygtį:

$$\Gamma = \frac{4IRT}{n^2F^2A}\nu \qquad (2)$$

kur I - didžiausia srovė, ν - potencialo svyravimo greitis, A - elektrodo plotas. ITO/poli-CzS/GOx paviršiaus aktyvumas esant pH 4,0 ir 7,2 be gliukozės buvo apskaičiuotas pagal tiesinės oksidacijos srovės priklausomybės nuo švytuoklės greičio nuolydį, kuris buvo apie 3×10^{-12} mol cm^{-2} . Apskaičiuojant teorinį paviršiaus padengimą, buvo pasiūlyta, kad GOx monomero skersmuo būtų 65 Å, o užpildymo santykis - 0,8. Tada apskaičiuota, kad teorinė GOx molekulių paviršiaus koncentracija elektrodo paviršiuje (elektrodo padengimas GOx) yra 4×10-12 mol cm-2. Ši vertė atitinka eksperimentinę G vertę. Labai panašus ITO/poli-CzS/GOx elektrodo aktyvumas buvo stebimas ir po vieno mėnesio laikymo +4 °C temperatūroje buferiniame tirpale. Todėl manome, kad skylėmis grįstas krūvio pernešimas iš GOx į organinį puslaidininkį apsaugojo fermentą nuo oksidacinės pažaidos.

Siekiant nustatyti efektyvų difuzijos koeficientą, taikyta Randleso ir Ševciko 3 lygtis:

$$I = 0.4463\, n\, A\, F\, C\sqrt{\frac{nF\nu D_{eff}}{RT}} \qquad (3)$$

kur C - fermento koncentracija paviršiuje. Tada Deff buvo apskaičiuotas pagal tiesinės priklausomybės I nuo √ν nuolydį 10-100 mV s-1 skenavimo greičių intervale. Fermento koncentracija monosluoksnyje buvo įvertinta atsižvelgiant į fermento (GOx) paviršiaus padengimą ir storį (h) kaip $C = \Gamma \times h^{-1}$. Šį storį sudaro žymės ilgis 15 Å ir fermento monomero skersmuo 65 Å, apskaičiuotas pagal GOx (*Aspergillus niger)* monokristalo rentgeno spindulių analizę. [76]. Greičio konstantos pagal difuzijos koeficientų duomenis apskaičiuotos taikant 4 lygtį. Difuzijos koeficientų ir greičio konstantų santrauka pateikta 1 lentelėje.

$$D_{CT} = \frac{1}{6}\, h_{\mathrm{CT}}^2 k_{CT} \qquad (4)$$

koeficientai buvo apskaičiuoti pagal Randleso-Sevciko lygtį, o C(glu)= 15 mM.

Apskaičiuotos monoelektroninės oksidacijos ir redukcijos CT greičio konstantos yra atitinkamai 70±10 s^{-1} ir 150±20 s^{-1} , kai pH 4,0, ir 130±20 s^{-1} ir 160±20 s^{-1} , kai pH 7,2. Palyginimui, ankstesniuose pranešimuose buvo išmatuoti FAD redokso sistemos (t. y. redukcijos potencialai yra apie -0,3 V prieš Ag/AgCl) elektronų pernašos CT greičiai: 0,1 s^{-1} greičio konstantos ant pliko sidabro elektrodo (Wen, Ye ir Zhou 1997), 0,03 s^{-1} ant trumpo savaime susiformavusio monosluoksnio ant aukso paviršiaus (J. Liu, Agarwal ir Varahramyan 2008), 1,6 s^{-1} ant boru legiruotų anglies nanovamzdelių modifikuoto elektrodo [79] ir 350 s^{-1} ant aminofenolio nitriloacto rūgštimi modifikuoto stiklinės anglies elektrodo. (Demin ir Hall 2009) buvo nustatyti. Be to, Willneris ir kt. [81] pranešė apie metodą, naudojamą GOx monosluoksniui ant Au elektrodo surinkti, apo-baltymą atstatant pirolochinolino chinino/FAD monosluoksniu, kurio dėka gaunamas funkcionalizuotas elektrodas, skirtas gliukozės elektrooksidacijai su precedento neturinčia didele greičio konstanta - apie 600 s^{-1} .

Ištirta ir palyginta pH įtaka ITO/poli-CzS/GOx struktūros greičio konstantoms esant pH 4,0 ir 7,2. Pirma, oksidacijos ir redukcijos paviršiaus aktyvumas esant pH 7,2 ir 4,0 yra labai panašus, t. y. apie 3×10^{-12} mol cm^{-2} . Antra, atsižvelgiant į gliukozės įtaką krūvio perdavimui, ITO/poli-CzS/GOx-elektrodas, esant pH 4,0 ir 7,2, buvo tiriamas naudojant palyginti didelę gliukozės koncentraciją - 15 mM. Apskaičiuota, kad oksidacijos ir redukcijos greičio konstantos, esant pH 7,2, statistiškai yra tos pačios vertės kaip ir užregistruotos panašioje sistemoje be gliukozės (1 lentelė, 3 ir 4 įrašai), nes tai yra krūvio (skylės) perdavimo procesas iš HTPS į kofaktorių. Tačiau sistemoje su gliukoze, esant pH 4,0, pastebėta nauja negrįžtamoji smailė ties maždaug 800 mV (9c pav.). Pirmasis signalas ties maždaug 180 mV (pradžia) rodo kofaktoriaus oksidaciją į radikalo katijoną per skyles iš organinio puslaidininkio. Antrąjį signalą, esantį maždaug 800 mV, galima priskirti FAD ir gliukozės komplekso oksidacijai iki gliukono rūgšties ir FAD (žr. toliau). Pagal [82], antros eilės gliukozės oksidacijos greičio konstanta, esant GOx, yra apie 3×10^4 M^{-1} s^{-1} . Todėl apskaičiuota, kad šio proceso pseudopirmosios eilės greičio konstanta, esant 15 mM gliukozės, yra 450 s^{-1} . Mažesnė redukcijos proceso k_{CT} , esant pH 4,0, nei gliukozės oksidacijos, rodo, kad gliukozė gali sušvelninti fermento KT kinetiką. Neseniai Bartlett ir Al-Lolage [83] išanalizavo mokslinius straipsnius, kuriuose aprašomi elektrocheminiai biojutikliai, pagrįsti gliukozės oksidazės (GOx), kuri buvo išgryninta skirtingų tiekėjų iš skirtingų GOx gaminančių mikroorganizmų, pagrindu. Jie numatė, kad ciklinėse voltamperogramose esančios redokso smailės, kurios paprastai

priskiriamos GOx krūvio perdavimui, kartais atsiranda dėl laisvo FAD ir galbūt dėl katalazės ir (arba) kitų priemaišų, esančių tiekiamame komerciniame fermente, kuris taip pat adsorbuojasi ant elektrodo paviršiaus. Buvo pranešta, kad imobilizuotos katalazės atveju stebimas labiau neigiamas akivaizdus katalitinės redukcijos smailės taškas (Salimi, Noorbakhsh ir Ghadermarz 2005) palyginti su mūsų naujausiais tyrimais. Laisvas FAD buvo išplautas taikant griežtą GOx modifikuotų elektrodų plovimo procedūrą. Be to, negalima atmesti galimybės, kad dalis laisvo FAD kofaktoriaus išsiskiria iš lėtai disocijuojančio GOx ir gali būti oksiduojamas/redukuojamas elektrodo paviršiuje, nes kofaktorius - FAD - su apo-GOx jungiasi nekovalentiškai, todėl šis ryšys yra palyginti silpnas ir holo-GOx linkęs lėtai disocijuoti į apo-GOx ir FAD.

ITO/poli-CzS/GOx elektrodo voltamperometrinė elgsena buvo tiriama ciklinės voltamperometrijos metodu potencialų diapazone nuo -200 mV iki +1000 mV, esant skirtingoms gliukozės koncentracijoms (1-15 mM) buferiniame tirpale, kurio pH 4,0 ir kuriame yra ištirpusio deguonies (9a pav.). Pridėjus gliukozės, apskaičiuotas oksidacijos (esant 800 mV) pikų srovių skirtumas. Pastebėta plati tiesinė smailės srovės tankio ir gliukozės koncentracijos nuo 2 iki 15 mM priklausomybė (9a pav., intarpas); oksidacijos srovių koreliacijos koeficientas 0,982. Be to, iš tiesinio priderinimo nuolydžio nustatyta, kad jautrumas gliukozei yra 0,64±0,03 μA mM^{-1} cm^{-2} . Pagal [85], apskaičiuota, kad antros eilės $FADH_2$ oksidacijos greičio konstanta GOx oksiduojant deguonimi esant žemam pH yra 1,6×106 M^{-1} s^{-1} . Todėl apskaičiuota, kad pseudo pirmos eilės oksidacijos greičio konstanta esant ~0,2 mM vandenyje ištirpusio O2 yra ~300 s-1 . Ši greičio konstanta yra šiek tiek didesnė, bet tos pačios eilės kaip ir $FADH_2$ oksidacijos, kurią vykdo CzS, greičio konstanta. Šiuo atveju ITO/poli-CzS/GOx-elektrodo jautrumas yra vidutinis, nes deguonis konkuruoja su CzS oksiduojant $FADH_2$.

Remiantis gautais rezultatais, buvo pasiūlytas gliukozės oksidacijos mechanizmas per skylutes ir nedalyvaujant ištirpusiam deguoniui (9b pav.). Pirmiausia skylutės iš elektrodo grįžtamuoju būdu oksiduoja $FADH_2$ kofaktorių į radikalo katijoną - $FADH_2^+$.

Todėl CV stebimos oksidacijos ir redukcijos smailės atitinkamai ties +400 mV ir +100 mV (8a pav.). Antrasis žingsnis - nukleofilinis gliukozės prisijungimas prie šio radikalo katijono ($FADH_2^+$) ir pereinamosios būsenos (TS) susidarymas. Neseniai panaši FAD ir gliukozės komplekso TS buvo sėkmingai identifikuota naudojant masių spektrometrijos [86]. Galiausiai susiformavusi TS oksiduojama antrosios skylės iš elektrodo, kad susidarytų pradinis $FADH_2$ ir gliukono rūgštis.

6.3.3. Poli-TPA/GOx, poli-CzEt/GOx, poli-CzPh/GOx modifikuotų elektrodų elektrocheminis įvertinimas

Gauti elektrodai buvo modifikuoti plonu imobilizuoto GOx sluoksniu, jį susiejant glutaraldehidu, ir išbandyta jų reakcija į gliukozę; matavimo rezultatai pateikti 10 paveiksle. Į PBS tirpalą pridėjus gliukozės, visuose tirtuose elektroduose stebimas nuolat didėjantis bendras srovės atsakas. Nuo 0,50 mM ir didesnės gliukozės koncentracijos CzPh polimeru (poly-CzPh) modifikuotame elektrode, 1,0 mM ir didesnės - CzEt polimeru (poly-CzEt) modifikuotame elektrode, voltamperogramose pastebėtas nuolat didėjantis ir apibrėžtas oksidacijos smailėmis pagrįstas jutiklio atsakas, esant maždaug 0,15 V potencialui prieš Ag/AgCl. Atsakymas įsisotina esant didesnei gliukozės koncentracijai. Smailųjį atsaką taip pat buvo galima pastebėti naudojant polimerizuotą TPA (poli-TPA) modifikuotą elektrodą, tačiau elektrodo charakteristikos skyrėsi. Oksidacijos smailė, stebima CV, buvo gerokai labiau išsklaidyta ir mažiau apibrėžta, todėl bendras signalo ir triukšmo santykis buvo mažesnis ir buvo stebimas proporcingas potencialo poslinkis, priklausomai nuo gliukozės koncentracijos. Deja, chronoamperometrijos metodas nesuteikė esminės informacijos bandant įvertinti srovės tankio kitimą priklausomai nuo gliukozės koncentracijos, nes buvo stebimas per didelis srovės triukšmo lygis.

Gauti matavimo duomenys, kai smailės padėtis yra 0,15 V, palyginti su Ag/AgCl, buvo panaudoti 11 paveiksle pateiktiems duomenims gauti. Tiek poli-CzPh/GOx, tiek poli-CzEt/GOx elektrodų atsakas atrodo prisotintas esant maždaug 5 mM gliukozės koncentracijai. Nors poli-CzP/GOx elektrodo srovės tankis nuolat didėjo kartu su didėjančia gliukozės koncentracija, nepavyko gauti pakankamai duomenų taškų kalibracinei kreivei sudaryti. Netikėtai, reaguojant į gliukozės koncentraciją, poli-TPA/GOx elektrodui būdinga smailė pasižymėjo žymiu potencialo nuokrypiu. Padidinę gliukozės koncentraciją nuo 0,5 iki 14 mM, išmatavome 15 mV stebimo CV oksidacijos smailės potencialo skirtumą. Tačiau smailės padėties nepavyko tiksliai nustatyti esant mažesnei nei 0,5 mM koncentracijai visuose elektroduose. Kaip matyti 10 pav. 10, srovės atsakas į skirtingas gliukozės koncentracijas poly-CzEt/GOx, poly-CzPh/GOx ir poly-TPA/GOx elektrodų atrodo lygiagretus, todėl didžiausias išmatuojamas skirtumas šioje srityje visada būtų ties stebimu smailės tašku. Be to, preliminarūs bandymai su galimomis trukdančiomis medžiagomis, tokiomis kaip askorbo rūgštis, šlapimo rūgštis, laktozė, sacharozė ir vandenilio peroksidas, rodo, kad GOx, kaip specifinio katalizatoriaus, ir žemas 0,15 V darbinis potencialas nerodė jokio signalo apie šių trukdančių medžiagų buvimą.

Aptikimo ribos (LOD) buvo nustatytos pagal mažos koncentracijos kalibravimo kreivių tiesiškumo intervalą pagal (5) lygtį:

$$LOD = \frac{3.0\,\sigma}{slope} \qquad (5)$$

kur σ yra atsako standartinis nuokrypis. Vidutinis jautrumas buvo įvertintas kaip srovės tankio ir gliukozės susitraukimo nuolydis, kuris buvo nustatytas pagal kalibravimo kreives. Buvo apskaičiuotos 240 ir 230 μM LOD vertės, imant signalo ir triukšmo santykį 3,0, ir atitinkamai 3,3 ir 3,7 μA cm^{-2} mM^{-1} biojutiklių, kurių pagrindą sudaro poli-CzEt ir poli-CzPh aktyvieji sluoksniai, vidutiniai jautrumo rodikliai.

Paėmę srovės tankio skirtumą esant stebimai maksimaliai įtampai ir baziniam srovės tankiui (J0 - srovės tankis esant 0 mM gliukozės), nustatėme elektrodo jautrumą gliukozei. Gauta kalibracinė kreivė atitinka Michaelio-Menteno kinetikos priklausomybę. Michaelio konstantos (KM) vertės buvo apskaičiuotos taikant Lineweaver-Burk metodą (6 lygtis) [87,88]:

$$\frac{1}{J} = \frac{1}{J_{max}} + \frac{K_M}{J_{max}C} \qquad (6)$$

kur J_{max} - didžiausias srovės tankis, o C - gliukozės koncentracija. 11b paveiksle parodyta tiesinė visų elektrodų substrato koncentracijos taškų priklausomybė. Be to, apskaičiuota, kad Michaelio konstantos poli-CzPh/GOx, poli-CzEt/GOx poli-CzEt ir poli-TPA/GOx elektrodų atveju yra atitinkamai 1,1, 2,0 ir 1,4 mM. Šios konstantos yra vienu laipsniu didesnės už gimtojo GOx Michaelio konstantą, kuri ištirpusio deguonies atžvilgiu yra apie 0,3 mM.[89] ir tai rodo, kad didžiausias greitis mūsų atveju buvo pasiektas esant didesnei substrato koncentracijai.

Tiriant GOx aktyvumą ant elektrodų paviršių, aktyvumas Γ (aprėptis) buvo nustatytas pagal I ir ν tiesės nuolinkį, naudojant 3 lygtį:[75]

$$I = \frac{n^2F^2A\,\Gamma}{4RT}\nu \qquad (7)$$

kur n - reakcijoje dalyvaujančių krūvių skaičius, A (cm^2) - elektrodo plotas, F - Faradėjaus konstanta, Γ (mol cm^{-2}) - reaguojančiųjų rūšių paviršinis tankis / aktyvumas, ν (V s^{-1}) - potencialo svyravimo greitis, R - idealiųjų dujų konstanta, T - absoliutinė temperatūra. Norint apskaičiuoti krūvio skaičių, buvo įvertinta CV smailės forma. Ji parodo sluoksnių homogeniškumą, kurį

galima įvertinti pagal pilnąjį plotį ties puse smailės aukščio (FWHM), kaip aprašyta 8 lygtyje:[90]

$$n = \frac{3.53\ RT}{FWHM \times F} = \frac{90.6\ mV}{FWHM} \qquad (8)$$

Šiuo atveju apskaičiuota, kad visoms elektroaktyviosioms medžiagoms n yra maždaug 1. Reaguojančiųjų rūšių paviršinį tankį galime apskaičiuoti pagal srovės matavimo vertę numatomoje smailės padėtyje esant 0,15 V įtampai prieš Ag/AgCl. Palyginti su ankstesniame darbe gautais rezultatais, gautas paviršiaus tankis yra maždaug 10^{-9} -10^{-10} mol cm^{-2} , kuris yra gerokai didesnis (trimis eilėmis), palyginti su GOx monosluoksniui apskaičiuotu tankiu (t. y. maždaug 10^{-12} mol cm^{-2}). Tokį didelį padidėjimą galima pagrįsti tuo, kad taikant kitokį imobilizavimo metodą, t. y. adsorbuotas GOx molekules ant paviršiaus susiejant kryžminiais saitais, nebesusidaro struktūrizuotas paviršinis monosluoksnis iš GOx, o elektrodų paviršiuje susidaro tankūs netvarkingi GOx aglomeratai.

Gauti suprojektuoto biojutiklio, pagrįsto karbazolo darinių biokompozitu, analitiniai parametrai buvo palyginti su kai kuriais kitais anksčiau aprašytais gliukozės biojutikliais, pagrįstais GOx, kai buvo nustatytas tiesinis srovės - koncentracijos diapazonas esant teigiamam potencialui prieš Ag/AgCl, o duomenys pateikti 2 lentelėje. Nustatytas linijinis diapazonas, jautrumas ir aptikimo ribos vertės poli-CzEt/GOx ir poli-CzPh/GOx pagrindu sukurtiems biojutikliams išliko panašios į kitų literatūroje aprašytų elektrocheminių metodų (žr. 2 lentelę). Palyginus mūsų paruoštus biojutiklius, nustatyta, kad karbazolų pagrindu pagamintų elektrodų jautrumas yra didesnis nei trifenilamino pagrindu pagamintų elektrodų, nes šie elektropolimerai turi labiau konjuguotą aromatinę sistemą, todėl krūvininkų nešiklių judrumas šiuose elektropolimeruose yra didesnis nei poli-TPA. Be to, aptikimo riba (LOD) rodo mažiausią analitės kiekį, kurį galima aptikti biojutikliais. Šios LOD vertės yra lygios deguonies koncentracijai ore prisotintame vandeniniame tirpale - apie 200 μM. Todėl deguonies molekulės konkuruoja dėl redukuoto kofaktoriaus ($FADH_2$) oksidacijos, kurią vykdo krūvio nešėjas (skylė) iš elektrodo į/iš GOx. Nors šie trečiosios kartos biojutikliai, pagrįsti skylutes pernešančiomis medžiagomis, pasižymi puikiu stabilumu, jų jautrumas mažas, o linijinis diapazonas vidutinis, nes krūvininkų tuneliavimas link elektrodo yra ribojantis viso proceso etapas šiuose biojutikliuose.[91]

6.3.4. Citochromo c ir chlorofilo a, kaip natūralių gliukoze maitinamų EBFC redokso mediatorių, įvertinimas

Srovės stabilumas, didžiausia išėjimo galios vertė ir didelė elektromagnetinė jėga yra trys pagrindinės biokuro elemento savybės [92]. Šiame tyrime pirmiausia buvo bandoma nustatyti sistemą, kuri generuoja pakankamą biokuro elemento galią. Taigi biokuro elemento galia ir paviršinis galios tankis buvo apskaičiuoti taikant Omo dėsnį ir galios apskaičiavimo formulę pagal grafito elektrodo paviršiaus plotą. Viso elemento OCP buvo apskaičiuotas pagal šią 9 lygtį:

$$OCP = (E_k - E_{ref}) - (E_a - E_{ref}) \quad OCP = \frac{(E_k - E_{ref})}{(E_a - E_{ref})} \qquad (9)$$

kur E_k yra katodo potencialo vertė, o E_a yra anodo potencialo vertė.

EFC galios tankis buvo apskaičiuotas pagal lygtį $P = U^2/R$ ir padalytas iš geometrinio paviršiaus ploto.

Galios tankio skaičiavimų rezultatai pateikti 12 paveiksle. Didžiausią galios tankį generavo sistema $EBFC_{CA}$. Šios sistemos paviršinis galios tankis yra apie 2500-4000 nW/cm^2 (12 pav.). Kitų sistemų $EBFC_{CC}$, $EBFC_{ChV}$ ir $EBFC_{Hep}$ sukurto galios tankio vertės buvo maždaug 10 kartų mažesnės. Kaip ir tikėtasi, sistemos be jokio redokso mediatoriaus generuojamas galios tankis buvo mažiausias. Pastebėti tam tikri skirtumai tarp anglies kompozito rezistoriaus apkrovos verčių, naudotų didžiausiam galios tankiui gauti. Didžiausias galios tankis, kurį generavo sistema su redokso tarpininku chlorofilu a, užfiksuotas esant 125 mV biokuro elemento potencialui. Galios tankis pavyko pasiekti palyginti didelę vertę sistemoje, kurioje naudojamas heparinas, esant 35 mV potencialui. Kitų biokuro ląstelių $EBFC_{CC}$ ir $EBFC_{ChV}$, kurių pagrindą sudaro citochromai ir ultragarsu suardytų *Chlorella vulgaris* ląstelių supernatantas, generuojami potencialai buvo gana panašūs, tačiau $EBFC_{CC}$ potencialas buvo 80 mV, o $EBFC_{ChV}$ - 143 mV.

Panašios sistemos su redokso substratu chlorofilu a, naudojant vandens valymo dumblo ir vaisių sulčių nuotekų mišinį 3:1, pasiektas 2397 nW/cm^2 galios tankis. [93]. Kitame tyrime didžiausias galios tankis buvo lyginamas skirtingais metų laikais ir pavasarį buvo pasiekta 5700 nW/cm^2 galios tankio vertė, o vasarą - tik 110 nW/cm^2 MBFC, naudojant biomasę su Chlorofilu a mikrobinio kuro elemente [94]. Biokuro elementų sistema sukūrė 1510 nW/cm^2 galios tankio vertę, kai gliukozės koncentracija sintetinėse nuotekose buvo 20 g/l. [95]. Biokuro elementų technologija naudojama nuotekoms biologiškai

nusausinti naudojant *Chlorella vulgaris,* o bioelektrogeninis aktyvumas padidėjo nuo 2317 nW/cm^2 iki 32767 nW/cm [296].

Apibendrinant galios tankio vertinimą, galima pažymėti, kad chlorofilo a substratas $EBFC_{CA}$ yra geriausias pasirinkimas iš įvertintų redokso mediatorių, naudojamų kuriant EBFC.

Gliukozė laikoma idealiu ekologišku kuru tiesioginio tipo biokuro elementams. Gliukozės privalumas yra tas, kad ji gali būti gausiai gaminama tiek iš natūralių augalų, tiek iš pramoninių procesų. Gliukozės koncentracijos poveikis sistemos galios tankiui ir elektromagnetinei jėgai buvo išmatuotas į penkias įvertintas sistemas pridėjus tam tikrą gliukozės kiekį. Didinant gliukozės koncentraciją nuo 0,10 ir 100 mM (13 pav.), sumažėjo biokuro elemento potencialas, o chlorofilo pagrindu veikiančio biokuro elemento atveju, padidinus gliukozės koncentraciją iki 100 mM, sistema beveik negeneruoja galios - paviršinis galios tankis yra labai artimas 0 nW/cm^2 . Kai $EBFC_{CC}$ sistemoje kaip redokso mediatorius buvo naudojamas citochromas c (13 pav.), didėjant gliukozės koncentracijai generuojama galia didėjo. Nors didžiausias galios tankis yra mažesnis nei $EBFC_{CA}$ ar $EBFC_{Ch}$ sistemose ir siekia apie 160 nW/cm^2 , šios sistemos signalas didėjo, kai didėjo gliukozės kiekis elektrolito tirpale, ir tokia sistema buvo daug stabilesnė.

Kontrolinis tyrimas atliktas tik su poliruotu grafito elektrodu - didžiausias paviršinis galios tankis buvo 24,71 nW/cm^2 , kai sistemoje nebuvo gliukozės. Didėjant gliukozės koncentracijai, mažėja biokuro elemento galios tankis. Galima teigti, kad šie redokso mediatoriai didina biokuro elementų efektyvumą, nes jie generuoja daug didesnę maksimalią paviršinę galią.

13 pav. lyginamas visų biokuro elementų galios tankis (13A pav.) ir elektromagnetinė jėga (13B pav.), kai gliukozės koncentracija tirpale yra 10 mM. Įtampos sumažėjimas paprastai registruojamas, kai padidėja išorinės grandinės apkrova [97]. Nors tokių biokuro elementų galios tankis paprastai nurodomas pagal elektrodo aktyviojo paviršiaus plotą, o ne tūrį, kaip dažnai būna daugelio kitų energijos šaltinių atveju, nes pažangesnių skaičiavimų neįmanoma atlikti dėl problemų, susijusių su aktyviojo paviršiaus skaičiavimu visame elektrodo tūryje.

6.3.5. Tarpininkaujant EBFC atliekamas ciklinės voltamperometrijos įvertinimas

Vertinant ciklinės voltamperometrijos rezultatus, daugiausia dėmesio buvo skiriama potencialo vertei, kuriai esant ciklinėje voltamogramoje (CV) pastebimas oksidacijos smailė. Šio eksperimento metu potencialas buvo

keičiamas gana plačiame potencialo verčių diapazone, t. y. potencialas buvo keičiamas nuo -1,5 V iki +1,5 V, kai skenavimo greitis buvo 50 mV/s (14 pav.). Potencialo keitimas tokiame plačiame elektrodų potencialų diapazone reikalavo labai kruopštaus ištirpusio deguonies pašalinimo degazuojant elektrocheminę sistemą azoto srautu. Pastebėta, kad sistemoje be jokio redokso tarpininko (14A pav.) nebuvo pastebėtas aiškiai išsiskiriantis oksidacijos smailė. Tačiau šioje sistemoje po jo sekė šiek tiek išreikštas srovės tankio padidėjimas esant 1,1 V potencialo vertei. Srovės tankio pokyčiai atitinka tiesinę koreliaciją, kurios $R^2 = 0,95$ ir $y = 0,11x + 1,85$. Įvertintose EBFC sistemose srovės tankis buvo gana skirtingas. $EBFC_{CC}$ (14B pav.) pastebėtas oksidacijos maksimumo potencialo vertės poslinkis. Didėjant gliukozės koncentracijai, stebėta potencialo vertė pasislinko į didesnes potencialo vertes. Potencialo vertės pasislinko nuo 0,63 V iki 0,77 V.

Tuo tarpu srovės tankio priklausomybės nuo gliukozės koncentracijos šioje sistemoje nepastebėta. Tokio potencialo vertės poslinkio nepastebėta jokioje kitoje vertintoje sistemoje. Vykstant potencialo ciklui, kai gliukozės koncentracija padidėjo, srovės tankio sumažėjimas buvo stebimas $EBFC_{CA}$ (14C pav.) ir $EBFC_{Hep}$ (14E pav.). $EBFC_{ChV}$ nepastebėta jokių srovės ar potencialo priklausomybių.

Kai kurie tyrėjai [92] atskleidė netinkamų - parazitinių O_2 reakcijų - atsiradimą. Mokslininkų grupė aprašė, kad, priklausomai nuo eksperimentinių sąlygų, parazitinės reakcijos gali atsirasti naudojant itin neigiamo arba teigiamo redokso potencialo redokso mediatorius. O_2 redukcija redokso polimeruose, kuri stebima esant žemo potencialo bioanodams, arba kai kurių kitų elektroaktyviųjų rūšių oksidacija, kuri stebima esant aukštam potencialui, taikomam biokatodams, yra nepageidaujami reiškiniai.

Potencialo, kuriam esant vyksta oksidacija visose įvertintose sistemose $EBFC_{CC}$, $EBFC_{CA}$, EBFC ,$_{ChV}$ ir $EBFC_{Hep}$, vertės apibendrintos 3 lentelėje. Remiantis 3 lentelėje pateiktais duomenimis, potencialo, kuriam esant vyksta oksidacija, vertė sumažėjo visose sistemose.

6.3.6. Chronoamperometrija pagrįstas tarpininkaujamų EBFC vertinimas

Elektrocheminės sistemos, kaip antros kartos biojutiklio, charakteristikos buvo tiriamos chronoamperometrijos metodu. $EBFC_{CC}$, $EBFC_{CA}$, $EBFC_{ChV}$, ir $EBFC_{Hep}$ reagavo į gliukozės pokyčius esant pastoviai būsenai. Šis poveikis gerai matomas iš grafikų (15 pav.), kad naudojant $EBFC_{ChV}$, stebimas pastovus srovės kritimas, o sistemos pusiausvyrą sunku stabilizuoti.

Naudojant $EBFC_{Hep}$, stebimas pastovus srovės didėjimas. Tokios sistemos nelaikomos pakankamai stabiliomis, kad būtų galima sukurti biojutiklį.

Elektrodai $EBFC_{CA}$ ir $EBFC_{CC}$ buvo tinkami EBFC kūrimui. Nustatyta, kad didinant gliukozės kiekį sistemoje, srovės tankis didėja, o pusiausvyra pasiekiama greitai. Dėl labai kintančių bazės lygių sunku tiesiogiai įvertinti ir palyginti sistemas pagal chronoamperometrijos duomenis. Matavimų rezultatai, pateikti 16 paveiksle, grindžiami 15 paveiksle pateiktais duomenimis, nes, matuojant srovės tankio pokytį, galima lengviau palyginti tirtų sistemų efektyvumą. Visos bandytos sistemos reaguoja į gliukozės pridėjimą, palaipsniui didinant gliukozės koncentraciją stebimas srovės tankio pokytis padidėja beveik viena eile, o didžiausias bendras padidėjimas stebimas $EBFC_{CC}$, kai ji prisotinta gliukoze, srovės tankio pokytis, palyginti su kontroline sistema, padidėjo 15 kartų. $EBFC_{ChV}$ taip pat rodo didelį santykinį srovės tankio pokytį, daugiau nei eilės tvarka, tačiau atrodo, kad ji greitai pasisotina, nes sumažėjęs atsako diapazonas pasisotina esant 20 mM/L gliukozės, o visos kitos bandytos sistemos rodė srovės tankio pokytį visame bandytame 0-100 mM/L gliukozės diapazone.

Visi mėginiai atitinka tikėtinas Michaelio-Menteno kinetikos kreives. Taip pateikti $EBFC_{Hep}$ ir "kontroliniai" mėginiai yra netikslus vaizdas dėl jų reakcijos pobūdžio, kaip matyti iš chronoamperometrijos duomenų. Tiek $EBFC_{Hep}$, tiek kontrolinis mėginys nepasiekia pusiausvyros ir nuolat didėja.

Santykinis srovės tankio pokytis apskaičiuotas pagal 10 lygtį:

$$log10\,\frac{J_i - J_{i-1}}{J_0 * 100\%} \qquad (10)$$

kur J_i - srovės tankis įpylus gliukozės, J_{i-1} - srovės tankis prieš įpylus gliukozės ir J_0 - srovės tankis, išmatuotas eksperimento pradžioje.

Naudojant citochromus $EBFC_{CC}$, buvo gautas didžiausias santykinis srovės atsakas į tolesnį gliukozės koncentracijos didinimą. Be to, iš 17 pav. pastebėta, kad sistema išlaiko didelį jautrumą visame vertinamame koncentracijos diapazone, rodydama registruotos srovės padidėjimą iki 50 mM gliukozės, o toliau didinant srovės atsaką palaipsniui mažėja. Didinant gliukozės koncentraciją nuo 20 mM iki 50 mM pastebėtas 167 % registruotos srovės padidėjimas, toliau didinant koncentraciją iki 50 mM - 80 %, o atsako greitis visame tiriamame koncentracijos intervale atitinka varpo formos kreivę. Didelis santykinis jautrumas rodo tolesnio iteracinio tobulinimo galimybę, nes šiuo metu sistema stabdoma tik dėl mažų absoliučių signalo srovės verčių.

$EBFC_{CA}$ taip pat pasižymėjo santykinai linijiniu srovės atsaku į gliukozės koncentracijos didėjimą visame diapazone.

$EBFC_{ChV}$ pasižymėjo stipriu atsaku žemutinėje koncentracijos intervalo dalyje, o esant didesnei nei 20 mM koncentracijai - plokščiajuosčiu atsaku. $EBFC_{Hep}$ ir kontrolinių mėginių atsako ir triukšmo santykis buvo palyginti mažas, abu mėginiai stipriai reagavo labai ribotame koncentracijos diapazone apatinėse tiriamojo diapazono ribose.

6.3.7. Bakterijų *Rhizobium anhuiense* kaip potencialaus biokatalizatoriaus mikrobiologiniams biodegalų elementams kurti įvertinimas

Zeta potencialo matavimai buvo atliekami siekiant įvertinti ląstelių paviršiaus elektrinį potencialą, kuris priklauso nuo aplinkos sąlygų [98]. Daugumos gramteigiamų bakterijų paviršius, esant neutraliam pH, dažniausiai yra neigiamai įkrautas. Tokį poveikį lemia neigiamai įkrautos lipopolisacharidų sudėtyje esančios fosfatinės ir karboksilatinės grupės y ir subalansuojamas priešingai įkrautais priešpriešiniais jonais, esančiais supančioje terpėje, todėl susidaro dvigubas elektrinis sluoksnis.

Menadionas (MQ) yra redokso ciklo junginys, kurio empirinė formulė yra $C_6\ H_4\ (CO)_2\ C_2\ H(CH_3\ )$, jis taip pat žinomas kaip vitaminas K_3, ir yra 1,4-naftochinono analogas, turintis papildomą metilo grupę. Menadionas yra prooksidantas, generuojantis superoksido anijonų radikalus. *Rizobijos,* veikiamos menadiono, reaguoja inaktyvuodamos dėl šio poveikio susidariusius laisvuosius anijonų radikalus [62].

Šiame tyrime maža menadiono koncentracija veikia kaip stresorius, todėl jis nenaikina bakterijų, bet stiprina jų atsparumą ir didina krūvio perdavimo efektyvumą po adaptacijos laikotarpio. Esant mažesnei nei 1 mM jonų koncentracijai, zeta potencialas nepriklausė nuo jonų stiprumo (19A pav.), o esant menadionui bakterijos pasižymėjo nedideliu zeta potencialo svyravimu ir šis poveikis nepriklausė nuo inkubacijos trukmės. Kai jonų koncentracija viršijo 1 mM, visų mėginių zeta potencialas didėjo kartu su didėjančia jonine jėga. Nepastebėta reikšmingo zeta potencialo skirtumo tarp įvairių mediatorių buvimo ar nebuvimo ir inkubacijos trukmės. Buvo įvertinta pH įtaka *Rhizobium anhuiense* zeta potencialui. Atsižvelgiant į tai, kad natūrali bakterijų gyvenamoji aplinka yra ~pH 7,0, o dėl medžiagų apykaitos procesų ir įvairių metabolitų sekrecijos pH dažnai pakinta į rūgštinę pusę, tolesni tyrimai atlikti pH intervale nuo 5,0 iki 8,0. Tyrimai atskleidė, kad šie pH pokyčiai neturėjo didelės įtakos bakterijų zeta potencialui. Zeta potencialas išliko neigiamas plačiame pH diapazone (19B pav.). Tai atskleidžia, kad pH

kitimas neturi įtakos bakterijų ir anodo elektrostatinei sąveikai. Taip pat buvo įvertinta auginimo terpės įtaka bakterijų zeta potencialui (19C pav.). Norriso terpė, pH 7,0, 25 g/l gliukozės, taip pat teigiamai veikė zeta potencialą. Vidutinis bakterijų zeta potencialas padidėjo iki -25 mV, palyginti su vidutiniu bakterijų zeta potencialu, kuris yra -60 mV PBS pagrindu pagamintuose tirpaluose su maža jonine jėga. Šis reiškinys pastebėtas greičiausiai dėl skirtingų ištirpusių jonų buvimo PBS ir Norris terpėje.

Bakterijų ląstelės, turinčios neigiamą krūvį, dėl elektrostatinės traukos lengviau prilimpa ir vėliau imobilizuojasi prie teigiamai įkrauto elektrodo. Šiame tyrime pastebėtas labai neigiamas zeta potencialas mažo joninio stiprumo tirpaluose. Stebėjimas rodo, kad *Rhizobium anhuiense* turi įgimtą gebėjimą stipriai prilipti prie anodo paviršiaus.

Atvirosios grandinės potencialas (OCP) buvo nustatytas išorinių grandinių apkrovose, o galios tankis apskaičiuotas remiantis šiais matavimo rezultatais.

Galios tankio ir poliarizacijos kreivės buvo surinktos BFC, pagrįstos *Rhizobium anhuiense* bakterijomis, kurios buvo apdorotos keliais redokso mediatoriais skirtingose aplinkose (20 ir 21 pav.).

Menadionas tarnauja kaip organinis hidrofobinis redokso mediatorius, didinantis krūvio perdavimą [53,54]. Redokso mediatorių efektyvumas didele dalimi priklauso nuo taikomo redokso mediatoriaus oksidacijos ir redukcijos potencialų. Redokso mediatoriai, kurių redokso potencialas didesnis, efektyviau pagauna elektronus iš elektronų donorų, tačiau elektronų pernaša iš redokso mediatorių, kuriems būdingas labai didelis redokso potencialas, į krūvio perdavimo grandinę nėra labai efektyvi [99]. Čia suprojektuoto MBFC elektrinis potencialas ir galios tankis pavaizduotas 21 paveiksle.

Riboflavinas yra žinomas kaip endogeninis redokso mediatorius, palengvinantis elektronų perdavimo greitį, skatinantis mažesnį generuojamos energijos kiekį. Funkciniai prietaisai, kuriems energiją tiekia kuro elementai, turi veikti sąlygomis, lygiomis didžiausiam galios tankiui arba jam lygiomis, kad veiktų labai efektyviai. Šio proceso metu perduodami elektronai yra tiesiogiai susiję su cheminėmis reakcijomis, kurias katalizuoja mikroorganizmų medžiagų apykaitos procesuose dalyvaujantys fermentai. Bakterijomis pagrįstiems kuro elementams būdingas netiesinis galios tankis. Šį netiesiškumą galima panaudoti efektyviam energijos taupymui, tuo pat metu pritaikant aktyvinimo našumą prie tam tikro charakteristikų rinkinio. Kuriant tokias sistemas siekiama didesnio bendro galios tankio esant didesniam potencialui, nes esant didžiausiai galios tankio vertei galima generuoti didžiausią elektros srovės kiekį.

Natūralaus redokso mediatoriaus - menadiono - panaudojimas MBFC konstrukcijoje leidžia padidinti suprojektuotų MBFC įtampą ir galią, o tai

padidina jų pritaikomumą. Priešingai, nepastebėta jokio teigiamo poveikio, kai vietoj menadiono buvo naudojamas riboflavinas. Šis poveikis gali būti susijęs su skirtingu šių natūralių redokso mediatorių tirpumu, nes menadionas tirpsta hidrofobinėje aplinkoje ir patenka į fosfolipidinę membraną, o riboflavinas tirpsta vandenyje ir gali būti ištirpintas ląstelėje, kaip ir ekstraląstelinėje aplinkoje. Tačiau riboflavinas nelabai tinka elektronams per ląstelės membraną perstumti. Todėl galime teigti, kad menadionas gali veiksmingiau pernešti krūvį per fosfolipidinę membraną link elektrodų, palyginti su riboflavino gebėjimu pernešti krūvį (20 pav.).

Žinoma, kad *Rhizobium anhuiense* gali veikti ir anaerobinėmis, ir aerobinėmis sąlygomis. Todėl *Rhizobium anhuiense* gebėjimas generuoti energiją buvo papildomai ištirtas anaerobinėmis sąlygomis, išstumiant ir prisotinant sistemą azoto dujomis. Tačiau anaerobinėmis sąlygomis nustatytas reikšmingas visų su energijos generavimu susijusių charakteristikų sumažėjimas (18 pav. ir 21 pav.).

Reikėtų pažymėti, kad čia aprašomo MBFC generuojamos srovės tankis, kaip ir daugumoje MBFC, nėra labai didelis, todėl norint padidinti srovės tankį 3D elektrodų medžiagos [100] ir (arba) laidžių polimerų pagrindu sukurtos struktūros [101] gali būti panaudotos elektrodinės konstrukcijos, kurios leistų padidinti srovės stiprį keliomis eilėmis. [64].

6.4.Išvados

1. Nustatėme, kad biojutiklių elektrodų konstrukcijoje galima taikyti skyles pernešančių (p tipo) organinius/polimerinius puslaidininkius. Atlikus elektrocheminius eksperimentus nustatyta, kad, esant palyginti mažam jonizacijos potencialui, vyksta tiesioginis skylių pernešimas iš elektrodo į fermentą. Pastebėta plati tiesinė priklausomybė tarp srovės tankio ir gliukozės koncentracijos nuo 2 iki 15 mM ir didelis ITO/poli-CzO/GOx-elektrodo stabilumas, o didžiausias jautrumas nustatytas grafito/poli-CzPh/GOx-elektrodo - 3,7 $\mu A\ cm^{-2}\ mM^{-1}$.

2. Sudarėme ir ištyrėme redokso tarpininkų pagrindu veikiančias bioelektrochemines sistemas su skirtingais redokso mediatoriais. Chlorofilo A ir Citochromomis medijuojama sistema pasižymėjo didžiausiu jautrumu į sistemos gliukozės koncentraciją, išmatuotas galios tankis buvo 2,5-4 $\mu W/cm^2$. Tačiau didinant gliukozės koncentraciją, šių sistemų veikimas buvo slopinamas. Chlorofilu A medijuojamos sistemos, padidinus gliukozės koncentraciją iki 100 mM, galios tankis nukrito iki < 10 nW/cm^2.

3. Naudodami *Rhizobium anhuiense* bakterijas, toliau kūrėme kuro elementus, pagrįstus elektrokatalitiniais procesais. Siekdami pagerinti krūvio perdavimą, išbandėme keletą redokso mediatorių: menadioną, riboflaviną ir 9,10-fenantrenchinoną. Nustatyta, kad geriausi rezultatai pasiekti *Rhizobium anhuiense* pagrindu sukurtame bioanode, kultivuotame didelio gliukozės kiekio aplinkoje, tarpininkaujant menadionui, išmatuotas 0,385 mV atviros grandinės potencialas, bei išmatuotas maksimalus 5,5 $\mu W/cm^2$ galios tankis, kuris generavo 50 $\mu A/cm^2$ anodinę srovę.

NOTES

NOTES

Vilniaus universiteto leidykla
Saulėtekio al. 9, III rūmai, LT-10222 Vilnius
El. p. info@leidykla.vu.lt, www.leidykla.vu.lt
Tiražas 15 egz.